DTIC FILE COPY

REPORT DOCUMENTATION PAGE

Form Approved
OMB No. 0704-0188

1a. REPORT SECURITY CLASSIFICATION UNCLASSIFIED	1b. RESTRICTIVE MARKINGS NONE

2a. SECURITY CLASSIFICATION AUTHORITY	3. DISTRIBUTION/AVAILABILITY OF REPORT

AD-A217 957

(S)

APPROVED FOR PUBLIC RELEASE;
DISTRIBUTION UNLIMITED.

5. MONITORING ORGANIZATION REPORT NUMBER(S)

AFIT/CI/CIA-89-025

6a. NAME OF PERFORMING ORGANIZATION AFIT STUDENT AT TX A&M UNIV	6b. OFFICE SYMBOL (If applicable)	7a. NAME OF MONITORING ORGANIZATION AFIT/CIA

6c. ADDRESS (City, State, and ZIP Code)	7b. ADDRESS (City, State, and ZIP Code) Wright-Patterson AFB OH 45433-6583

8a. NAME OF FUNDING/SPONSORING ORGANIZATION	8b. OFFICE SYMBOL (If applicable)	9. PROCUREMENT INSTRUMENT IDENTIFICATION NUMBER

8c. ADDRESS (City, State, and ZIP Code)

10. SOURCE OF FUNDING NUMBERS

PROGRAM ELEMENT NO.	PROJECT NO.	TASK NO.	WORK UNIT ACCESSION NO.

11. TITLE (Include Security Classification) (UNCLASSIFIED)
Ligand-Centered Electron-Transfer Redox Processes for Manganese, Iron, and Cobalt Complexes in Relation to Selected Catalytic Systems.

12. PERSONAL AUTHOR(S)
Silvia Ann Richert

13a. TYPE OF REPORT THESIS/DISSERTATION	13b. TIME COVERED FROM _____ TO _____	14. DATE OF REPORT (Year, Month, Day) 1989	15. PAGE COUNT 130

16. SUPPLEMENTARY NOTATION   APPROVED FOR PUBLIC RELEASE IAW AFR 190-1
ERNEST A. HAYGOOD, 1st Lt, USAF
Executive Officer, Civilian Institution Programs

17.	COSATI CODES		18. SUBJECT TERMS (Continue on reverse if necessary and identify by block number)
FIELD	GROUP	SUB-GROUP	

19. ABSTRACT (Continue on reverse if necessary and identify by block number)

DTIC
ELECTE
FEB 13 1990
S D

90 02 12 018

20. DISTRIBUTION/AVAILABILITY OF ABSTRACT ☒ UNCLASSIFIED/UNLIMITED ☐ SAME AS RPT. ☐ DTIC USERS	21. ABSTRACT SECURITY CLASSIFICATION UNCLASSIFIED	
22a. NAME OF RESPONSIBLE INDIVIDUAL ERNEST A. HAYGOOD, 1st Lt, USAF	22b. TELEPHONE (Include Area Code) (513) 255-2259	22c. OFFICE SYMBOL AFIT/CI

DD Form 1473, JUN 86   Previous editions are obsolete.   SECURITY CLASSIFICATION OF THIS PAGE
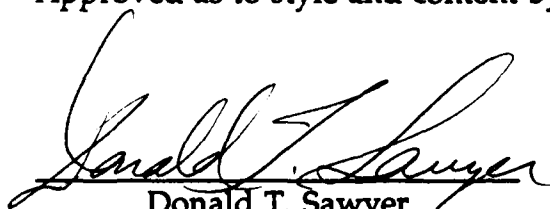
AFIT/CI "OVERPRINT"

LIGAND-CENTERED ELECTRON-TRANSFER REDOX PROCESSES FOR MANGANESE, IRON, AND COBALT COMPLEXES IN RELATION TO SELECTED CATALYTIC SYSTEMS

A Dissertation

by

SILVIA ANN RICHERT

Submitted to the Office of Graduate Studies of
Texas A&M University
in partial fulfillment of the requirements for the degree of

DOCTOR OF PHILOSOPHY

May 1989

Major subject: Chemistry

LIGAND-CENTERED ELECTRON-TRANSFER REDOX PROCESSES FOR MANGANESE, IRON, AND COBALT COMPLEXES IN RELATION TO SELECTED CATALYTIC SYSTEMS
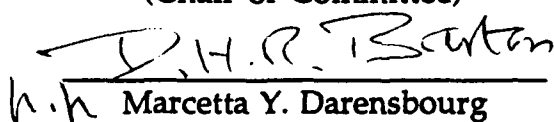
A Dissertation

by

SILVIA ANN RICHERT

Approved as to style and content by:
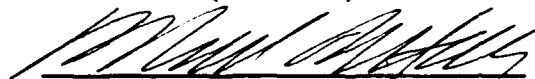
_____
Donald T. Sawyer
(Chair of Committee)

_____
Marcetta Y. Darensbourg
(Member)

_____
Arthur E. Martell
(Member)

_____
Thomas O. Baldwin
(Member)

_____
Michael B. Hall
(Head of Department)

May 1989

ABSTRACT

Ligand-Centered Electron-Transfer Redox Processes for Manganese, Iron, and Cobalt Complexes in Relation to Selected Catalytic Systems. (May 1989)

Silvia Ann Richert, B.S., United States Air Force Academy;

A.M., Harvard University

Chair of Advisory Committee: Dr. Donald T. Sawyer

The oxidation potentials for a series of MnL_3, FeL_3, and CoL_3 complexes [L = acetylacetonate, 8-quinolinolate, picolinate, 2,2'-bipyridine, and 1,10-phenanthroline] have been determined by cyclic voltammetry. The oxidations of these complexes occur at substantially less positive potentials than those for their zinc analogues and are clearly ligand-centered. The removal of an electron from the valence shell of the ligand is facilitated by the formation of a metal (d-electron)–ligand (p-electron) covalent bond. The negative shift in oxidation potential for a ligand is proportional to the metal-ligand covalent bond energy. The X-ray absorption edge energies for a series of manganese complexes have been determined and correlated with the electrochemical results. A change in the sp covalency of manganese ($d^5sp \rightarrow d^4sp^2$) corresponds to a shift of 4.3 eV, and the formation of a d-p covalent bond from a ligand-centered oxidation to a shift of 2.3 eV per bond formed.

The direct conversion of cyclohexane to cyclohexanone via iron-induced activation of dioxygen species has been investigated. The addition of hydrogen peroxide to a solution that contains bis(picolinato)iron(II) and cyclohexane in a pyridine/acetic acid solvent

(2:1 mole ratio) results in the direct transformation of cyclohexane to cyclohexanone. Other hydrocarbon substrates are transformed to ketones via the oxygenation of a methylenic carbon. Acetylenes and arylolefins are dioxygenated to α-dicarbonyls and aldehydes. A μ-dioxygen binuclear iron picolinate intermediate appears to be the active form of the catalyst.

> Keywords: Oxidation in solution reactions,
Electrical

To Brent.

ACKNOWLEDGMENTS

I would like to express my gratitude to Professor Donald T. Sawyer for his invaluable advice and patience. His insight and encouragement have made my graduate studies a truly rewarding experience. I am indebted to the other members of my committee for their constructive comments and criticisms.

I would like to express my deepest appreciation to Dr. Hiroshi Sugimoto for the many hours of valuable discussions and for his expertise and patience in demonstrating experimental techniques. I would like to acknowledge Drs. Lee Spencer and Paul Tsang for their incisive comments and counsel. Special thanks go to Dr. Takayuki Matsushita who kindly supplied several manganese complexes used in the X-ray absorption edge studies, to Ceshing Sheu who supplied information on several substrate transformations, and to Dr. Pablo Cofré who supplied supporting electrochemical data. I am grateful to Drs. K. M. Barkigia, J. Fajer, L. Hanson, and M. W. Renner of Brookhaven National Laboratory for their collection of the X-ray absorption edge data. I would also like to express my appreciation to my fellow graduate students and postdoctoral fellows for their gracious assistance and consideration.

Finally, I would like to thank my family and friends, and most of all my husband Brent, for their support of my educational goals and their understanding when I needed it most.

TABLE OF CONTENTS

CHAPTER

LIST OF TABLES

TABLE   Page

LIST OF FIGURES

CHAPTER I

INTRODUCTION

Ligand-Centered Electron-Transfer Redox Processes for Manganese, Iron, and Cobalt Complexes

Chemists are interested in transition metal complexes because of their applications as catalysts and as models for metalloenzymes. In discussing the nature and bonding of these complexes the common practice has been to assign formal oxidation states (sometimes inappropriately referred to as valences) to each atom or group of atoms within the complex.[1] While formal oxidation states are useful for electron counting and have been used to predict structures and reactivities, the actual electron distribution within a complex is often far different. To consider the formal oxidation state to be equivalent to the actual charge on a metal center gives a false impression of the ionicity, bond energies (ionic being misconstrued as "weak"), oxidative power, and reactivity of the complex.[2] Although there is no consensus on how to determine the actual charge on an atom in a complex,[1,3] a parameter that gives an indication of the extent of charge transfer within a molecule is electronegativity. There are several methods for the evaluation of electronegativities,[4] which Pauling first defined as "the power of an atom in a molecule to attract electrons to itself."[5,6] He introduced a method to calculate electronegativities from thermochemical data for bond energies,

---

The journal model is *J. Am. Chem. Soc.*

with fluorine assigned a value of 4.0. Soon after the introduction of the
Pauling scale, Mulliken suggested an electronegativity scale based on the
average of an atom's first ionization potential and electron affinity.[7]
Allred and Rochow proposed a definition of electronegativity dependant
on the effective nuclear charge and covalent radius of an atom.[8]
Sanderson has used a similar definition of electronegativity[3] to calculate
bond energies, bond lengths, and partial charges with great success.

A variation of the Mulliken electronegativity scale, based on the
most recent values for ionization potentials and electron affinities[9] and
scaled to χ_F = 4.0, is presented in Table I. This scale has smaller values of
electronegativity for carbon, nitrogen, oxygen, and sulfur, and a larger
electronegativity value for hydrogen. The electronegativities of nitrogen
and hydrogen are nearly identical, which indicates that the N-H bond is
fully covalent. Earlier studies had indicated extremely small charge
transfer in NH_3 (δ_H, +0.06).[3] Recent experiments have determined there
is absolutely no tendency for ammonia to act as a proton donor in
hydrogen bonding.[10]

The increase in electronegativity with increased positive
charge[3,11-15] (one recent estimate[16] gives the change in electronegativity
corresponding to the acquisition of unit charge as $\Delta\chi_i = 1.57\chi^{1/2}$) and the
principle of electronegativity equalization within compounds[3,17-19]
preclude the formation of highly oxidized metal centers with donors such
as C, N, O, and S. The metal centers in complexes that contain such donor
ligands have recently begun to be represented as having low or zero
charge.[2,20,21] A recent analysis suggests the valence-electron hybridization

Table I. Periodic Table of the Elements: Electronegativities.

Group I	II											III	IV	V	VI	VII	VIII
H a 13.60 b 0.75 c 2.76																	**He** 24.59
Li 5.39 0.62 1.15	**Be** 9.32 0.0 1.79											**B** 8.30 0.28 1.65	**C** 11.26 1.26 2.41	**N** 14.53 0.0 2.79	**O** 13.62 1.46 2.90	**F** 17.42 3.40 4.00	**Ne** 21.56
Na 5.14 0.55 1.09	**Mg** 7.65 0.0 1.47											**Al** 5.99 0.44 1.23	**Si** 8.15 1.38 1.83	**P** 10.49 0.75 2.16	**S** 10.36 2.08 2.39	**Cl** 12.97 3.62 3.19	**Ar** 15.76
K 4.34 0.50 0.93	**Ca** 6.11 0.0 1.17	**Sc** 6.54 0.19 1.29	**Ti** 6.82 0.08 1.33	**V** 6.74 0.52 1.40	**Cr** 6.77 0.67 1.43	**Mn** 7.44 0.0 1.43	**Fe** 7.87 0.15 1.54	**Co** 7.86 0.61 1.64	**Ni** 7.64 1.16 1.69	**Cu** 7.73 1.24 1.72	**Zn** 9.39 0.0 1.80	**Ga** 6.00 0.3 1.2	**Ge** 7.90 1.23 1.75	**As** 9.81 0.81 2.04	**Se** 9.75 2.02 2.26	**Br** 11.81 3.36 2.92	**Kr** 14.00
Rb 4.18 0.49 0.90	**Sr** 5.70 0.0 1.10	**Y** 6.38 0.31 1.28	**Zr** 6.84 0.43 1.40	**Nb** 6.88 0.89 1.49	**Mo** 7.10 0.75 1.51	**Tc** 7.28 0.55 1.50	**Ru** 7.37 1.05 1.62	**Rh** 7.46 1.14 1.65	**Pd** 8.34 0.56 1.71	**Ag** 7.58 1.30 1.71	**Cd** 8.99 0.0 1.73	**In** 5.79 0.30 1.17	**Sn** 7.34 1.11 1.62	**Sb** 8.64 1.07 1.87	**Te** 9.01 1.97 1.10	**I** 10.45 3.06 2.60	**Xe** 12.13

Table I. (Continued).

Group	I	II											III	IV	V	VI	VII	VIII
	Cs	Ba	La*	Hf	Ta	W	Re	Os	Ir	Pt	Au	Hg	Tl	Pb	Bi	Po	At	Rn
	3.89	5.21	5.58	7.0	7.89	7.98	7.88	8.7	9.1	9.0	9.22	10.44	6.11	7.42	7.29	8.42	-	10.75
	0.47	0.0	0.5	~0	0.32	0.81	0.15	1.10	1.56	2.13	2.31	0.0	0.2	0.36	0.95	1.9	2.8	
	0.84	1.00	1.2	1.3	1.58	1.69	1.54	1.9	2.0	2.1	2.22	2.01	1.2	1.49	1.58	2.0		
	Fr	Ra	Ac‡															
		5.28	6.9															
		0.0																
		1.02																

*Lanthanide Series

Ce	Pr	Nd	Pm	Sm	Eu	Gd	Tb	Dy	Ho	Er	Tm	Yb	Lu
5.47	5.42	5.49	5.55	5.63	5.67	6.14	5.85	5.93	6.02	6.10	6.18	6.25	5.43

‡Actinide Series

Th	Pa	U	Np	Pu	Am	Cm	Bk	Cf	Es	Fm	Md	No	Lr
				5.8	6.0								

[a] Ionization potential in electron volts (Ref. 9).
[b] Electron affinity in electron volts (Ref. 9).
[c] Electronegativity $\chi = \dfrac{IP+EA}{5.205}$, scaled so $\chi_F = 4.00$.

in palladium and platinum complexes should be formulated with zero-charge metal centers to form the maximum number of covalent bonds.[22] Similarly, the moiety O^{2-} is incompatible with oxidized transition metal complexes. A theoretical analysis[23] for the d^5 Cr(I) ion (isoelectronic with the d^5 Mn(II) ion) concludes that the electron-density distribution for the CrO^+ ion is between d^5 and d^4 $[Cr^I(\cdot O\cdot)^+ \leftrightarrow Cr^{II}(\cdot O^-)^+]$. Therefore the oxidation state for the more electronegative manganese in the isoelectronic MnO^+ ion must be essentially $[Mn^{II}(\cdot O\cdot)^{2+}]$. Manganous fluoride (MnF_2) has been calculated to be only 49% ionic,[16] and nominal Mn(IV) cannot be achieved in a stable form even with fluoride ligands $(MnF_4$ rapidly decomposes to MnF_3 and $F_2)$.[24] Thus, high oxidation-state metal and oxo-dianion formulations are even less appropriate. The degree of covalency for manganese-oxygen bonds that is indicated from these electronegativity and charge-density considerations confirms that the presence of an electropositive center of highly oxidized manganese is unlikely in biological complexes. The same arguments hold true for other first row transition metals. Indeed, a model for the reactive intermediate of cytochrome P-450 was recently shown to have reaction chemistry and electronic characteristics that are consistent with an oxygen atom covalently bonded to an iron(II)-porphyrin radical species.[25]

The issue of assigning oxidation states becomes even more ambiguous with complexes that contain "non-innocent" ligands.[26] Many biological-type ligands belong in this category due to their delocalized electronic structures and the presence of N, O, and S donors. For complexes of this type both the metal center and the ligand can be redox

active and the electrochemical properties of both the ligand and the metal ion are altered so that inner-sphere electron transfer between the two is possible.[27]

Perhaps the most scrutinized redox-active ligand is the catechol ligand, which may exist as the dianion catecholate, the monoanion radical semiquinato, or the neutral quinone. Which form of the ligand coordinates to a metal center has been shown to depend on solvent, charge, counterligands, temperature, and physical state,[28-31] and in numerous cases the redox activity of catechol complexes has been shown to be ligand-centered.[32-36] Additional examples of ligand-centered redox systems include the formation of ligand-centered radical cations in the oxidation of phthalocyanine complexes,[37] and the oxidations of metal-dithiolate[38] and metal-hydroxide[39] complexes.

In the cases of the metal-dithiolate[38] and metal-hydroxide[39] complexes the ligand-centered oxidations are facilitated by the stabilization of the ligand-radical product via covalent bond formation with an unpaired d-electron of the transition metal center. The negative shift in the potential for ligand oxidation relative to that for the free ligand anion is proportional to this covalent bond energy

$$E^{\circ\prime}{}_{ML/ML^-} = E^{\circ\prime}{}_{L\cdot/L^-} + (-\Delta G)_{B.F.}/23.1 \text{ kcal } V^{-1} \qquad (1)$$

where $(-\Delta G)_{B.F.}$ is the free energy of formation for the M-L covalent bond $(M\cdot + \cdot L)$.

These observations have prompted an investigation into the relevance of a ligand-centered redox approach to the electrochemistry of transition metal complexes in general, and in particular to biologically significant systems. The results of this investigation are presented in Chapter III. Manganese, iron, and cobalt, which are present in numerous metalloenzymes,[40] comprised the metal centers in these investigations. The ligands that have been studied include 8-quinolinolate (8Q⁻), acetylacetonate (acac⁻), α-picolinate (PA⁻), 2,2'-bipyridine (bpy), and 1,10-phenanthroline (phen). These ligands contain oxo- and pyridyl-nitrogen donor groups which are analogous to the tyrosine, glutamic acid, aspartic acid, and histidine residues that can act as ligands in metallo-proteins. The investigations have utilized dipolar aprotic solvents such as acetonitrile, dimethylformamide, and dimethyl sulfoxide, which more closely model the matrix of biological metals than does water (the transition metals of metalloproteins are often buried within the protein matrix, which is a distinctly different environment than bulk water in regard to dielectric constant, proton availability, and ionic solvation[41]). Cyclic voltammetry has been employed to determine the electron-transfer thermodynamics and the site of electron transfer; first, in a series of manganese complexes to determine if the redox processes are ligand- or metal-centered for these oxygen and nitrogen donor ligands, and later for iron and cobalt complexes to ascertain if the nature of the transition metal–ligand interaction is general or metal specific. Additionally, X-ray absorption edge energies have been used to estimate the relative charge densities[42-46] on the metal centers of a series of manganese compounds.

These edge positions are correlated with the oxidation states and bonding of the manganese centers. Various spectroscopic and magnetic measurements have been employed to characterize the complexes in their several oxidation states.

Iron-Induced Activation of Hydrogen Peroxide

The mild oxidizing action of hydrogen peroxide is enhanced in the presence of certain metal catalysts. For nearly 100 years[47] aqueous solutions of ferrous ion-hydrogen peroxide have been used to oxidize most organic compounds by a process known as Fenton chemistry. The mechanism of Fenton chemistry involves the iron(II)-catalyzed decomposition of hydrogen peroxide to generate hydroxyl radicals as transient intermediates, as shown in Scheme I.[41,48-50] The initial reaction is the reductive cleavage of the peroxy-bond by ferrous ion to produce ferric ion, hydroxide ion, and hydroxyl radical. The subsequent reaction of hydroxyl radical with organic substrates via hydrogen-atom abstraction produces carbon radicals that propogate chain reactions and autooxidations in the presence of dioxygen. Thus, traditional Fenton chemistry in aqueous media produces a diverse group of products from ·OH induced radical chemistry.

In contrast to the indiscriminant reactivity of ·OH with organic substrates in aqueous media, pronounced regio- and stereo-selectivity has been observed in the hydroxylation of cyclohexanol to cyclohexanediols by iron(II) and hydrogen peroxide in 90% acetonitrile-water.[51] The active

Scheme I.

$$HOOH + Fe(II) \xrightarrow{pH\,2} Fe(III)(^-OH) + \cdot OH \qquad k, \sim 100\ M^{-1}s^{-1}$$

$$\cdot OH + Fe(II) \longrightarrow Fe(III)(^-OH) \qquad k, 2 \times 10^8\ M^{-1}s^{-1}$$

$$\cdot OH + RH \longrightarrow R\cdot + H_2O \qquad k, 10^7\text{-}10^{10}\ M^{-1}s^{-1}$$

$$\cdot OH + HOOH \longrightarrow HO_2\cdot + H_2O \qquad k, 1 \times 10^7\ M^{-1}s^{-1}$$
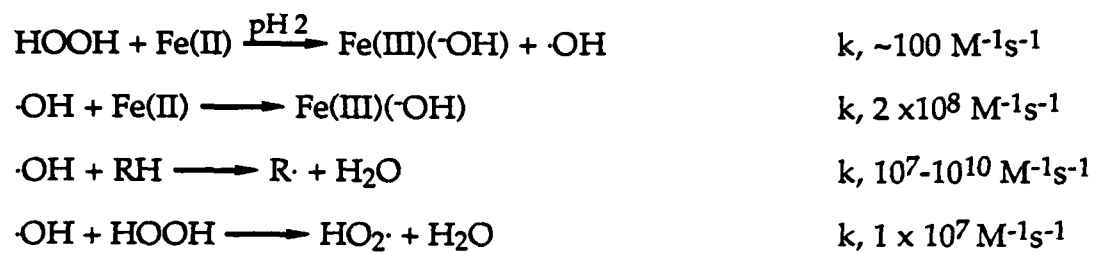
oxidant is postulated to be a ferryl ion (FeO^{2+}) or possibly a dimeric μ-oxo bridged iron species (Scheme II).[50-52]

The contrast in products between traditional Fenton chemistry in aqueous solution and the reaction of iron(II) and hydrogen peroxide in dipolar aprotic media is even more dramatic when dry acetonitrile is used as the solvent.[53,54] Solutions of $[Fe(MeCN)_4](ClO_4)_2$ catalyze the rapid disproportionation of hydrogen peroxide to dioxygen and water, but the catalyst remains in the Fe(II) state. In the presence of organic substrates, products resulting from dehydrogenation or monooxygenation are obtained (products of Fenton chemistry are not observed). The system cleanly oxidizes alcohols, aldehydes, thioesters, and substituted hydrazines by a two-electron process to yield products consistent with those obtained from catalase- and some peroxidase-catalyzed processes.[54,55] In the presence of excess hydrogen peroxide, the system reacts with singlet oxygen trapping reagents, like diphenylbenzofuran, 9,10-diphenyl-anthracene, and rubrene, to yield exclusively dioxygenated products.[53]

In the same medium, ferric chloride ($FeCl_3$) activates hydrogen peroxide to oxygenate alkanes, alkenes, aldehydes, and thioesters, and to dehydrogenate alcohols.[56,57] Anhydrous $FeCl_3$ in dry acetonitrile also catalyzes the demethylation of N,N-dimethylaniline, the epoxidations of olefins (stereospecifically in the case of norbornene), and the cleavage of 1,2-diols by hydrogen peroxide.[56,57]

The postulated reaction sequence for the $[Fe(MeCN)_4](ClO_4)_2$ chemistry in dry acetonitrile (Scheme III) involves an initial strong Lewis-acid interaction of the iron center with hydrogen peroxide to weaken the

Scheme II.

Ferryl Ion

$$Fe^{2+} + HOOH \longrightarrow \left[Fe\text{-}O\text{-}O\begin{smallmatrix}H\\ \\H^+\end{smallmatrix} \right]^+ \longrightarrow FeO^{2+} + H_2O$$

or

$$Fe^{3+} + \cdot OH \longrightarrow FeO^{2+} + H^+$$

Fe(III) μ-oxo bridged dimer

$$Fe^{IV}\!\!=\!\!O \xrightarrow{Fe^{II}} Fe^{III}\text{-}O\text{-}Fe^{III}$$

Scheme III.

a. [Fe(MeCN)$_4$](ClO$_4$)$_2$

$$Fe^{2+} + HOOH \longrightarrow Fe(II)(HOOH)^{2+}$$

$$
\left[
\begin{array}{ccc}
Fe(II) \overset{\displaystyle O \diagup H}{\underset{\displaystyle O \diagdown H}{|}} & \longleftrightarrow & Fe(II)\text{-}O\text{-}O \overset{\diagup H}{\diagdown H} \\[2em]
\updownarrow & & \updownarrow \\[1em]
Fe(II) \overset{\diagup OH}{\diagdown OH} & & Fe(\dot{O})(OH_2)
\end{array}
\right]^{2+}
$$

$$Fe(\dot{O})(OH_2) + RH \longrightarrow ROH + Fe^{2+} + H_2O$$
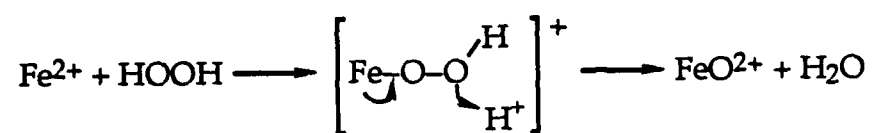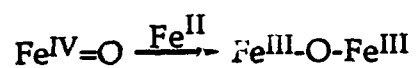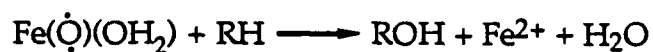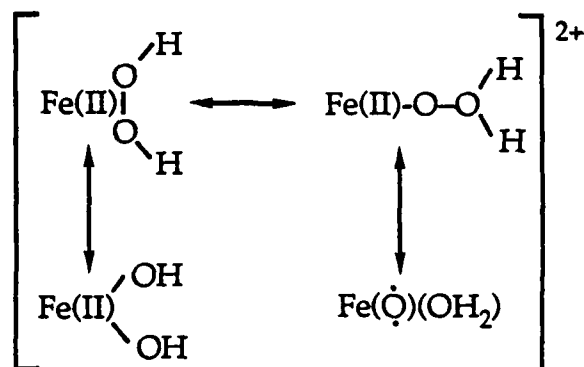
oxidase and monooxygenase model

b.

$$
\left[Fe(II) \overset{\displaystyle O \diagup H}{\underset{\displaystyle O \diagdown H}{|}} \right]^{2+} + HOOH \longrightarrow
\left[\underset{\displaystyle O \diagdown H \ \ O \diagdown H}{\overset{\displaystyle O \diagup H \ \ O \diagup H}{| \ Fe(II) \ |}} \right]^{2+} \longrightarrow
$$

$$
\left[\left(\begin{array}{c} O \\ | \\ O \end{array} \right) Fe(II)(OH_2)_2 \right]^{2+}
$$

$$
\left[\left(\begin{array}{c} O \\ | \\ O \end{array} \right) Fe(II)(OH_2)_2 \right]^{2+} + PhCH{=}CHPh \longrightarrow 2PhCH(O) + Fe^{2+} + 2H_2O
$$

$$\Big\downarrow HOOH$$

$$^3O_2 + Fe^{2+}$$
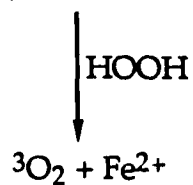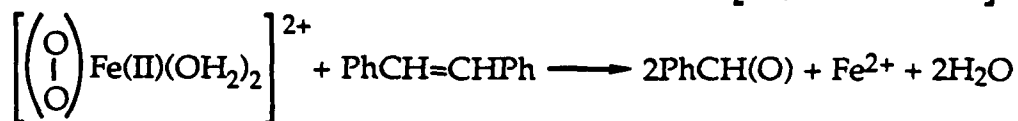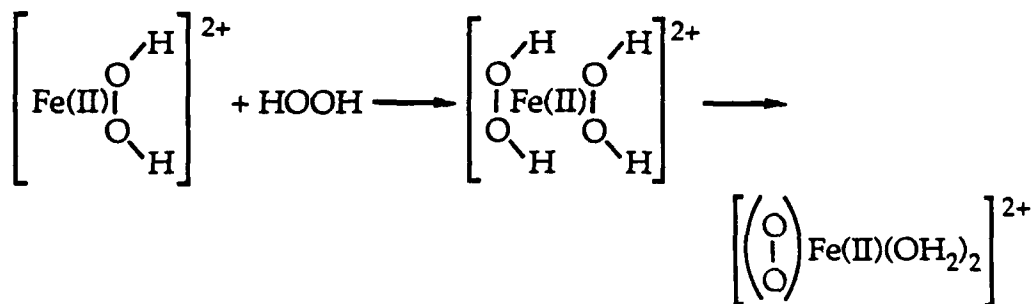
catalase and dioxygenase model

O–O bond.[41,54,55] This gives the peroxide a biradical nature, which results in the two-electron oxidation of organic substrates without necessitating intramolecular electron transfer from the iron(II) center. A similar activation is postulated for epoxidations by $FeCl_3$ (Scheme IV),[41,55-57] where the hydrogen peroxide acquires substantial oxene character for the direct biradical electrophilic insertion into the π-bond of the substrate.

Tris(picolinato)manganese(III)[58] also facilitates the decomposition of hydrogen peroxide in aprotic solvents in the absence of substrates. The reaction apparently proceeds via the one-electron oxidation of hydrogen peroxide to the hydroperoxyl radical (HOO·), followed by disproportionation to hydrogen peroxide and dioxygen. The tris(picolinato)manganese(II) complex, $Mn(PA)_2(PAH)(H_2O)$, efficiently catalyzes the disproportionation of superoxide (O_2^-) in acetonitrile or dimethyl sulfoxide at a rate that is two orders of magnitude faster than the disproportionation of hydroperoxyl radical (k, 1×10^4 $M^{-1}s^{-1}$).[59] In the presence of strong acids, superoxide decomposes by a rapid protonation to form hydroperoxyl radical, followed by disproportionation to hydrogen peroxide and dioxygen. The addition of superoxide to the manganese complex results in a coordinated hydroperoxy-manganese adduct that reacts with a second superoxide to yield hydrogen peroxide and dioxygen. The bis(8-quinolinolato)manganese(II) complex also has a catalytic effect on the decomposition of superoxide.[60]

The picolinato-iron complexes have not been studied in regard to their reaction with hydrogen peroxide or superoxide in aprotic media, but the bis(8-quinolinato)iron(II) complex catalytically decomposes

Scheme IV.

FeCl$_3$

$$FeCl_3 + HOOH \longrightarrow \left[Cl_3Fe\begin{array}{c} OH \\ OH \end{array} \longleftrightarrow Cl_3Fe(\dot{O})(OH_2) \right]$$

$$\left[Cl_3Fe(\dot{O})(OH_2) \right] + RCH=CHR' \longrightarrow RCH\overset{\displaystyle O}{-}CHR' + FeCl_3 + H_2O$$

$$\downarrow HOOH$$

$$O_2 + FeCl_3 + 2H_2O$$
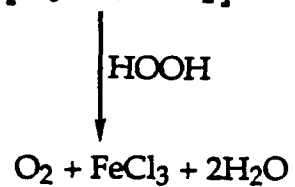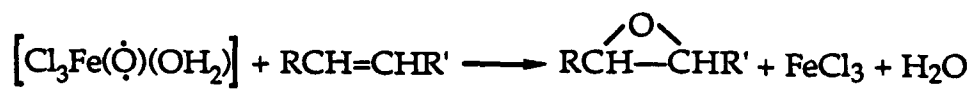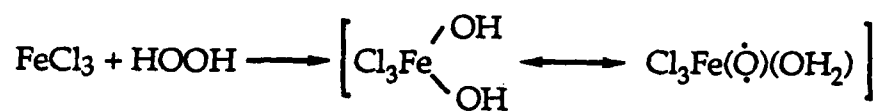
superoxide.[61] In aqueous media tris(picolinato)iron(II) catalyzes the decomposition of superoxide via the generation of hydroxyl radicals, while tris(picolinato)iron(II) anion catalyzes the decomposition of hydrogen peroxide to produce hydroxyl radicals.[62]

Although [Fe(MeCN)$_4$](ClO$_4$)$_2$ and FeCl$_3$ in anhydrous acetonitrile activate hydrogen peroxide for the oxidation of a wide variety of organic substrates, these systems are essentially unreactive with saturated hydrocarbons. Ferric chloride/HOOH epoxidizes aliphatic mono-olefins while [Fe(MeCN)$_4$](ClO$_4$)$_2$/HOOH does not react with these substrates. The presence of basic ligands (H$_2$O or pyridine) promotes Fenton chemistry. During the past five years, several reports[63-67] have described the selective transformation of methylenic groups $\left(\gtrdot CH_2 \right)$ to ketones via four heterogeneous iron-dioxygen systems (a) iron powder/sodium sulfide/O$_2$, (b) Fe$_3$O(OAc)$_6$·3.5Py/zinc dust/O$_2$, (c) (Py)$_4$FeCl$_2$/KO$_2$(s), and (d) (Py)$_4$FeCl$_2$/(O$_2$ + e$^-$ → O$_2^{\cdot -}$) in 4:1 pyridine/HOAc. These systems are postulated to contain the same iron-carbon σ-bonded intermediates[68] and to have superoxide ion as the active form of reduced oxygen that oxidizes the iron catalyst within the catalytic cycle. Pyridine is believed to be essential to the system as a trap for hydroxyl radicals, and thereby to prevent Fenton chemistry.

This background has prompted studies to optimize the catalyst/solvent system for the ketonization of $\left(\gtrdot CH_2 \right)$ via superoxide (KO$_2$ or O$_2$ + e$^-$ → O$_2^{\cdot -}$) and to investigate the use of iron catalysts with hydrogen peroxide in pyridine/acetic acid solvents. The results of these studies are presented in Chapter IV. Catalyst concentrations for a variety

of metal complexes (predominantly iron complexes) and solvent

compositions have been varied to optimize ketone yields. The

transformations of several substrates that contain methylenic carbons,

acetylenes, and arylolefins have been investigated. Capillary gas

chromatography and mass spectrometry have been used to identify and

assay the reaction products. Various spectroscopic and electrochemical

measurements have been used to characterize the reactions.

CHAPTER II

EXPERIMENTAL TECHNIQUES

Electrochemistry

Cyclic Voltammetry

Cyclic voltammetry was accomplished with a Bioanalytical Systems (BAS) Model CV-27 voltammograph and a Houston Instruments Model 200 XY recorder. The electrochemical measurements were made with a microcell assembly (10 mL capacity) closed with a Teflon cap that contained holes for a three electrode system and two additional small bore holes for deaeration and sample injection. The working electrode was a Bioanalytical Systems glassy-carbon inlay electrode (area 0.09 cm^2). The auxiliary electrode was a platinum wire isolated from the bulk solution by a glass tube closed with a fine porosity glass-frit and filled with a concentrated solution of supporting electrolyte. A Ag/AgCl reference electrode (filled with aqueous tetramethylammonium chloride solution and adjusted to 0.00 V vs. SCE) with a solution junction via a Pyrex tube with a soft-glass (soda lime) cracked tip (resistance 15-25 kΩ) was used.[69] The reference electrode was placed inside a Luggin capillary in the cell assembly. Prior to use, the electrochemical cell assembly was treated with HNO_3 overnight, repeatedly soaked in a distilled water bath (residual acid tended to concentrate in the glass frit), and oven dried at 140 °C for several hours.

Dry tetraethylammonium perchlorate (TEAP, GFS Chemicals) was used as the supporting electrolyte (0.1 M) for the electrochemical

experiments. Solutions were deaerated with high purity argon (presaturated with solvent) for 10 minutes prior to each experiment or until a background scan of the solvent and supporting electrolyte confirmed the absence of dioxygen (5 μA scale). A blanket of argon was maintained during the experiments. The cyclic voltammograms were initiated at the rest potential of the solution with a scan rate of 0.1 V s^{-1}. The working-electrode surface was polished with Buehler No. 3 (0.05 μm) polishing alumina prior to each scan. Experiments were performed at room temperature (22 $\pm$ 2 °C) unless otherwise indicated.

For oxidation-reduction couples that were reversible in appearance, the half-wave potential, $E_{1/2} = (E_{p,a} + E_{p,c})/2$, where $E_{p,a}$ and $E_{p,c}$ are the peak anodic and cathodic potential values, is reported (estimated error, $\pm$ 0.01 V). When a redox feature appeared irreversible, $E_{1/2}$ has been estimated by the relation $E_{1/2} = (E_{p,a} - 0.03$ V) or $(E_{p,c} + 0.03$ V) for a one electron process at 25 °C.[69]

Controlled-Potential Electrolysis

Controlled-potential electrolysis was performed with a three-electrode potentiostat (Princeton Applied Research Model 173 potentiostat/galvanostat, Model 175 universal programmer, and Model 179 digital coulometer). The same microcell assemblies and Ag/AgCl reference electrodes as those employed for cyclic voltammetry were used. Platinum-flag auxiliary electrodes (contained in a glass tube with medium or coarse porosity glass frit and filled with a concentrated solution of the supporting electrolyte) and glassy-carbon plate working electrodes (on

platinum wires) were used for the controlled-potential electrolyses. The glassy-carbon plate working electrodes were polished with alumina (Buehler No. 3, 0.05 μm) and rinsed with methanol prior to use.

X-ray Absorption Edge Spectroscopy (XAES)

X-ray absorption spectra were collected for powdered samples spread on tape by use of beam line X-11 at the National Synchrotron Light Source at Brookhaven National Laboratory. Samples were mounted on a movable stage placed between two detectors, perpendicular to the x-ray path. The number of counts per detector for a given wavelength was recorded as the monochrometer scanned through a set wavelength range. Data were then treated as an absorption plot of $\ln(I_0/I)$ vs. energy. These data were further treated by subtracting a linear background determined from fitting the pre-edge region and by normalizing the edge height. The edge position was defined as the inflection point of the major absorption edge. The E_0 of energy was taken as the beginning of the pre-edge feature attributed to $1s \rightarrow 3d$ quadrupole transitions for Mn compounds.[70-72] First derivative plots were used to determine edge positions when available. Maximum error in edge position is estimated to be ± 0.5 eV.

Magnetic Susceptibility Measurements

Solution magnetic susceptibilities of the complexes were measured by the Evans' method[73-76] with concentric NMR tubes in a Varian XL-200 or XE-200 NMR Spectrometer (Wilmard Glass Co., Inc. 5 mm diameter, 6" NMR tube with a WGS-5BL coaxial insert with capillary end). Prior to use,

the NMR tubes were treated with acid and distilled water baths in the

same manner as the electrochemical cells, followed by a NH_3-EDTA bath.

The tubes were then rinsed with distilled water and oven dried. The outer

tube contained 0.6-1.0 mL of solution while the capillary end of the inner

tube held 60-100 μL. The solution of the complex under study (1-5 mM)

was placed in either the outer or inner tube; the outer tube was preferred

for ease in sample handling. Samples were prepared with deuterated

solvents in a glovebox (Vacuum Atmospherics Model HE-493 Dri-Lab

with a Model HE-493 Dri-Train system) under a nitrogen atmosphere.

Tetramethylsilane (TMS) was used as a non-interacting chemical-shift

indicator.

The paramagnetic shift of the TMS protons was the measured NMR

parameter, which was used in the relation[73,74]

$$\chi_M{}^{corr} = (4/3\pi)\,(\Delta ppm \times 10^{-6})\,MW/c - \chi_{diamag} \qquad (2)$$

where $\chi_M{}^{corr}$ is the corrected molar susceptibility, Δppm the shift in the

TMS proton resonance in parts per million, MW the molecular weight of

the complex, c the concentration of the complex in solution in

grams/milliliter, and χ_{diamag} a correction for the diamagnetic

susceptibility of the ligand atoms as estimated from Pascal's constants.[74,75]

A factor of $(4/3\pi)$ appears in the equation rather than $(2/3\pi)$ because the

probe geometry in the newer superconducting magnet spectrometers has

the applied magnetic field parallel to the sample tube axis, whereas the

iron magnet instruments in use when the Evans' method was developed

have the applied magnetic field perpendicular to the sample tube axis.[76]
The major sources of error in the measurement of χ_M^{corr} were the small
sample size and solubility limitations (weighing error, ± 0.0001 g (Mettler
H31 or Ainsworth Type 10 Analytical Balance); error in χ_M^{corr}, ± 10%).

Assuming Curie Law behavior, the magnetic moment was
calculated from the molar susceptibility,[74]

$$\mu_{corr} = (3kT\ \chi_M^{corr}/N_0)^{1/2} = 2.84\ (\chi_M^{corr} \cdot T)^{1/2} \qquad (3)$$

where μ_{corr} is the magnetic moment in Bohr magnetons corrected for
diamagnetism, k is Boltzmann's constant, N_0 is Avogadro's number, and
T is the temperature (K). Measurements were performed at ambient
temperature, 21-22 °C.

Gas Chromatography

The reaction products were separated and identified with a Hewlett-
Packard 5880A Series gas chromatograph equipped with a HP-1 capillary
column (cross-linked methyl silicone gum phase, 12 m x 0.2 mm i.d.) and
by gas chromatography-mass spectrometry (Hewlett-Packard 5790A Series
gas chromatograph with mass selection detector). Reference samples were
used to confirm product identifications. The quantities of products were
calculated from standard curves for authentic samples. Linear regressions
of the ratios of standard solutions (0.2 mM, 0.5 mM, 1 mM, 2 mM, 3 mM, 5
mM, 10 mM, and 20 mM) to 1 M cyclohexane were used to determine
product yields for cyclohexanone or cyclohexanol. Direct injections of the

product solution (1-2 µL) were made. Conditions: injection temperature, 220 °C; detector temperature, 250 °C; chart speed, 0.25 cm/min; attenuation, 2^2 or 2^3; threshold, -2. Gas flow rates: hydrogen, 40 psi; air, 40 psi; carrier, 6 psi; auxiliary 1, 16 psi. Other parameters were left at the default values. The oven temperature profile was adjusted for the substrate under study and its products.

Spectroscopy

Optical Spectroscopy

The UV/visible spectrophotometric measurements were performed on a Hewlett-Packard Model 8450 diode-array spectrophotometer. The error in wavelength measurement was ± 2 nm. Quartz cells (Precision Cells, Inc.) were cleaned by the same regimen as that used for the electrochemical cell assemblies.

Infrared Spectroscopy

Infrared spectra were recorded with an IBM IR/44 (IR/40S Spectrometer with IR/30S upgrade unit) FTIR instrument. Solid-state samples were made by use of a KBr pellet press.

Nuclear Magnetic Resonance Spectroscopy

The NMR spectra were recorded on a Varian XL-200 NMR Spectrometer with the sample dissolved in deuterated solvents that contained an internal TMS reference.

Elemental Analysis

Elemental analyses were performed by Galbraith Microanalytical Laboratories, Inc., Knoxville, TN.

Chemicals and Reagents

The reagents for the investigations and syntheses were the highest purity commercially available and were used without further purification, unless noted otherwise. Burdick and Jackson "distilled in glass" grade acetonitrile (MeCN, 0.004% H_2O), dimethylformamide (DMF, 0.011% H_2O), dimethyl sulfoxide (DMSO, 0.016% H_2O), and pyridine (Py, 0.014% H_2O) were used without further purification as the solvents for the electrochemical experiments. The solvents for the magnetic susceptibility measurements, deuterated d_3-MeCN, d_7-DMF, and d_6-DMSO that contained 1% tetramethylsilane (TMS), were purchased from Aldrich. Tetraethylammonium perchlorate (TEAP, GFS Chemicals) was vacuum dried for 24 hours prior to use as the supporting electrolyte for the electrochemical experiments. High purity argon gas was used to deaerate the solutions. All compounds were dried in vacuo over $CaSO_4$ for 24 hours prior to use.

A number of reagents and complexes were purchased commercially:

General Reagents

Ammonium acetate (NH_4OAc, Fisher); absolute ethanol (EtOH, Mallinkrodt); hydrogen peroxide (HOOH, 30% Mallinkrodt and 50% Fisher); methanol (MeOH, Fisher); perchloric acid ($HClO_4$, 70%, MCB

Reagents); potassium superoxide (KO_2, Aldrich); sodium bicarbonate ($NaHCO_3$, Fisher); sodium perchlorate ($NaClO_4$, GFS); and tetramethyl-ammonium hydroxide pentahydrate (TMAOH·$5H_2O$, Fluka).

The substrates and reference compounds for the products for the catalyses described in Chapter IV were purchased from Aldrich with the exceptions of cyclohexanol ($C_6H_{11}OH$, Baker), cyclohexene (C_6H_{10}, Fisher), and acetophenone (PhC(O)CH_3, Mallinkrodt).

Ligands

Glacial acetic acid (HOAc, ACS grade, Fisher Scientific or Chempure); 2,2'-bipyridine (bpy, Aldrich); 8-hydroxyquinolinol (8HQ, Aldrich Gold Label); 2,4-pentanedione (acacH, Aldrich Gold Label); 1,10-phenanthroline monohydrate (phen, Aldrich Gold Label); α-picolinic acid (PAH, Aldrich); 2,6-pyridinedicarboxylic acid (DPAH$_2$, Aldrich); tetrabutylammonium hydroxide ((Bu_4N)OH, 1 M, obtained from Aldrich as a 25% solution in methanol and concentration determined by acid-base titration); and triphenylphosphine oxide (OPPh$_3$, Aldrich).

Manganese Complexes

[Mn(H_2O)$_6$](ClO_4)$_2$ (Fluka); Mn(OAc)$_2$·$4H_2O$ (Alfa); Mn(OAc)$_3$·$2H_2O$ (Aldrich); Mn(acac)$_2$ (McKenzie); Mn(acac)$_3$ (McKenzie), recrystallized from benzene before use; MnCl$_2$ (Aldrich); MnF$_3$ (Alfa); Na$_3$[Mn(P_2O_7)$_3$] (K&K Laboratories); MnTPP(OAc) (TPP = tetraphenylporphinato, Strem); MnO$_2$ (Mallinkrodt); and KMnO$_4$ (Fisher).

Iron Complexes

$[Fe(H_2O)_6](ClO_4)_2$ (GFS); $Fe(ClO_4)_3$ (Strem); $FeCl_3 \cdot 6H_2O$ (Fisher); $Fe(acac)_2$ (McKenzie); $Fe(acac)_3$ (McKenzie), recrystallized from dry acetonitrile before use; $[Fe(bpy)_3](ClO_4)_2$ (GFS); $[Fe(phen)_3](ClO_4)_2$ (GFS); $Fe(CO)_5$ (Aldrich); and ferrocene ($Fe(Cp)_2$, Cp = cyclopentadienyl, Aldrich UV standard).

The IR spectrum of $Fe(acac)_3$ (absorption maxima (cm^{-1}); 1572(vs), 1525(vs), 1466(vw), 1442(w), 1424(m), 1390(m), 1363(s), 1275(s), 1189(w), 1023(s), 930(s), 802(w), 772(m), 668(s), 560(m), 550(m), 435(vs)) was in accord with published spectra,[77,78] as was its UV/visible spectrum[79,80] (λ_{max}; 235, 273, 353, and 434 nm). The solution magnetic moment for $Fe(acac)_3$ was $\mu_{corr} = 5.88$ B.M.

Cobalt Complexes

$[Co(H_2O)_6](ClO_4)_2$ (GFS); $Co(CO_3)$ (Allied Chemicals, Baker & Adamson); $Co(NO_3)_2$ (Allied Chemicals); $CoCl_2 \cdot 6H_2O$ (Mallinkrodt); $Co(acac)_2$ (Aldrich), dried in vacuo over P_2O_5 overnight; and $Co(OAc)_2 \cdot 4H_2O$ (Aldrich), heated in vacuo overnight at 60-90 °C with an oil bath to obtain $Co(OAc)_2$.

Zinc Complexes

$[Zn(H_2O)_6](ClO_4)_2$ (GFS); $Zn(acac)_2 \cdot H_2O$ (Aldrich); and $Zn(OAc)_2 \cdot 2H_2O$ (Aldrich).

Syntheses

Several complexes were prepared by conventional methods:

Manganese Complexes

$Mn(8Q)_3$[81,82]; $Mn(PA)_3 \cdot H_2O$[58,81,82]; $[Mn(bpy)_3](ClO_4)_2$[82]; $[Mn(phen)_3](ClO_4)_2$[83-85]; and $[Mn(OPPh_3)_4](ClO_4)_2$[86].

Dr. T. Matsushita kindly provided a number of compounds used in the XAES study of manganese: $[Mn(urea)_6](ClO_4)_3$[87]; $[Mn(DMU)_6](ClO_4)_2$[88] (DMU = dimethylurea); $[Mn(DMSO)_6](ClO_4)_3$[89]; $Mn(DPA)(DPAH)(EtOH)$[81]; $Na[Mn(DPA)_2]$[58]; $Bu_4N[Mn(DPA)_2]$[58]; $Mn(PA)_2 \cdot 2H_2O$[90]; $[Mn(terpyO_3)_2](ClO_4)_2 \cdot 2H_2O$[91] (terpyO_3 = 2,2',2"-terpyridine 1,1',1"-trioxide); $[Mn(bpyO_2)_3]_2(S_2O_8)_3 \cdot 8H_2O$[92] (bpyO_2 = 2,2'-bipyridine 1,1'-dioxide); $[Mn_2(bpy)_4(\mu-O)_2](ClO_4)_3 \cdot 4H_2O$[93,94]; $[Mn_2(phen)_4(\mu-O)_2](ClO_4)_4 \cdot 4H_2O$[95]; $Mn(salpn)Cl$[96] (salpnH_2 = N,N'-disalicylidenepropanediamine); and $Mn(salen)Cl \cdot H_2O$[96] (salenH_2 = N,N'-disalicylidenethanediamine).

Iron Complexes

$Fe(8Q)_3$[97]; $[Fe(OPPh_3)_4](ClO_4)_2$[98]; and $(Py)_4FeCl_2$[99].

The IR spectrum of $Fe(8Q)_3$ is consistent with published spectra[100-102] (absorption maxima (cm^{-1}); 1597(w), 1574(s), 1562(w), 1496(vs), 1462(vs), 1438(w), 1424(w), 1421(w), 1377(vs), 1322(vs), 1278(s), 1237(m), 1227(m), 1109(vs), 824(s), 804(m), 788(m), 738(vs), 620(m), 524(s)). The UV/visible spectrum of $Fe(8Q)_3$ has three absorption bands (λ_{max}; 372 nm, 462 nm, and 574 nm, with a shoulder at 315 nm). The $Fe(8Q)_3$ complex has a solution magnetic moment of $\mu_{corr} = 6.35$ B.M.

Cobalt Complexes

Co(8Q)$_2$[103]; Co(PA)$_2$[104]; Co(acac)$_3$[105]; Na$_3$[Co(CO$_3$)$_3$]·3H$_2$O[106];

[Co(bpy)$_3$](ClO$_4$)$_2$[104]; [Co(phen)$_3$](ClO$_4$)$_2$[84]; [Co(phen)$_3$](ClO$_4$)$_3$·2H$_2$O[84]; and

[Co(OPPh$_3$)$_4$](ClO$_4$)$_2$[86].

The IR spectrum of Co(8Q)$_2$ confirmed that it was anhydrous. The

NMR spectrum of Co(acac)$_3$ had two clean lines (δ; 2.046 ppm and 5.543

ppm, areas 6:1, TMS internal reference) for CH$_3$ and ‑CH.

Anhydrous Hydrogen Peroxide

Anhydrous hydrogen peroxide (HOOH) was prepared by careful

removal of water from 10 mL of 50% HOOH at 0 °C under vacuum to give

1.5-3 mL of pure hydrogen peroxide.[54] This was quickly dissolved in dry

acetonitrile (25 mL). The resulting solutions were assayed by iodometric

titration[107] and found to be 1.6 M (94%) and 3.6 M (82%).

Hazard Warning: Pure HOOH is an exceptional oxidant. Trace

quantities of reduced transition-metal ions can initiate its violent

decomposition and oxidation of organic materials. It is necessary to

exercise extreme care, use adequate safety precautions, and work with a

small quantity during its purification, storage, and use.

Tetramethylammonium Superoxide

Tetramethylammonium superoxide (Me$_4$N)O$_2$ was prepared by

combining KO$_2$ and (Me$_4$N)OH·H$_2$O (from TMAOH·5H$_2$O which was

sequentially dried under vacuum at 65 °C with continuous stirring for

18 hours, 80 °C for 24 hours, and 93 °C for 24 hours) and subsequent
extraction in liquid ammonia.[108,109]

Ligand Anion Solutions

Ligand anion solutions of $8Q^-$, $acac^-$, ^-OAc, and PA^- were prepared
by mixing the appropriate ligand (8HQ, acacH, HOAc, or PAH) with
$(Bu_4N)OH$ (1 M tetrabutylammonium hydroxide in methanol).

$(Me_4N)PA$ and $(Me_4N)_2DPA$

Tetramethylammonium picolinate ($(Me_4N)PA$) and
tetramethylammonium dipicolinate ($(Me_4N)_2DPA$) were prepared by the
neutralization of PAH or $DPAH_2$ by $TMAOH \cdot 5H_2O$ in aqueous
solution.[110] Recrystallizations of $(Me_4N)PA$ were from acetonitrile;
$(Me_4N)_2DPA$ was recrystallized from 95% MeCN-5% MeOH. The
extremely hydroscopic products were stored under vacuum.

$[M(MeCN)_4](ClO_4)_2$, M = Mn, Fe, Co, and Zn

The $[M(MeCN)_4](ClO_4)_2$ complexes of Mn, Fe, Co, and Zn were
prepared by multiple recrystallizations of the commercial hydrated
perchlorates in dry MeCN.

Iron Picolinate and Iron Dipicolinate Solutions

Solutions (1-5 mM) of iron picolinate and iron dipicolinate were
prepared in situ by mixing $Fe(ClO_4)_3$ (anhydrous) or $[Fe(MeCN)_4](ClO_4)_2$

with varying stoichiometries of the appropriate ligand anion (PA⁻, $(Me_4N)PA$, or $(Me_4N)_2DPA$).

$Fe(PA)_2$ and $Fe(DPA)$

The nominal complexes $Fe(PA)_2$ and $Fe(DPA)$ were prepared by mixing $[Fe(MeCN)_4](ClO_4)_2$ and the stoichiometric amount of the tetramethylammonium salt of the ligand in acetonitrile under argon. A brick-red precipitate was obtained for "$Fe(PA)_2$". The isolated powder gradually turned light brown upon exposure to air. Exposure of the $Fe(PA)_2$ solution to air resulted in the precipitation of a pale green powder. The precipitate obtained for "$Fe(DPA)$" was an orange-brown powder that became light brown upon exposure to air. Exposure of the $Fe(DPA)$ solution to air caused the precipitation of a dark mustard-colored powder.

$Co(PA)_3$ and $Co(8Q)_3$

These complexes were prepared by a variation of a literature method for the synthesis of $Co(acac)_3$.[105] Three equivalents of ligand (approximately 4 g) in 150 mL of solvent were mixed with $Na_3[Co(CO_3)_3] \cdot 3H_2O$ in the presence of 2 mL of 70% $HClO_4$. $Co(PA)_3$ was prepared in water and $Co(8Q)_3$ in 95% ethanol. The products were recrystallized from water, then heptane, and absolute ethanol, respectively. Purple crystals were obtained for $Co(PA)_3$ (λ_{max}; 376 nm and 528 nm). <u>Analysis</u>. Calculated for $CoC_{18}H_{12}N_3O_6$ ($Co(PA)_3$): C, 50.84; H, 2.84; N, 9.88; O, 22.57; Co, 13.86. Found: C, 50.78; H, 2.84; N, 9.76; O, 23.05; Co, 13.77.

The NMR spectrum for $Co(8Q)_3$, although fairly noisy, was consistent with the published spectrum.[111] The NMR spectrum of $Co(PA)_3$ consisted of a doublet (δ; 7.519, 7.549 ppm), a triplet (δ; centered at 7.794 ppm), and two larger multiplets. One of the latter had a complex pattern (δ; 7.942, 7.973, 8.006, 8.042, 8.065, 8.076, 8.088, 8.100, 8.132 ppm), and the other appeared to consist of a triplet (δ; 8.321, 8.359, 8.397 ppm) and a doublet of doublets (δ; 8.451, 8.478, 8.524, 8.552 ppm). The UV/visible spectrum of $Co(PA)_3$ contained two maxima (λ_{max}; 376 nm and 528 nm), consistent with that reported in the literature (λ_{max}; 380 nm and 528 nm)[112] for a pale pink crystalline product (deep purple crystals were obtained in the present work). The corresponding synthesis[112] did not include the addition of acid needed to drive the reaction to completion[106] or a rigorous drying procedure.

$Zn(8Q)_2 \cdot 2H_2O$ and $Zn(PA)_2 \cdot 2H_2O$

$Zn(8Q)_2 \cdot 2H_2O$ was prepared by a modified procedure[113] that made use of $[Zn(H_2O)_6](ClO_4)_2$ in place of $Zn(NO_3)_2$, where 0.5 equivalent of $[Zn(H_2O)_6](ClO_4)_2$ was added to an equimolar mixture of NaOH and 8HQ in water. The resulting yellow precipitate was collected on a glass frit, washed with ethanol, and dried in vacuo over $CaSO_4$. A similar synthesis was used for $Zn(PA)_2 \cdot 2H_2O$. The IR spectrum of $Zn(PA)_2 \cdot 2H_2O$ was reasonable in comparison to the spectra of other $M(PA)_2$ compounds[90] (absorption maxima (cm^{-1}); 1097(m), 1051(s), 1023(s), 860(m), 765(vs), 722(s), 699(vs), 642(s)).

CHAPTER III

LIGAND-CENTERED REDOX PROCESSES FOR MnL$_3$, FeL$_3$, AND CoL$_3$ COMPLEXES (L = 8-QUINOLINOLATE, ACETYLACETONATE, PICOLINATE, 2,2'-BIPYRIDINE, AND 1,10-PHENANTHROLINE)

Results

Manganese

The oxidation and reduction potentials for the ligands used in these studies are summarized in Table II. The ligand anions (formed by the addition of one equivalent of hydroxide ((Bu$_4$N)OH) to a solution of the ligand) exhibited one-electron irreversible oxidations, whose potentials are summarized in Table III. The isolated tetramethylammonium picolinate salt had identical electrochemistry to the picolinate ion formed in solution [PAH + $^-$OH].

The potentials for the irreversible one-electron oxidations of the ligand anions (or neutral ligands) in the presence of Zn(II), a transition-metal ion with a filled d^{10} subshell, are summarized in Table IV. The oxidations are shifted slightly positive (~0.03 V) of the oxidations for the free ligand anions. Identical electrochemical results are obtained with the ligand anions whether the ZnL$_3$$^-$ complexes are formed by the addition of three equivalents of ligand anion to [Zn(MeCN)$_4$](ClO$_4$)$_2$ or by the addition of one L$^-$ to the ZnL$_2$ complex. In the latter case, an excess of L$^-$ (1.5-2 equivalents) is required to obtain a sharp oxidation peak. The ZnL$_2$ complexes (from isolated complexes or formed in situ by mixing 2L$^-$ and [Zn(MeCN)$_4$](ClO$_4$)$_2$) are insoluble, but are solubilized upon addition

Table II. Redox Potentials for Ligands in Acetonitrile.[a]

	$E_{1/2}$[b], V vs. SCE[c]	
Ligand[d]	Oxidations	Reductions
a. 8HQ	+1.17, +1.80	—[e]
acacH	+1.85(2e⁻)	—[e]
HOAc	—[e]	—[e]
PAH	—[e]	—[e]
b. bpy	+2.08	-2.19(2e⁻)
phen	+1.83	-2.10(2e⁻), -2.27
OPPh$_3$	—[e]	—[e]

[a] 3 mM solutions in acetonitrile (0.1 M tetraethylammonium perchlorate).

[b] $E_{1/2}$ taken as $E_{p,a}/2$ + 0.03 V for oxidations, $E_{p,c}/2$ - 0.03 V for reductions (Ref. 69).

[c] Saturated calomel electrode (SCE) vs. NHE, +0.242 V.

[d] Key: 8HQ, 8-hydroxyquinolinol; acacH, acetylacetone; HOAc, acetic acid; PAH, picolinic acid; bpy, 2,2'-bipyridine; phen, 1,10-phenanthroline; OPPh$_3$, triphenylphosphine oxide.

[e] No redox features observed within MeCN solvent window, +2.3 to -2.5 V.

Table III. Oxidation Potentials for Ligand Anions (L⁻/L·).[a]

Ligand Anion (L⁻)	$E_{1/2}$[b], V vs. SCE[c]		
	MeCN	DMF	DMSO
8Q⁻	-0.03	-0.03	-0.01
acac⁻	+0.31	+0.35	+0.41
⁻OAc	+1.14	+1.17	+1.16
PA⁻	+1.26	+1.18	+1.19
⁻OH	+0.35	+0.75(+0.35)[d]	+0.72(+0.34)[d]

[a] 3 mM solutions (0.1 M tetraethylammonium perchlorate).
[b] $E_{1/2}$ taken as $E_{p,a}/2$ + 0.03 V (Ref. 69).
[c] Saturated calomel electrode (SCE) vs. NHE, +0.242 V.
[d] A new oxidation peak appears for concentrations > 6 mM or at times > 30 min.

Table IV. Oxidation Potentials for Zinc Complexes.[a]

Zinc Complex	$E_{1/2}$[b], V vs. SCE[c]		
	MeCN	DMF	DMSO
a. $Zn(8Q)_3^-$	-0.02	0.00	+0.02
$Zn(acac)_3^-$	+0.34	+0.40	+0.42
$Zn(OAc)_3^-$	+1.17	+1.16	+1.18
$Zn(PA)_3^-$	+1.30	+1.19	+1.21
b. $[Zn(MeCN)_4](ClO_4)_2$	>2.3		
$[Zn(bpy)_3](ClO_4)_2$	>2.3		
$[Zn(phen)_3](ClO_4)_2$	>2.3		
$[Zn(OPPh_3)_4](ClO_4)_2$	>2.3		

[a] 3 mM solutions (0.1 M tetraethylammonium perchlorate).
[b] $E_{1/2}$ taken as $E_{p,a}/2 + 0.03$ V (Ref. 69).
[c] Saturated calomel electrode (SCE) vs. NHE, +0.242 V.

of the third equivalent of L⁻. Addition of one equivalent of hydroxide to ZnL_2 results in dissolution, but a second equivalent causes the formation of a white precipitate and electrochemistry that is characteristic of the 2L⁻ species. The $[Zn(MeCN)_4](ClO_4)_2$ used to form the zinc complexes is electrochemically inactive except for electrode plating and stripping processes at $E_{p,c}$, -1.10 V and $E_{p,a}$, -0.57 V vs. SCE, respectively, in MeCN.

Figure 1 illustrates the cyclic voltammograms for picolinate anion (PA⁻), $Zn(PA)_3^-$, and $Mn(PA)_3 \cdot H_2O$. The latter is reversibly reduced to $Mn(PA)_3^-$ and reoxidized by two reversible one-electron steps (nominally attributable to the Mn(II)/Mn(III) and Mn(III)/Mn(IV) redox couples). The cyclic voltammograms for the 8-quinolinolate, acetylacetonate, and acetate anions and their zinc and manganese complexes have similar features. The cyclic voltammogram for $Mn(acac)_3$ includes a small couple at +0.23 V (probably due to $Mn(acac)_2^+$). Although the ligand anions and zinc complexes exhibit irreversible oxidation peaks, the manganese complexes undergo two reversible oxidations; their $E_{1/2}$ values are summarized in Table V(a). The results for the acetate complex of manganese are anomalous. Instead of two reversible couples, the positive voltage scan yields broad, complex irreversible oxidation peaks (apparently due to the propensity of $Mn(OAc)_3 \cdot H_2O$ to polymerize).[114]

The electrochemistry for these species does not vary appreciably with solvent, with the exception of some oxidative features that are observed in MeCN, which are beyond the solvent edges of DMF and DMSO. Identical electrochemical features are observed for the MnL_3 compounds, for the addition of three equivalents of ligand anion to

Figure 1. Cyclic voltammograms: (a) 3 mM picolinate (PA⁻)

[PAH + (Bu$_4$N)OH, 1:1]; (b) 3 mM Zn(PA)$_2$·2H$_2$O plus two equivalents of

PA⁻; (c) 3 mM Mn(PA)$_3$·H$_2$O in MeCN (0.1 M tetraethylammonium

perchlorate). Conditions: scan rate, 0.1 V s⁻¹; ambient temperature; glassy-

carbon working electrode (0.09 cm²); saturated calomel electrode (SCE) vs.

NHE, +0.242 V.

(a) PA⁻

50μA

(b) Zn(PA)₂(OH₂)+2 equiv PA⁻

50μA

(c) Mn(PA)₃(OH₂)

20μA

+2.0   +1.0   0   -1.0
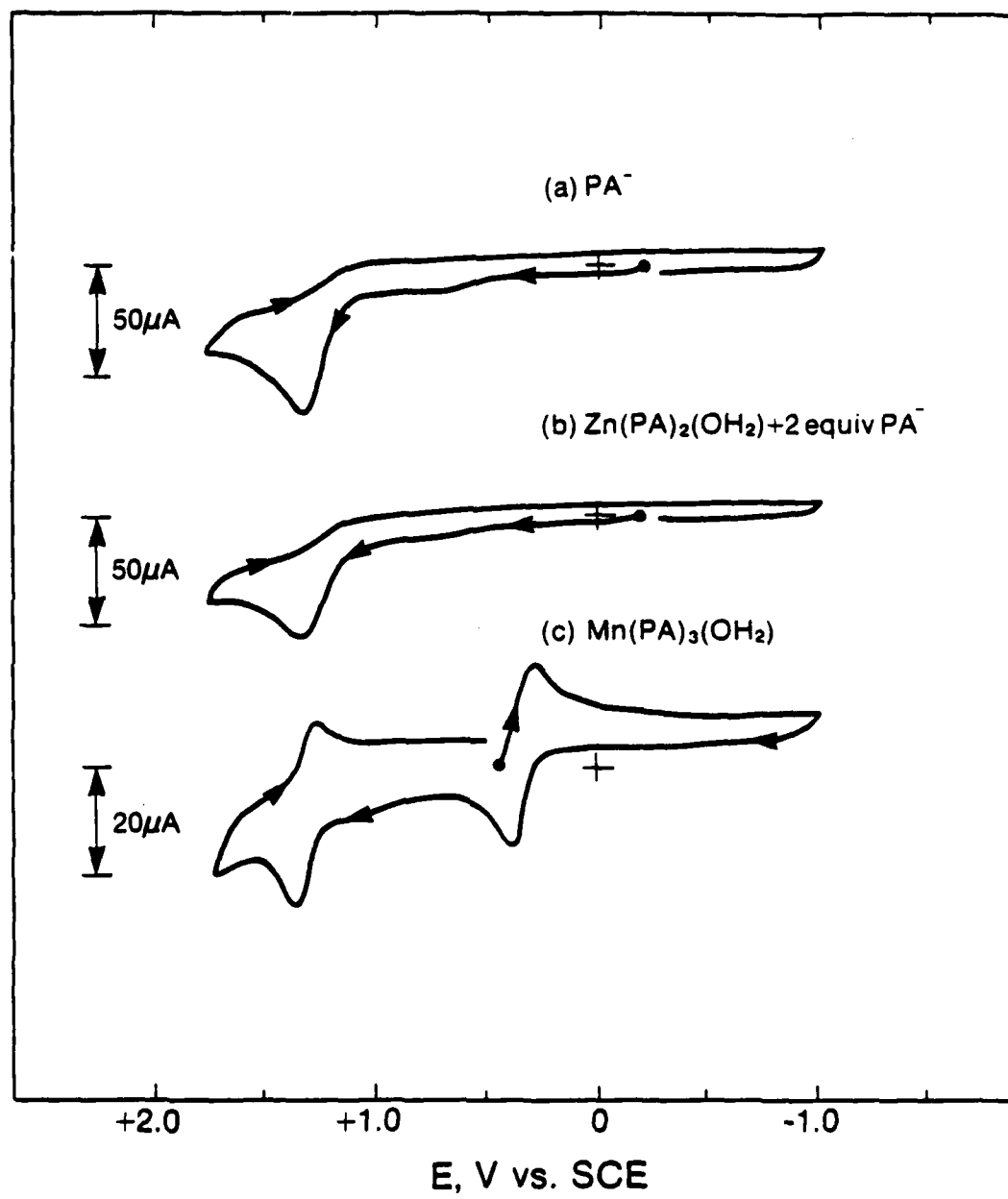
E, V vs. SCE

Table V. Oxidation Potentials for Manganese Complexes.[a]

	$E_{1/2}$, V vs. SCE[b]		
Mn Complex	MeCN	DMF	DMSO
a. $Mn(8Q)_3$	-0.30/+0.73	-0.25/___[c]	-0.21/___[c]
$Mn(acac)_3$	-0.06/+0.96	-0.06/+1.04	+0.01/+1.00
$Mn(OAc)_3$[d]	+0.20/+1.17	———	———
$Mn(PA)_3$	+0.36/+1.35	+0.36/+1.38	+0.21/___[c]
b. $[Mn(MeCN)_4](ClO_4)_2$	>2.3		
$[Mn(bpy)_3](ClO_4)_2$	+1.31		
$[Mn(phen)_3](ClO_4)_2$	+1.32		
$[Mn(OPPh_3)_4](ClO_4)_2$	>2.3		
c. Mn^{2+}/Mn^{3+} (H_2O, pH 0)[e]	+1.27		

[a] 3 mM solutions (0.1 M tetraethylammonium perchlorate).
[b] Saturated calomel electrode (SCE) vs. NHE, +0.242 V.
[c] Second couple past solvent edge.
[d] Poorly resolved cyclic voltammograms. $E_{1/2}$ taken as $E_{p,a}/2$ + 0.03 V (Ref. 69).
[e] Standard reduction potential (Ref. 115).

[Mn(MeCN)$_4$](ClO$_4$)$_2$, and for the addition of one equivalent of ligand anion to MnL$_2$. Attempts to use [Mn(DMU)$_6$](ClO$_4$)$_2$ as the source of manganese ion failed with the exception of the picolinate species. The ligand anions appear to attack DMU instead of replacing it in the coordination complex. Because DMU can undergo partial enolization, the anions (which are all relatively strong bases in MeCN) deprotonate the enolized form. Picolinate, as the weakest base, forms the manganese complex. The E$_{1/2}$ values for the oxidations of several other manganese complexes are summarized in Table V(b) and Table VI contains additional redox data for various manganese complexes in aqueous and acetonitrile solutions.

The X-ray absorption spectrum for Mn(PA)$_3$·H$_2$O (Figure 2) indicates that the edge energies have been taken at the inflection point of the absorption band. Table VII summarizes the near-edge energies for a series of solid state (a) MnL$_2$ complexes, (b) and (c) their oxidized analogues (traditionally viewed as Mn(III) complexes), (d) binuclear manganese complexes, and (e) and (f) oxidized manganese-oxygen compounds (MnO$_2$ and KMnO$_4$). Both [Mn$_2$(bpy)$_4$(μ-O)$_2$](ClO$_4$)$_3$·4H$_2$O and MnO$_2$ exhibit shoulders along the major absorption edge; the edge values are for the first inflection point.

Table VI. Redox Chemistry of Manganese Complexes.[a]

I. Metal-Centered, Mn(II)/Mn(III)

aqueous media	$E^{o'}$, V vs. SCE	complex in acetonitrile	$E^{o',b}$ V vs. SCE
3 M HClO$_4$	+1.32	[Mn(MeCN)$_4$]$^{2+}$	>+2.3
7.5 M H$_2$SO$_4$	+1.25	[Mn(DMU)$_6$]$^{2+}$	+1.90

II. Ligand-Centered, MnL$_n$/Mn($\cdot$L)L$_{n-1}$

aqueous media	$E^{o'}$, V vs. SCE	complex in acetonitrile	$E^{o',b}$ V vs. SCE
0.4 M H$_2$P$_2$O$_7^{2-}$ (pH 7.1)	+0.77	(i) (HTDT$^-$/HTDT$\cdot$)	-0.05
		[Zn(TDT)$_2$]$^{2-}$	+0.18
0.1 M N(CH$_2$CH$_2$OH)$_3$ (pH 12)	-0.72	[Mn(TDT)$_2$]$^{2-}$	-0.63
0.1 M gluconate (pH 13.5)	-0.27	(ii) (DTBCH$^-$/DTBCH$\cdot$)	-0.12
		[Mn(DTBC)$_2$]$^{2-}$	-0.51
0.1 M catechol (pH 13.5)	-0.52		
		[Mn(bpyO$_2$)$_3$]$^{2+}$	+0.87
MnO$_4^{2-}$/MnO$_4^-$ (pH 14)	+0.32		
		[Mn(terpyO$_3$)$_3$]$^{2+}$	+1.06

[a] Ref. 116.
[b] Based on anodic voltammograms.
[c] Key: DMU, dimethylurea; TDT, 3,4-toluenedithiolate; DTBC, 3,5-di-*tert*-butylcatecholate; bpyO$_2$, 2,2'-bipyridine 1,1'-dioxide; terpyO$_3$, 2,2',2"-terpyridine 1,1',1"-trioxide.
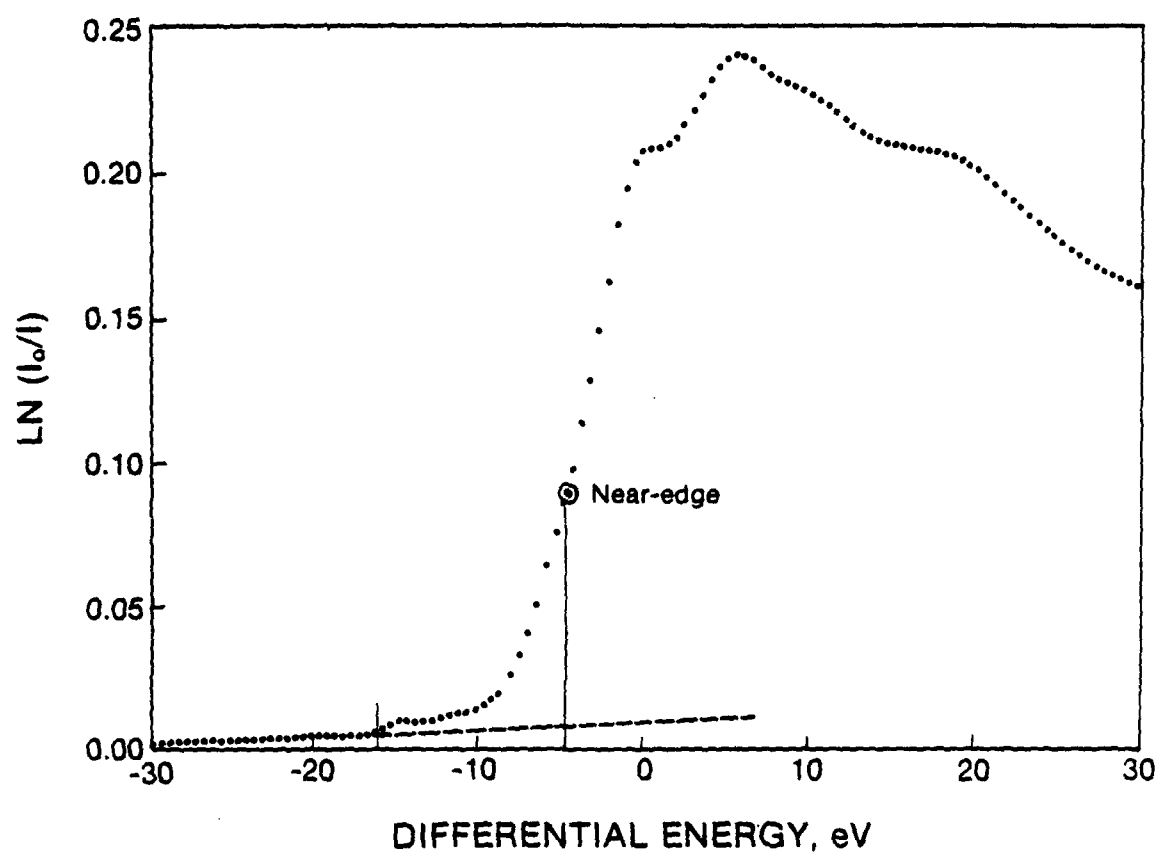
Figure 2. X-ray absorption spectrum for solid $Mn(PA)_3 \cdot H_2O$. The reference energy, E_0, is the K-edge for manganese metal at 6537.4 eV (~ -16 eV on the differential energy scale).

Table VII. X-ray Absorption Edges for Solid Manganese Complexes and Compounds.

Complex	major edge,[a] eV	assignment; edge, eV
a. $Mn(OAc)_2(OH_2)$	6546.5	
$Mn(PA)_2(OH_2)_2$	6546.5	
$Mn(acac)_2$	6546.0	
$[Mn(terpyO_3)_2](ClO_4)_2 \cdot 2H_2O$	6546.0	
$[Mn(bpy)_3](ClO_4)_2$	6546.0	
$[Mn(OPPh_3)_4](ClO_4)_2$	6545.5	
$MnCl_2$	6545.5	
		$Mn (d^5sp + 2 \cdot L)$ 6546.0 ± 0.3
b. $[Mn(bpyO_2)_3]_2(S_2O_8)_3 \cdot 8H_2O$	6550.0	$Mn (d^4sp^2 + 3 \cdot L)$ 6550.0 ± 0.5
c. MnF_3	6549.0	
$Na_3[Mn(P_2O_7)_3]$	6549.0	
$Mn(OAc)_3 \cdot 2H_2O$	6549.0	
$[Mn(urea)_6](ClO_4)_3$	6548.5	
$[Mn(DMSO)_6](ClO_4)_3$	6548.5	
$Mn(PA)_3 \cdot H_2O$	6548.5	
$Mn(acac)_3$	6548.5	

Table VII. (Continued).

Complex'	major edge,[a] eV	assignment; edge, eV
Mn(salpn)Cl	6548.5	
Mn(salen)Cl·H$_2$O	6548.0	
Mn(8Q)$_3$	6548.0	
MnTPP(OAc)	6548.0	
Mn(DPA)(DPAH)(EtOH)	6548.0	
(Bu$_4$N)[Mn(DPA)$_2$]	6548.0	
		Mn (d^{5}sp + 2·L, + ·L) 6548.3 ± 0.5
d. [Mn$_2$(bpy)$_4$(μ-O)$_2$](ClO$_4$)$_3$·4H$_2$O	6548.5	Mn (d^{5}sp + 2·L, + 1.5·L) 6548.5 ± 0.5
[Mn$_2$(phen)$_4$(μ-O)$_2$](ClO$_4$)$_4$·4H$_2$O	6549.0	Mn (d^{5}sp + 2·L, + 2·L) 6549.0 ± 0.5
e. MnO$_2$	6551.0	Mn (d^{5}sp + 2·L, + 2·L) 6551.0 ± 0.5
f. KMnO$_4$	6557.5	Mn (d^{5}sp + 2·L, + 4·L + ·L$^-$) 6557.5 ± 0.5

[a] Position of first major inflection point after Mn K-edge at 6537.4 eV; reproducibility, ± 0.5 eV.

Iron

The electrochemical results for the control experiments with the ligand anions and zinc complexes have been presented in the previous section. The cyclic voltammograms for the FeL_3 complexes, each of which exhibits a reversible one-electron couple, are shown in Figure 3. The $E_{1/2}$ values for these iron complexes are summarized in Table VIII(a). Because $Fe(8Q)_3$ is slightly soluble in MeCN (<1 mM), there is only a faint reversible couple in this solvent. The electrochemical behavior of $Fe(acac)_3$ is in accord with that previously observed.[117,118] $Fe(PA)_3$ was formed in situ. Identical electrochemical features are obtained for $[Fe(ClO_4)_3 + 3PA^-]$ and for $[Fe(MeCN)_4(ClO_4)_2 + 3PA^-]$. The solution magnetic moments for $Fe(8Q)_3$ and $Fe(acac)_3$ indicate the iron complexes are 5/2 spin systems. Ferric acetate exists only in polymeric forms,[119,120] and was not studied.

Addition of hydroxide ion $((Bu_4N)OH)$ to a solution of $Fe(acac)_3$ results in an initial green color that persists for several seconds at room temperature. Addition of 1, 2, or 3 equivalents of ^-OH yields a dark-green solution, which rapidly returns to an orange color that is slightly different from that of the original solution. In MeCN and DMF an orange precipitate forms after the addition of the third equivalent of hydroxide (on occasion, this occurs in DMSO). Addition of hydroxide ion to the same concentration of $FeCl_3$ or $Fe(ClO_4)_3$ also results in an orange precipitate. Experiments in DMSO yield a precipitate in ~60% of the cases. The solubility of "$Fe(OH)_3$" in DMSO appears to depend on the water content (typically 3-10 mM, approximately the same concentration as the

Figure 3. Cyclic voltammograms: (a) 1 mM Fe(8Q)$_3$; (b) 1 mM Fe(acac)$_3$; (c) 1 mM Fe(PA)$_3$ [Fe(ClO$_4$)$_3$ + 3PA$^-$] in DMF (0.1 M tetraethylammonium perchlorate). Conditions: scan rate, 0.1 V s^{-1}; ambient temperature; glassy-carbon working electrode (0.09 cm^2); saturated calomel electrode (SCE) vs. NHE, +0.242 V.

(a) Fe(8Q)₃

10μA

(b) Fe(acac)₃

(c) Fe(PA)₃
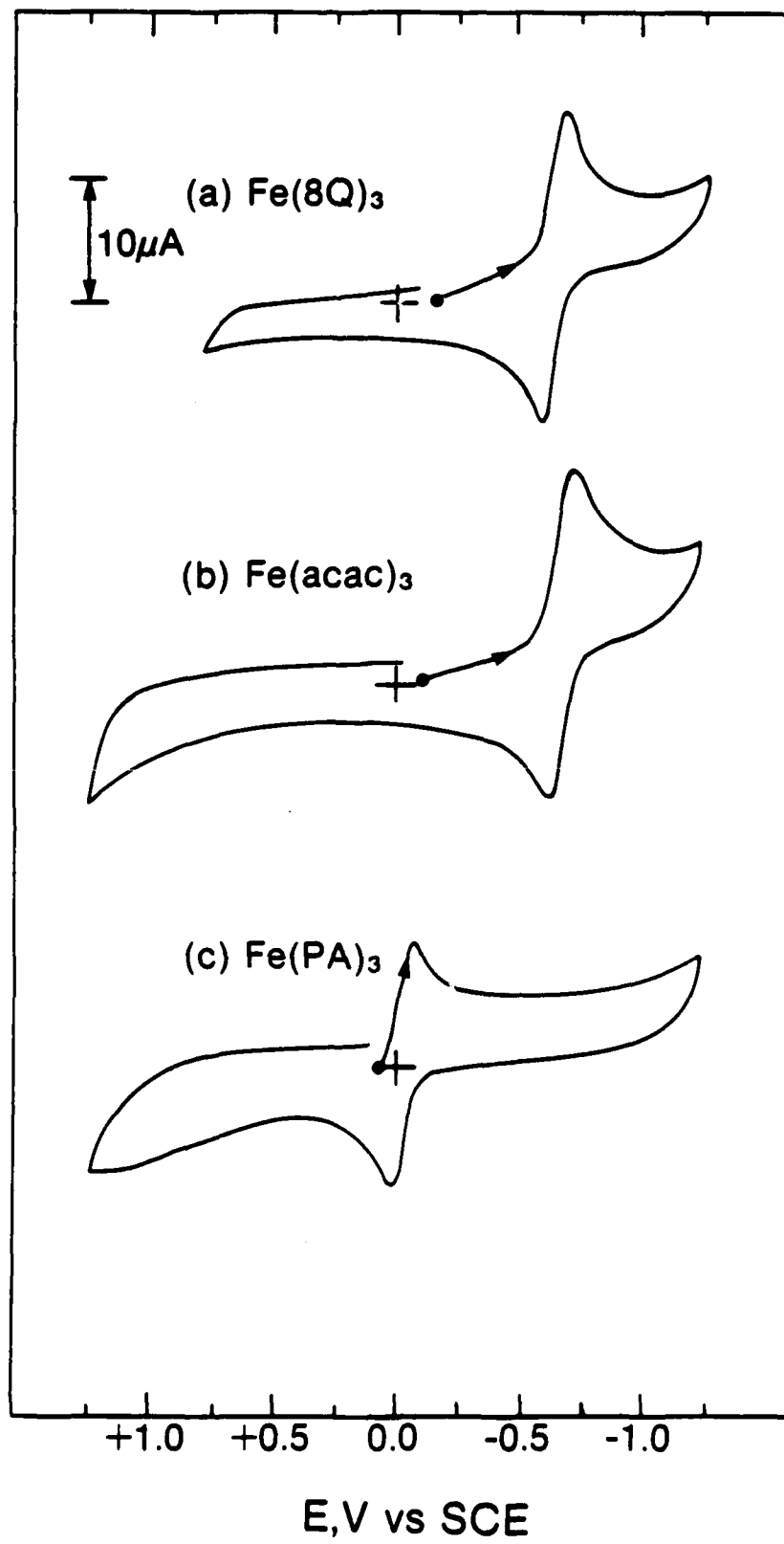
E,V vs SCE

Table VIII. Oxidation Potentials for Iron Complexes.[a]

	$E_{1/2}$, V vs. SCE[b]		
Iron Complex	MeCN	DMF	DMSO
a. $Fe(8Q)_3$	-0.65[c]	-0.65[d]	-0.58[d]
$Fe(acac)_3$	-0.66	-0.66[e]	-0.63[e]
$Fe(PA)_3$	-0.04	-0.04	-0.03
b. $[Fe(MeCN)_4](ClO_4)_2$	+1.61		
$[Fe(bpy)_3](ClO_4)_2$	+1.06		
$[Fe(phen)_3](ClO_4)_2$	+1.08		
$[Fe(OPPh_3)_4](ClO_4)_2$	+1.03		
c. Fe^{2+}/Fe^{3+} (H_2O, pH 0)[f]	+0.53		

[a] 3 mM solutions (0.1 M tetraethylammonium perchlorate).
[b] Saturated calomel electrode (SCE) vs. NHE, +0.242 V.
[c] Solubility in MeCN <1 mM.
[d] In addition to the reversible couple at -0.65 V, $Fe(8Q)_3$ has three irreversible one-electron oxidations at +1.37 V, +1.52 V, and +1.68 V in DMF; only two of these are observed in DMSO, at +1.29 V and +1.48 V.
[e] $Fe(acac)_3$ exhibits an additional small couple at +0.07 V in DMF and at -0.03 V in DMSO (probably due to $Fe(acac)_2^+$ in analogy to the equilibria for $Fe(8Q)_3$) (Ref. 61).
[f] Standard reduction potential (Ref. 115).

iron species). Iron(II) salts give brown precipitates upon the addition of two equivalents of ^-OH, as does $[Fe(bpy)_3](ClO_4)_2$.

The titration of $Fe(acac)_3$ with 3 equivalents of ^-OH results in a linear decrease in the peak currents for the -0.66 V couple and the appearance of an oxidation peak that corresponds to that of free $acac^-$. The increase in amplitude of this oxidation peak corresponds to the release of one $acac^-$ per ^-OH added. Addition of excess ^-OH results in a second oxidation peak that overlaps the $acac^-$ peak to form a shoulder. In these solvents the oxidation peaks of $acac^-$ and of ^-OH (in DMF and DMSO the oxidation is of the product that forms from ^-OH attack on the solvent) occur at the same potentials as the product species of the $^-OH/Fe(acac)_3$ titration. The use of a fast positive voltammetric scan immediately upon addition of hydroxide ion to $Fe(acac)_3$ failed to resolve whether the $acac^-$ is initially released upon formation of the green species, or is released when it decomposes. With a large excess of $acac^-$ (10 equivalents) present in solution, the green color is not observed upon addition of ^-OH, but ligand substitution and disproportionation to $Fe(acac)_3$ and "$Fe(OH)_3$"($\downarrow$) are rapid processes. With only two $acac^-$ ligands in excess a brief green color is observed with the addition of ^-OH.

With MeCN at -30 °C as the solvent matrix, the green intermediate can be stabilized for study by UV/visible spectroscopy and electro-chemistry. The initial $Fe(acac)_3$ solution has two absorption bands (λ_{max}; 356 nm and 430 nm) which shift to 344 nm and a shoulder at 390 nm, respectively, within two seconds after addition of hydroxide ion. At the same time, the solution becomes green and a broad absorption band

appears between 600 nm and 800 nm; this feature grows to a maximum within 30 seconds, and then begins to decay. After several minutes the green color (and this broad absorbance) completely disappears to give a solution with a spectrum, slightly shifted and reduced in absorbance, for $Fe(acac)_3$.

Figure 4 illustrates that the addition of hydroxide ion to $Fe(acac)_3$ causes a reduction in its peak current and the appearance of an oxidation peak at +0.02 V vs. SCE and a broad reduction at -1.5 V. The reduction is coupled with an oxidation at ~ -1.14 V. With time the oxidation at +0.02 V disappears and is replaced by the oxidation peak for free $acac^-$ at +0.34 V, the broad reduction peak decreases, and the initial $Fe(acac)_3$ couple regains some of its amplitude.

Addition of hydroxide ion to a $Fe(8Q)_3$ solution causes a decrease in the amplitude for the -0.65 V couple and the appearance of the oxidation peak for free $8Q^-$. UV/visible spectroscopy indicates that the magnitudes of the $Fe(8Q)_3$ absorbances decrease with a concomitant increase in the absorbances for free $8Q^-$ upon addition of each of three equivalents of hydroxide ion.

Figure 5 illustrates the cyclic voltammograms for a number of other iron complexes. The voltammograms of $[Fe(MeCN)_4](ClO_4)_2$ and $FeCl_3$, in addition to a reversible couple, displayed typical electrode plating and stripping processes. The voltammogram of $Fe(acac)_3$ exhibits oxidation features common to $acac^-$ and its complexes. Table VIII(b) summarizes the $E_{1/2}$ values for the oxidations of a number of other iron complexes.

Figure 4. Cyclic voltammograms: (a) 0.5 mM $Fe(acac)_3$; (b) a + 2 equiv. of ^-OH $((Bu_4N)OH)$, initial scan; (c) b, after 1.5 min; (d) b, after 3 min; (e) b, after 5 min in cold MeCN (0.1 M tetraethylammonium perchlorate, MeCN/dry ice). Conditions: scan rate, 0.1 V s^{-1}; ~ -30 °C; glassy-carbon working electrode (0.09 cm^2); saturated calomel electrode (SCE) vs. NHE, +0.242 V.

(a) Fe(acac)₃ (orange)

10μA

(b) [Fe(acac)₃ + 2⁻OH] (green)

(c) Solution (b) after 1½ min (green)

(d) Solution (b) after 3 min (green)

(e) Solution (b) after 5 min (orange)

E,V vs. SCE

Figure 5. Cyclic voltammograms: (a) 3 mM $[Fe(MeCN)_4](ClO_4)_2$; (b) 3 mM $FeCl_3$; (c) 3 mM $Fe(acac)_3$; (d) 3 mM $Fe(Cp)_2$; (e) 3 mM $Fe(CO)_5$ in MeCN (0.1 M tetraethylammonium perchlorate). Conditions: scan rate, 0.1 V s^{-1}; ambient temperature; glassy-carbon working electrode (0.09 cm^2); saturated calomel electrode (SCE) vs. NHE, +0.242 V.

(a) Fe(MeCN)$_4$(ClO$_4$)$_2$

100μA

(b) FeCl$_3$

(c) Fe(acac)$_3$

(d) FeCp$_2$

(e) Fe(CO)$_5$

+2.0   +1.0   0.0   -1.0   -2.0

E,V vs SCE

Cobalt

The electrochemical results for the control experiments with the ligands, ligand anions, and zinc complexes have been presented in Tables II, III, and IV. Figure 6 illustrates the cyclic voltammograms for the CoL_3 complexes. The electrochemistry of these complexes is characterized by coupled, irreversible oxidation and reduction peaks separated by 0.5-1.0 V. The peaks are broader than those for the reversible couples of the manganese and iron complexes, and the cobalt peak heights are less than expected for one-electron redox processes (Figure 7). The oxidation peak is not observed for an initial positive scan, but appears after reduction to an anionic species. The $E_{1/2}$ values for the cobalt complexes, based on the reductive features,[69] are summarized in Table IX(a). The $Co(8Q)_3$ complex is only slightly soluble (<0.5 mM in MeCN, <1 mM in DMF or DMSO). Cobaltic triacetate exists as a binuclear compound containing μ-hydroxo bridges[121] or as a trinuclear oxo-bridged structure[122] and was not included in this study. The solution magnetic moments for a number of cobalt complexes are listed in Table X. The CoL_2 complexes are 3/2 spin systems and the CoL_3 complexes are diamagnetic.

The same electrochemical features, slightly reduced in magnitude, are observed for the combination of CoL_2 and L⁻. Both the oxidation peak and the reduction peak are seen in initial positive and in initial negative scans. In the case of [$Co(acac)_2$ + acac⁻], a combination of the redox features for $Co(acac)_3$ and the oxidation peak for free acac⁻ is observed. Although crystalline $Co(acac)_2$ is tetrameric and in solution is [$Co(acac)_2]_n$, n=1-4, at concentrations less than 10 mM (the concentrations used in these studies)

Figure 6. Cyclic voltammograms: (a) 1 mM Co(8Q)$_3$ (not completely soluble); (b) 1 mM Co(acac)$_3$; (c) 1 mM Co(PA)$_3$ in DMF (0.1 M tetraethylammonium perchlorate). Conditions: scan rate, 0.1 V s^{-1}; ambient temperature; glassy-carbon working electrode (0.09 cm^2); saturated calomel electrode (SCE) vs. NHE, +0.242 V.

10μA

(a) Co(8Q)₃

(b) Co(acac)₃

(c) Co(PA)₃

+1.0 +0.5 0.0 -0.5 -1.0

E,V vs SCE
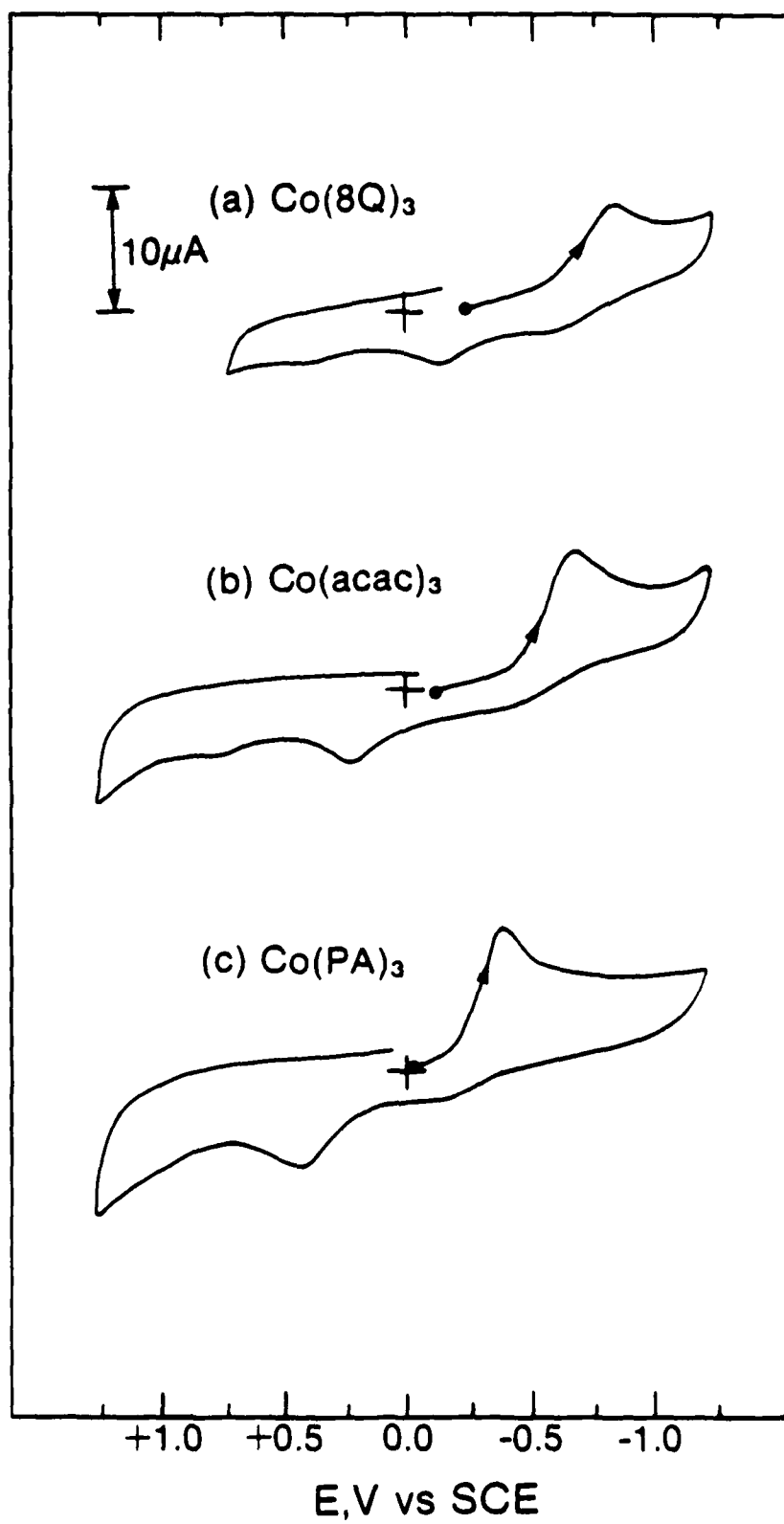
Figure 7. Cyclic voltammograms: (a) 3 mM acetylacetonate (acac⁻)

[acacH + (Bu$_4$N)OH, 1:1]; (b) 3 mM Mn(acac)$_3$; (c) 3 mM Fe(acac)$_3$;

(d) 3 mM Co(acac)$_3$ in DMF (0.1 M tetraethylammonium perchlorate).

Conditions: scan rate, 0.1 V s⁻¹; ambient temperature; glassy-carbon

working electrode (0.09 cm^2); saturated calomel electrode (SCE) vs. NHE,
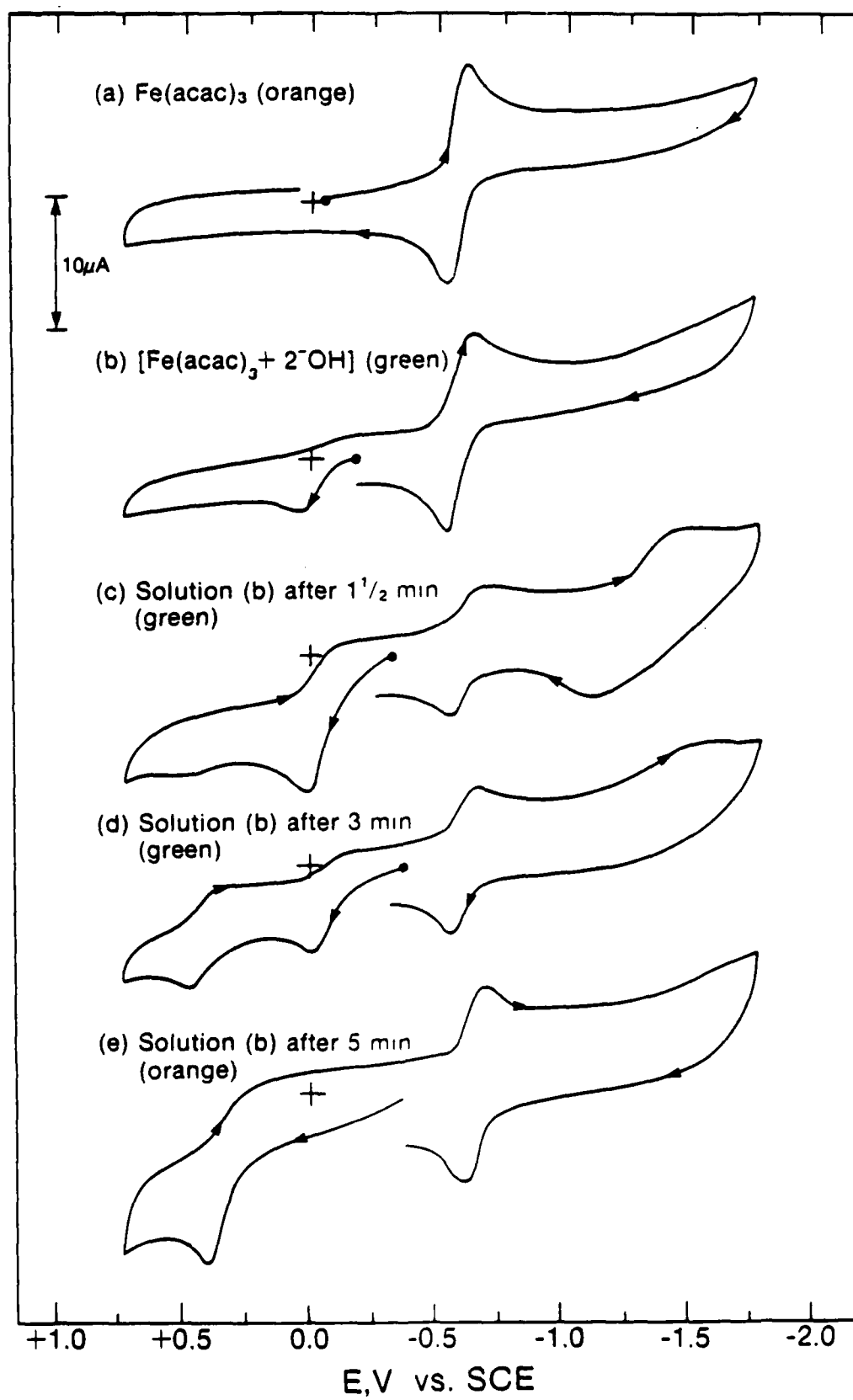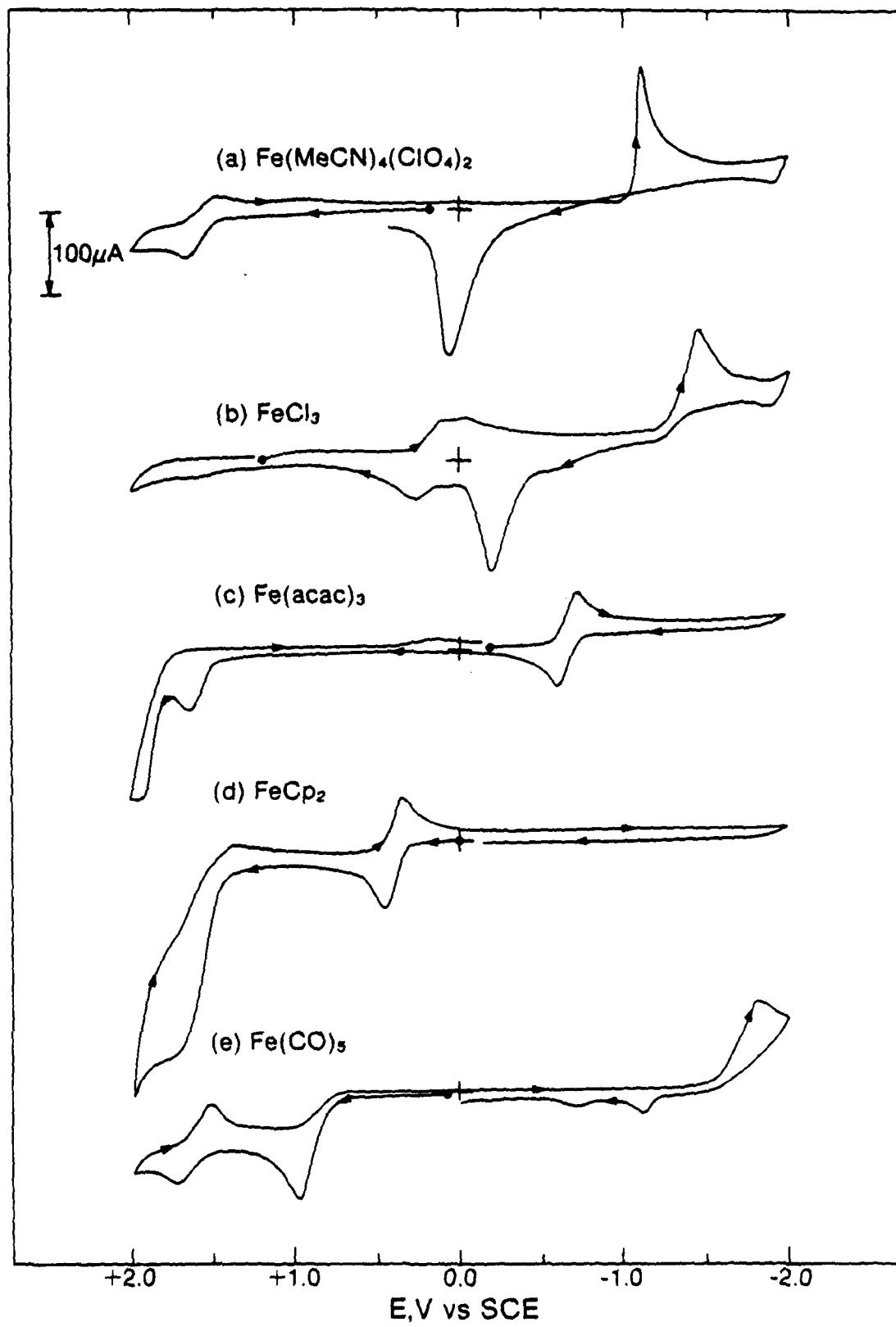
+0.242 V.

(a) Acac-

20μA

(b) Mn(acac)₃

(c) Fe(acac)₃

(d) Co(acac)₃

+1.0   +0.5   0.0   -0.5   -1.0
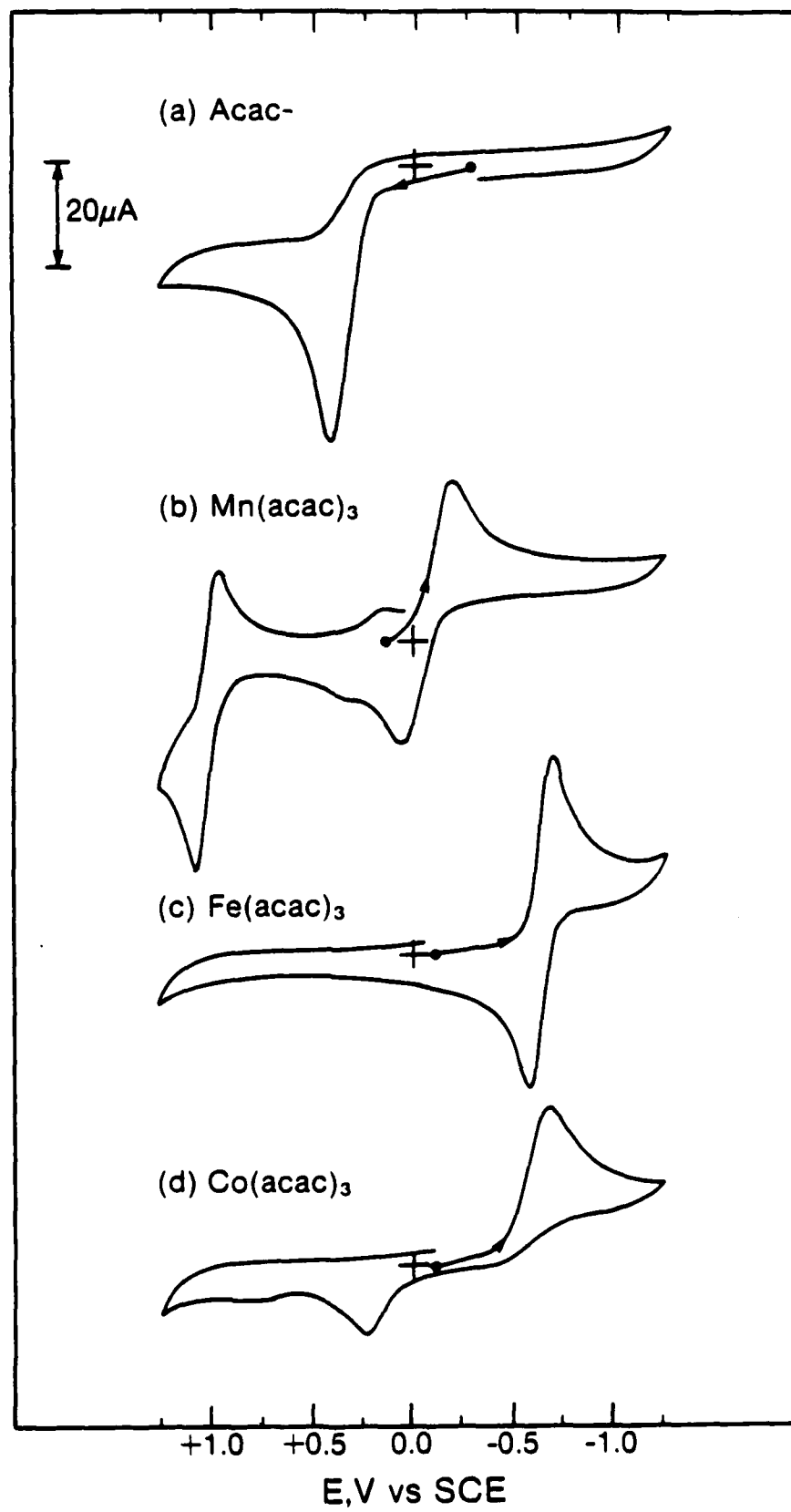
E,V vs SCE

Table IX. Oxidation Potentials for Cobalt Complexes.[a]

Co Complex	$E_{1/2}$[b] V vs. SCE[c]		
	MeCN	DMF	DMSO
a. Co(8Q)$_3$[d]	-0.71	-0.70	-0.69
Co(acac)$_3$	-0.59	-0.60	-0.52
Co(PA)$_3$	-0.20	-0.34	-0.29
b. [Co(MeCN)$_4$](ClO$_4$)$_2$	>2.3		
[Co(bpy)$_3$](ClO$_4$)$_2$	+0.34		
[Co(phen)$_3$](ClO$_4$)$_2$	+0.38		
[Co(OPPh$_3$)$_4$](ClO$_4$)$_2$	>2.3		
c. Co^{2+}/Co^{3+} (H$_2$O, pH 0)[e]	+1.68		

[a] ; mM solutions (0.1 M tetraethylammonium perchlorate).
[b] $E_{1/2}$ taken as $E_{p,c}/2$ - 0.03 V (Ref. 69).
[c] Saturated calomel electrode (SCE) vs. NHE, +0.242 V.
[d] Solubility in MeCN <0.5 mM, in DMF, DMSO <1 mM.
[e] Standard reduction potential (Ref. 115).

Table X. Solution Magnetic Moments for Cobalt Complexes.[a]

	μ_{corr}, B.M.			
Compound	MeCN	DMF	DMSO	Lit.
a. Co(8Q)₂[b]	—	—	—	
Co(acac)₂	4.60	4.13	4.98	4.18-4.37, 4.93 (Ref. 75, 123)
Co(OAc)₂	—[b]	4.77	5.03	5.0-5.1 (Ref. 124)
Co(PA)₂	4.73	3.43[b]	4.71	4.94 (Ref. 104)
[Co(phen)₃](ClO₄)₂	4.95	4.91	5.03	
b. Co(8Q)₃	—[b]	diamag.	diamag.	
Co(acac)₃		0.61		0.38 (Ref. 117, 125)
Co(PA)₃	0.66	0.66		
[Co(phen)₃](ClO₄)₃		0.95		

[a] 1-5 mM solutions in deuterated solvent (samples at 21 °C, 1% TMS internal reference).

[b] Solubility too low for accurate measurements by the Evan's method.

the monomer predominates;[126,127] therefore, the [Co(acac)$_2$ + acac$^-$]

experiments are valid comparisons with Co(acac)$_3$.

The addition of one equivalent of hydroxide ion to CoL$_2$ [CoL$_2$ +

$^-$OH] produces a solution with the same electrochemical features as those

that occur upon the addition of one equivalent of ligand to CoL$_2$

[CoL$_2$ + L$^-$], but with the peaks (primarily the reduction peaks) shifted by a

few hundredths of a volt. The addition of a second equivalent of $^-$OH to

CoL$_2$ causes a brown precipitate to form and the appearance of the

oxidation peak for two free ligand anions (L$^-$) in the cyclic voltammogram.

The oxidation potentials for a number of other cobalt complexes are

summarized in Table IX(b). Figure 8 illustrates the redox chemistry for

2,2'-bipyridine, and its zinc, iron, and cobalt complexes ([Zn(bpy)$_3$](ClO$_4$)$_2$,

[Fe(bpy)$_3$](ClO$_4$)$_2$, and [Co(bpy)$_3$](ClO$_4$)$_2$). The E$_{1/2}$ values for the redox

couples of the tris bipyridyl complexes [M(bpy)$_3$](ClO$_4$)$_2$, M = Mn, Fe, Co,

and Zn, are summarized in Table XI.. The manganese and iron complexes

have three reversible reduction couples while the cobalt complex only has

two, but the second is a two-electron process. [Co(phen)$_3$](ClO$_4$)$_2$ exhibits

electrochemistry that is similar to that of [Co(bpy)$_3$](ClO$_4$)$_2$; identical redox

features are observed for [Co(phen)$_3$](ClO$_4$)$_2$ and [Co(phen)$_3$](ClO$_4$)$_3$·2H$_2$O.

The [Zn(bpy)$_3$](ClO$_4$)$_2$ complex is not oxidized prior to the solvent edge,

but displays the sharp redox features that are characteristic of reductive

metal plating to and anodic stripping from the electrode surface. The

three reversible reduction couples for the Mn(bpy)$_3$(ClO$_4$)$_2$ and

Fe(bpy)$_3$(ClO$_4$)$_2$ complexes have essentially identical potentials (which also

is the case for the first reduction couple of [Zn(bpy)$_3$](ClO$_4$)$_2$).

Figure 8. Cyclic voltammograms: (a) 3 mM bpy; (b) 3 mM
[Fe(bpy)$_3$](ClO$_4$)$_2$; (c) 3 mM [Co(bpy)$_3$](ClO$_4$)$_2$; (d) 3 mM [Zn(bpy)$_3$](ClO$_4$)$_2$ in
MeCN (0.1 M tetraethylammonium perchlorate). Conditions: scan rate,
0.1 V s^{-1}; ambient temperature; glassy-carbon working electrode (0.09 cm^2);
saturated calomel electrode (SCE) vs. NHE, +0.242 V.

50μA

(a) bpy

(b) Fe(bpy)₃(ClO₄)₂

(c) Co(bpy)₃(ClO₄)₂

(d) Zn(bpy)₃(ClO₄)₂
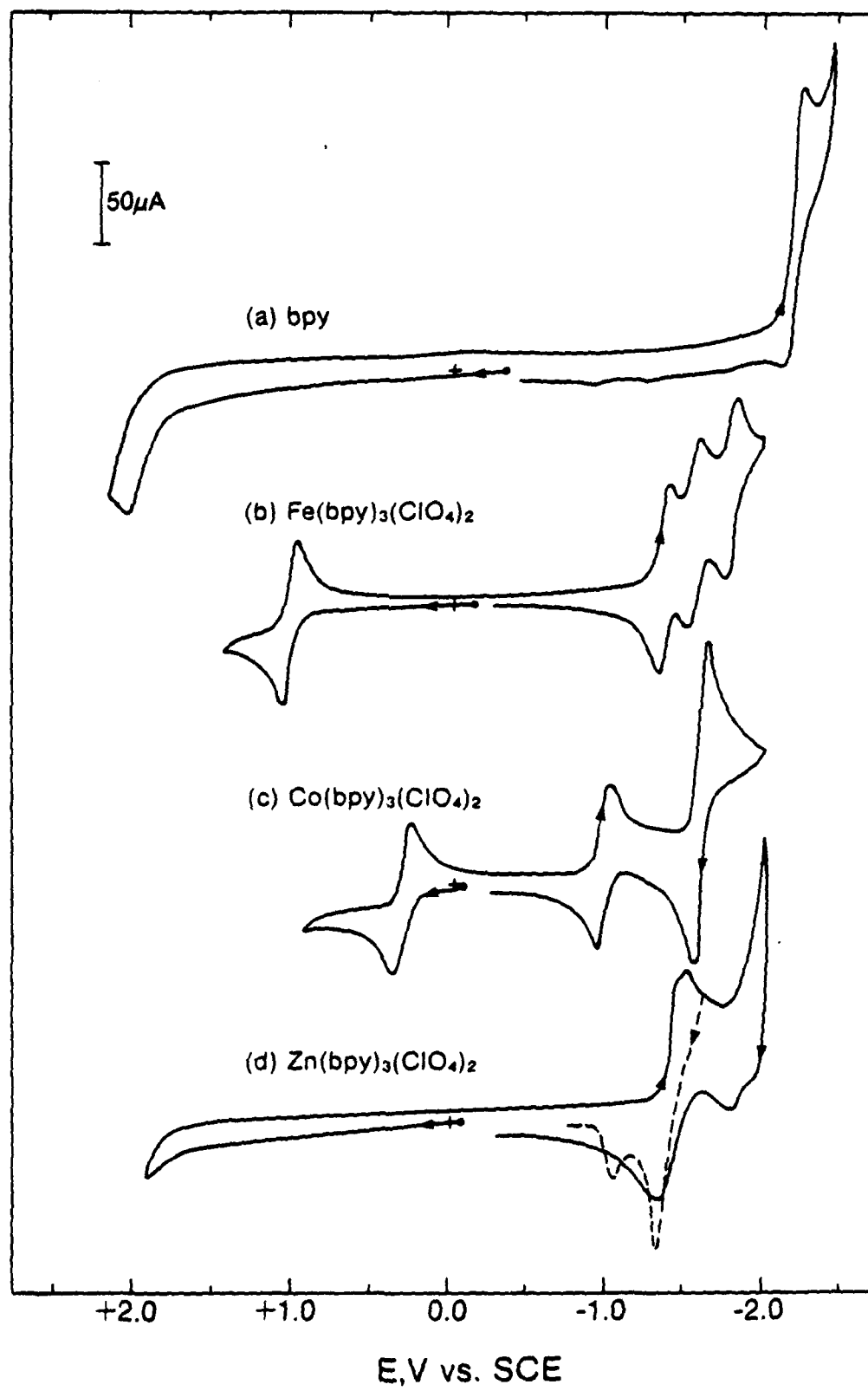
E,V vs. SCE

Table XI. Redox Potentials for the Tris Bipyridyl Complexes of Manganese, Iron, Cobalt, and Zinc.[a]

Complex	$E_{1/2}$, V vs. SCE[b]			
	3+/2+	2+/+	+/0	0/−
bpy[c]	+2.08(+/0)			-2.19(2e⁻)
Zn(bpy)₃(ClO₄)₂	>+2.3	-1.37(2e⁻)	—	-1.85[d]
Mn(bpy)₃(ClO₄)₂	+1.31	-1.36	-1.54	-1.75
Fe(bpy)₃(ClO₄)₂	+1.06	-1.35	-1.54	-1.78
Co(bpy)₃(ClO₄)₂	+0.34	-0.95	-1.57(2e⁻)	

[a] 3 mM solutions in MeCN (0.1 M tetraethylammonium perchlorate).

[b] Saturated calomel electrode (SCE) vs. NHE, +0.242 V.

[c] $E_{1/2}$ taken as $E_{p,a}/2$ + 0.03 V for the oxidation, $E_{p,c}/2$ - 0.03 V for the reduction (Ref. 69).

[d] Overlap of $Zn^{2+/0}$ plating onto electrode surface and reduction of complex.

Discussion

The free ligands (Table II) do not exhibit redox features that could interfere with the redox features of the ligand anions (Table III) or the metal complexes (Tables IV, V, VIII, and IX). The trend in oxidation potentials of the free-ligand anions, which covers a range of 1.3 V, is the opposite of that for the pKa values of the protonated ligands in aprotic solvents.[128] Thus the strongest Brønsted base has the least positive oxidation potential. The oxidation of hydroxide ion involves an EC process[39]

$$2\ ^-OH \rightarrow O^{\bar{\cdot}} + H_2O + e^- \qquad E_{1/2}, +0.35\ V\ vs.\ SCE. \quad (4)$$

More positive potentials are observed at higher concentrations (Table III) due to increased levels of water and to uncompensated iR.[39]

The oxidation potentials for the ZnL_3^- complexes in Table IV are slightly positive (by ~0.03 V) of those for the free-ligand anions (L^-) in Table III, which is due to the Lewis acidity interaction of Zn(II) with the ligand anion. In the cases where electron transfer does not occur, coordination to a cationic metal ion usually increases the oxidation potential of the ligand anion. The positive metal center delocalizes the electron density of the anion to make removal of an electron more difficult (a more positive oxidation potential). Likewise, the reduction potential of a neutral ligand becomes less negative upon coordination to a cationic metal ion (e.g., $Zn(bpy)_3^{2+}$, Table IV).[27]

Although Mn(II) has an acidity similar to that of Zn(II), the oxidation potentials for the MnL_3^- complexes are less positive by 0.28-0.97 V (Table V), and the oxidation processes are reversible (the oxidation potentials of ZnL_3^- and L^- are irreversible). Also, a second reversible couple is observed for the MnL_3^- complexes. Although these couples traditionally are attributed to the Mn(II)/Mn(III) and Mn(III)/Mn(IV) metal-centered oxidation processes, the first (nominally Mn(II)/Mn(III)) occurs at a substantially less positive potential than (a) that for the oxidation of solvated Mn(II) (in MeCN an oxidation peak is not observed before the solvent edge at +2.3 V vs. SCE) or (b) that for the oxidation of the free ligand anion or the ZnL_3^- complex. This negative shift in potential traditionally has been rationalized as due to enhanced stabilization of high oxidation states of the metal. The trend of the oxidation potentials for the MnL_3^- complexes parallels that for the ZnL_3^- complexes and the free ligand anions. If stabilization of Mn(III) were the process, then $Mn(PA)_3^-$ should have the least positive oxidation; instead, it has the most positive potential.

The shifts in the oxidation potentials for the MnL_3^- complexes in Table XII are consistent with a ligand-centered oxidation. The ligand radical product ($L^- \rightarrow L\cdot$) is stabilized by covalent bond formation with the d-electron manifold of the manganese center. Manganese, MnL_3^-, is a high-spin d^5 center with the orbitals half-filled in a spherical array and available for bond formation via the unpaired p-electron of an oxidized ligand radical. The stabilization that results from covalent bond formation causes the oxidation potential of the ligand anion in the complex to

Table XII. Oxidation Potentials and Shifts for ML_3^- Complexes in Acetonitrile.[a]

Complex	$E_{1/2}$,[b] V vs. SCE[c]	ΔE,[e] V
a. $Zn(8Q)_3^-$	-0.02	
$Zn(acac)_3^-$	+0.34	
$Zn(OAc)_3^-$	+1.17	
$Zn(PA)_3^-$	+1.30	
b. $Mn(8Q)_3$	-0.30	0.28
$Mn(acac)_3$	-0.06	0.40
$Mn(OAc)_3$	+0.20	0.97
$Mn(PA)_3$	+0.36	0.94
c. $Fe(8Q)_3$	-0.65[d]	0.63
$Fe(acac)_3$	-0.66	1.00
$Fe(PA)_3$	-0.04	1.34
d. $Co(8Q)_3$	-0.71[d]	0.69
$Co(acac)_3$	-0.59	0.93
$Co(PA)_3$	-0.20	1.50

[a] 3 mM solutions in acetonitrile (0.1 M tetraethylammonium perchlorate).

[b] $E_{1/2}$ taken as $(E_{p,a} + E_{p,c})/2$ for reversible couples of Mn and Fe complexes; as $E_{p,a}/2 + 0.03$ V for ZnL_3^-; and as $E_{p,c}/2 - 0.03$ V for Co complexes, which exhibit separated redox couples (Ref. 69).

[c] Saturated calomel electrode (SCE) vs. NHE, +0.242 V.

[d] Solubility in MeCN; $Fe(8Q)_3$ <1 mM, $Co(8Q)_3$ <0.5 mM.

[e] $\Delta E = E_{1/2(ZnL_3^-/ZnL_3)} - E_{1/2(ML_3^-/M(\cdot L)L_2)}$.

be less than that of the free anion. Therefore, the redox couple for the Mn(PA)$_3^-$ complex is best represented as a ligand-centered redox process [Mn(PA)$_3$]$^-$/[Mn($\cdot$PA)(PA)$_2$] (a Hückel LCAO-MO calculation[129] concludes Mn(acac)$_3$ has covalent metal-(ligand-radical) bonds, Mn($\cdot$acac)(acac$^-$)$_2$).

The apparent free energy of covalent-bond formation, $-\Delta G_{B.F.}$, can be estimated from the shift in potential between the ZnL$_3^-$/ZnL$_3$ and the ML$_3^-$/ML$_3$ oxidation processes,

$$(-\Delta G)_{B.F.} = [E_{1/2(ZnL_3^-/ZnL_3)} - E_{1/2(ML_3^-/M(\cdot L)L_2)}] \times 23.1 \text{ kcal V}^{-1}. \qquad (5)$$

The apparent bond-formation energies for the ML$_3$ complexes, based on the data in Table XII, are summarized in Table XIII.

A comparison of the oxidation potentials for the ZnL$_3^-$ anions with the potentials of the first oxidation couple for MnL$_3^-$ indicates a Mn-L covalent-bond energy of 6-22 kcal/mol ([0.28 V-0.97 V] $\times$ 23.1 kcal V^{-1}). These values are in accord with the covalent-bond energy (8 kcal) that has been observed for the hydroxide complex Mn(OPPh$_3$)$_4$(OH)$^+$.[39]

The shifts in potential between the first redox couple and the oxidation peak of the free ligand anion parallel the ease of oxidation for the free ligand anions. The ligands with oxidizable carboxylate groups ($^-$OAc and PA$^-$) have the largest voltage shifts, which indicates that the Mn-OC(O)R covalent bond is much stronger than the Mn-OR bond. The second oxidation couple [Mn($\cdot$L)(L$^-$)$_2$]/[Mn($\cdot$L)$_2$(L$^-$)]$^+$, is approximately 1.0 V positive of that for the first couple, which is due to the electrostatic effect of oxidizing a neutral complex rather than an anion. Additional redox

Table XIII. Apparent Metal-Ligand Covalent Bond-Formation Free Energies ($-\Delta G_{B.F.}$) for Several Manganese, Iron, and Cobalt Complexes.[a]

Complex	$-\Delta G_{B.F.}$,[a] kcal/mole
a. $Mn(8Q)_3$	6
$Mn(acac)_3$	9
$Mn(OAc)_3$	22
$Mn(PA)_3$	22
b. $Fe(8Q)_3$	15
$Fe(acac)_3$	23
$Fe(PA)_3$	31
c. $Co(8Q)_3$	16
$Co(acac)_3$	21
$Co(PA)_3$	35

[a] $-\Delta G_{B.F.} = [E_{1/2(ZnL_3^-/ZnL_3)} - E_{1/2(ML_3^-/M(\cdot L)L_2)}] \times 23.1$ kcal V^{-1}.

data are presented in Table VI for various manganese complexes in aqueous and acetonitrile solutions, and are grouped as metal-centered and ligand-centered processes.

The X-ray absorption edge data of Table VII can be categorized so as to be consistent with the interpretation of the electrochemical results. The edge energies for the MnL_2 complexes (with a covalency of two, d^5sp) are in the range 6545.5-6546.5 eV, while that for $[Mn(bpyO_2)_3]_2(S_2O_8)_3 \cdot 8H_2O$ is 6550.0 eV. The metal center of this complex traditionally is formulated as $Mn^{III}(L)_3^{3+}$, but, given the Mn(II)/Mn(III) redox potential of >+2.3 V vs. SCE (Table V(b)) and the fact that pyridine-N-oxides (L) can be oxidized to $\cdot L^+$ at lesser potentials, a more reasonable formulation is $Mn(\cdot L^+)_3^{3+}$ with three manganese(d^4sp^2)-(ligand cation-radical) covalent bonds. Thus, the shift in edge energy with valence (not oxidation state) is about +4.3 eV per change in sp covalency ($d^5sp \rightarrow d^4sp^2$; the shift for Co d^7sp to Co d^6sp^2 is +4 eV[43]), which is consistent with an edge energy of 6537.4 eV for zero-valent manganese metal. For organic ligand complexes (traditionally formulated as $Mn^{III}(L^-)_3$), the average edge energy is 6548.5 eV (Table VII), which corresponds to an edge shift of +2.3 eV from the formation of a d-p covalent bond [MnL_2 ($d^5sp + 2\cdot L$) $\rightarrow$ $Mn(\cdot L)(L^-)_2$ ($d^5sp + 2\cdot L, + \cdot L$)] (indicated by the electrochemical results). The more ionic complexes with weak covalent bonds, like MnF_3, have slightly higher edge energies. The edge of 6548.5 eV for the Nyholm complex is consistent with the formulation $[(bpy)_2Mn(\mu\text{-}O\cdot)(\mu\text{-}O^-)Mn(bpy)_2]^{3+}$, with an average of 3.5 covalent bonds per manganese ($d^5sp + 2\cdot L, + \cdot L$ and $d^5sp + 2\cdot L, + 2\cdot L$), where the observed edge is for $Mn(d^5sp + 2\cdot L, + \cdot L)$. The Goodwin

complex, $[Mn_2(phen)_4(\mu\text{-}O)_2](ClO_4)_4 \cdot 4H_2O$, with 4.0 covalent bonds per manganese ($d^5sp + 2 \cdot L, + 2 \cdot L$), has a lower edge energy than expected.

In the case of the (TPP)Mn(OAc) porphyrin complex the edge energy is consistent with a d^5sp Mn center with a covalency of three; two covalent bonds to TPP (as in H_2TPP) and one to a neutral ligand radical ($\cdot OAc$). The data for MnO_2 can be rationalized with a formulation of four covalent bonds (two sp and two d orbitals of d^5sp Mn) to two oxygen atoms (two p orbitals of s^2p^4 O) to give $O=Mn=O$; and for $KMnO_4$ seven covalent bonds (d^5sp; 2 sp and 5 d orbitals) are indicated, $[Mn(\cdot O \cdot)_3(\cdot O^-)]^-$. As such, its estimated edge energy is 6557.5 eV [6537.4 eV + (2 x 4.3 eV) + (5 x 2.3 eV)], which is identical to that observed[130] (Table VII(f)). The estimated edge for MnO_2 is 6550.6 eV [6537.4 eV + (2 x 4.3 eV) + (2 x 2.3 eV)], close to its observed value of 6551.0[130,131] (Table VII(e)).

From these results it appears that the conclusion that the oxidation of Mn complexes is ligand-centered almost certainly applies to all anionic manganese complexes and most neutral complexes with organic ligands (Tables V and VI). Hence, the extensively studied catechol complexes[132] ($Mn^{IV}(DBTC)_3^{2-}$ and $Mn^{III}(DTBC)_2^-$ where DTBC = 3,5-di-tert-butylcatechol dianion) are more accurately formulated as $[Mn(\cdot DTBC \cdot)(\cdot DTBSQ^-)_2]^{2-}$ with a covalency of 4 to Mn (d^5sp) and S=3/2; and $[Mn(\cdot DTBC \cdot)(\cdot DTBSQ^-)]^-$ with a covalency of 3 and S=4/2, respectively. Likewise, the polyol complexes[116] (gluconate and sorbitol dianions) that have been formulated as $Mn^{IV}(L^{2-})_3^{2-}$ and $Mn^{III}(L^{2-})_2^-$ are more appropriately represented by the formulae $[Mn(\cdot L \cdot)(\cdot L^-)_2]^{2-}$ (with a covalency of 4) and $[Mn(\cdot L \cdot)(\cdot L^-)]^-$ (with a covalency of 3), respectively. The

same modifications are in order for the "Mn(IV)" and "Mn(III)" complexes with Schiff bases, EDTA, and phthalocyanines. In each system the manganese has its full complement of valence electrons (d^5sp); a covalency of 2, 3, or 4; and an oxidation state of zero.

The oxidation potentials for the FeL_3^- complexes also are substantially less positive (by 0.63-1.34 V) than those for the zinc complexes (Table XII) or for the oxidation of solvated Fe(II) ion in MeCN. The same trend in oxidation potentials is observed for the FeL_3^- complexes as in the parallel series of MnL_3^- and ZnL_3^- complexes. Thus, the iron complexes appear to undergo ligand-centered oxidations, facilitated by stabilization of the ligand radical product via covalent bond formation with an unpaired d-electron of the transition metal center, in much the same manner as did the manganese complexes. The FeL_3 complexes have stronger (by 8-11 kcal) bond energies than the MnL_3 complexes (Table XIII).

The overall reaction for the addition of hydroxide ion to $Fe(acac)_3$ is shown below

$$Fe(acac)_3 + {}^-OH \rightarrow [green] \rightarrow 2/3Fe(acac)_3 + 1/3"Fe(OH)_3"\downarrow + acac^-. \quad (6)$$
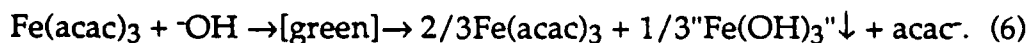
Reference to Figure 4 confirms that the addition of ^-OH to $Fe(acac)_3$ does not immediately displace an $acac^-$ ion upon formation of the green intermediate. With time the intermediate decomposes to a "$Fe(OH)_3$" precipitate and the original tris complex. The green intermediate has not been isolated or structurally characterized, but a reaction sequence that is consistent with the experimental results and the bond energies of

Table XIII is outlined in Scheme V. The electroactive intermediate is most likely the hydroxide adduct $[Fe(acac)_3(OH)]^-$ so that the oxidation of hydroxide ($^-OH \rightarrow \cdot OH$) is shifted to +0.02 V. This electroactive adduct may also be the green species. In contrast, $Fe(8Q)_3$ simply undergoes ligand substitution and disproportionation

$$Fe(8Q)_3 + {}^-OH \rightarrow 2/3Fe(8Q)_3 + 1/3"Fe(OH)_3"\downarrow + 8Q^- \qquad (7)$$
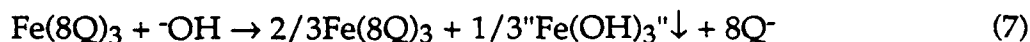
to yield the iron hydroxide precipitate and the original iron quinolinate complex.

While many nominal Co(III) complexes are considered to have substantial covalent character[133,134] they are considered to have strong donor bonds rather than covalent bonds after ligand-metal electron transfer. However, cobalt is more difficult to oxidize to the +3 oxidation state than manganese or iron. The relevant oxidation potentials are +1.68 V vs. SCE for Co(II)/Co(III) as compared to +1.27 V for Mn(II)/Mn(III) and +0.53 V for Fe(II)/Fe(III).[115] Thus cobalt also should exhibit ligand-centered oxidation for the same ligands as manganese and iron.

In contrast to the reversible redox couples of MnL_3 and FeL_3, the cobalt complexes exhibit electrochemistry characterized by widely separated irreversible oxidation and reduction peaks (Figures 6 and 7). The similar electrochemistry observed for $[CoL_2 + L^-]$ and $[CoL_2 + {}^-OH]$ indicate that the irreversible reduction for the CoL_3 complexes is the result of the propensity of CoL_3^- anions to hydrolyze as shown in Scheme VI.

Scheme V.

$$Fe(acac)_3 + {}^-OH \longrightarrow [Fe(acac)_3OH]^- \xrightarrow[(-1.3 \text{ V vs. SCE})]{e^-} Fe(acac)_2 + {}^-OH + acac^-$$

$(d^5sp^2; S=5/2)$ green$(d^5sp^2; S=5/2)$

^-OH

$-e^- (0.00 \text{ vs. SCE})$

$(acac)_2Fe=O + H_2O + acac^-$

$(d^6sp; S=0, 2/2)$

$2/3 \text{ "Fe(OH)}_3\text{"}\downarrow + 1/3 \text{ Fe(acac)}_3 + 2 \text{ acac}^-$

Scheme VI.

CoL$_3$

$$CoL_3 \xrightarrow{+e^-} \text{"}CoL_2 + L^-\text{"}$$

CoL$_2$ + L$^-$

$$CoL_3^- + H_2O \rightleftharpoons [CoL_2(OH)]^- + LH$$

$$\downarrow {\scriptstyle -e^-}$$

$$CoL_2OH$$

$$\Updownarrow {\scriptstyle LH}$$

$$CoL_3 + H_2O$$

CoL$_2$ + $^-$OH

$$CoL_2OH^- + OH^- \longrightarrow Co(OH)_2 \downarrow + 2L^-$$
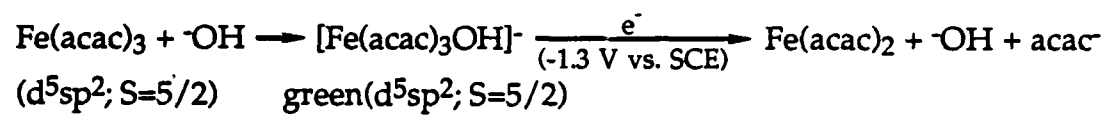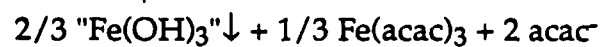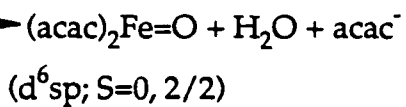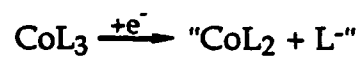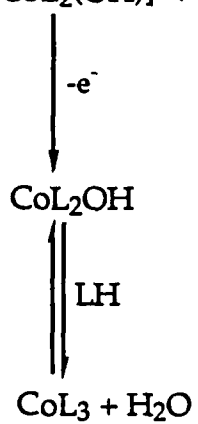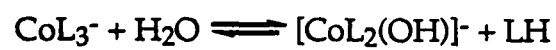
Therefore, the observed reduction is due to CoL_3, but the re-oxidation is due to $[CoL_2(OH)]^-$. The split redox couple has been seen previously for $Co(acac)_3$.[117,125] The electrochemical reduction of $Co(acac)_3$ is known to yield $Co(acac)_2$ and $acac^-$.[127,135-137] Apparently the equilibrium

$$Co(acac)_3^- \rightleftharpoons Co(acac)_2 + acac^- \qquad (8)$$

lies to the right and the process is sufficiently rapid that the re-oxidation of $Co(acac)_3^-$ cannot be observed on the electrochemical time scale (in MeCN some free $acac^-$ is detected, but for the other ligands and the other solvents hydrolysis prevents observation of the free ligand anions).

The $E_{1/2}$ values (taken from the reduction peaks[47]) for the CoL_3 complexes are negative of the potentials for the ZnL_3^-/ZnL_3 redox processes (Table XII). As with manganese and iron, the cobalt complexes appear to have ligand-centered electrochemistry. The bond energies for the CoL_3 complexes (Table XIII) are stronger than in the manganese (by 10-13 kcal/mole) or iron (by 2-4 kcal/mole) complexes. The exception is $Co(acac)_3$, whose bond is 1 kcal weaker than in $Fe(acac)_3$. This exception is in accord with the known predilections of iron to bond strongly with oxygen and of cobalt with nitrogen.[133] Stronger bonds also are observed for iron in its porphyrin complexes with hydroxide, (Por)M-OH, and phenoxide, (Por)M-OPh, as compared to the cobalt and manganese complexes.[39] This can be rationalized in that iron in these systems has a

valence-electron hybridization of d^5sp^2 (covalency, 3; S=5/2), while cobalt is d^6sp^2 (covalency, 3; S=0) and manganese is d^5sp (covalency, 3; S=4/2).

With neutral ligands ($OPPh_3$, bpy, and phen), the redox processes for the $ML_{3,4}^{2+}$ complexes (Table XIV) also are consistent with ligand-centered electron transfer. As with the anionic ligands, oxidation of the free ligands occurs at much more positive potentials than it does for those associated with Mn, Fe, or Co. Because oxidations are not observed for the zinc complexes prior to the solvent edge, only lower limits may be obtained for the apparent free energies of covalent bond formation (Table XV).

Because the three metal-ligand bonds for the ML_3^{3+} complexes shown in Table XIV are equivalent and covalent, the valence electrons for the uncharged metal centers ($Mn(d^5s^2)$, $Fe(d^6s^2)$, and $Co(d^7s^2)$) must be hybridized to accommodate the molecular orbital geometries and energetics, MnL_3^{3+} (d^5sp; S=4/2), FeL_3^{3+} (d^5sp^2; S=5/2), and CoL_3^{3+} (d^6sp^2; S=0). Oxidation of an aromatic pyridine nitrogen yields a radical cation that can couple with an unpaired metal valence electron (d^5sp^2 in the case of iron) to give a quaternerized nitrogen center (analogous to methylviologen (Me–N(O)$_2$)). Reduction of $Mn(bpy)_3^{3+}$ systems adds to the aromatic π-manifold and yields an uncharged nitrogen that remains covalently bound to the metal (again as with methylviologen). The final reduction (Table XI) yields $[M(bpy)_3]^-$ with the electron delocalized in a bound ligand (analogous to the reduction of free bipyridine to bpy$^-$).

Table XIV. Oxidation Potentials and Shifts for $ML_{3,4}^{2+}$ Complexes in Acetonitrile.[a]

Complex	$E_{1/2}$[b] V vs. SCE[c]	ΔE,[d] V
a. $[Zn(bpy)_3](ClO_4)_2$	>2.3	
$[Zn(phen)_3](ClO_4)_2$	>2.3	
$[Zn(OPPh_3)_4](ClO_4)_2$	>2.3	
b. $[Mn(bpy)_3](ClO_4)_2$	+1.31	>0.99
$[Mn(phen)_3](ClO_4)_2$	+1.32	>0.98
$[Mn(OPPh_3)_4](ClO_4)_2$	>2.3	
c. $[Fe(bpy)_3](ClO_4)_2$	+1.06	>1.24
$[Fe(phen)_3](ClO_4)_2$	+1.08	>1.22
$[Fe(OPPh_3)_4](ClO_4)_2$	+1.03	>1.27
d. $[Co(bpy)_3](ClO_4)_2$	+0.34	>1.96
$[Co(phen)_3](ClO_4)_2$	+0.38	>1.92
$[Co(OPPh_3)_4](ClO_4)_2$	>2.3	

[a] 3 mM solutions in acetonitrile (0.1 M tetraethylammonium perchlorate).

[b] $E_{1/2}$ taken as $(E_{p,a} + E_{p,c})/2$ for reversible couples of Mn, Fe, and Co complexes; and as $E_{p,a}/2 + 0.03$ V for ZnL_3^- (Ref. 69).

[c] Saturated calomel electrode (SCE) vs. NHE, +0.242 V.

[d] $\Delta E = E_{1/2(ZnL_{3,4}^{2+}/ZnL_{3,4}^{3+})} - E_{1/2(ML_{3,4}^{2+}/ML_{3,4}^{3+})}$.

Table XV. Apparent Metal-Ligand Covalent Bond-Formation Free Energies ($-\Delta G_{B.F.}$) for Several Manganese, Iron, and Cobalt Complexes with Neutral Ligands.[a]

Complex	$[(M-L^+)(L^+)_2]^{3+}$ $-\Delta G_{B.F.,}$[a] kcal/mole
a. $Mn(bpy)_3{}^{3+}$	>23
$Mn(phen)_3{}^{3+}$	>23
b. $Fe(bpy)_3{}^{3+}$	>29
$Fe(phen)_3{}^{3+}$	>28
$Fe(OPPh_3)_4{}^{3+}$	>29
c. $Co(bpy)_3{}^{3+}$	>45
$Co(phen)_3{}^{3+}$	>44

[a] $-\Delta G_{B.F.} = [E_{1/2(ZnL_{3,4}{}^{2+}/ZnL_{3,4}{}^{3+})} - E_{1/2(ML_{3,4}{}^{2+}/ML_{3,4}{}^{3+})}] \times 23.1$ kcal V^{-1}.

Bond dissociation energies play an important role in chemistry in the design of syntheses, the prediction of stable molecular structures, and the prediction of reaction mechanisms and products. The conclusion from the present results is that the electron-transfer redox reactions of most transition-metal complexes are ligand-centered. This concept is important to an appreciation of the redox character of transition-metal complexes, and to an understanding of the energetics of the metal-ligand bonds. Electrochemical measurements provide a convenient means to assess the covalent bond energies. The latter can be used to predict the reactivity of bound ligands (e.g., atomic oxygen, $\cdot$OH, and $\cdot$Cl) with substrates. In particular, work is in progress to apply these concepts in the design of effective models for methane-monooxygenases, dioxygenases, and the oxygen-evolving complex of photosystem II.

CHAPTER IV

IRON-INDUCED ACTIVATION OF HYDROGEN PEROXIDE FOR THE
DIRECT KETONIZATION OF METHYLENIC CARBON AND THE
DIOXYGENATION OF ACETYLENES AND ARYLOLEFINS

Results

Optimization for Reaction with Electrochemically Reduced Dioxygen

The reaction efficiencies for the $(Py)_4FeCl_2$-catalyzed conversion of
cyclohexane to cyclohexanone (based on $4e^-$/ketone or $4KO_2(s)$/ketone) by
various sources of reduced dioxygen are summarized in Table XVI. The
sole observed product is cyclohexanone. The optimal catalyst
concentration is 60 mM. Similar efficiencies are obtained for $(Py)_4FeCl_2$
concentrations that range from 2.5 mM to 45 mM. The efficiencies hold
constant for samples taken at 5C, 10C, 15C, 25C, 50C, 75C, and 100C. In the
absence of iron catalyst the substrate is not oxidized. Introduction of
2.5 mM $(Py)_4FeCl_2$ to the resulting electrolyzed O_2-solution causes the
formation of cyclohexanone at a reduced efficiency. Variation in the
electrolysis potential gives decreased efficiencies (<-0.3 V, 0%; -0.45 V, 50%;
and -0.8 V, 47%). Use of a platinum-mesh working electrode (-0.6 V vs.
SCE) with 2.5 mM $(Py)_4FeCl_2$ gives an efficiency of 48%. Gas evolution
and the formation of a dark brown product occur in the auxiliary electrode
compartment during the controlled-potential electrolyses, with the
exception of that performed at -0.3 V vs. SCE.

The use of $KO_2(s)$ as the source of reduced dioxygen gives
substantially lower efficiencies (Table XVI(b)) and a much greater

Table XVI. Reaction Efficiencies for the $(Py)_4FeCl_2$ Catalyzed Conversion of Cyclohexane to Cyclohexanone by Electrochemically Reduced Dioxygen in Pyridine/HOAc.

catalyst conc. (mM)	reaction efficiency (±5%)

a. $(O_2 + 2e^-)^a$

catalyst conc. (mM)	reaction efficiency (±5%)
60 (suspension)	83
45	59
30	60
15	58
7.5	64
3.8	56
2.5[b]	59
1.9	49
0.9	45
0.5	<30
0	0

[a] Controlled-potential electrolysis (-0.6 V vs. SCE) performed with glassy-carbon plate working electrodes to 25C. Solvent composition: Py/HOAc/H_2O (10:1:1 by volume), 1 M C_6H_{12}, 0.1 M tetraethyl-ammonium perchlorate, 1 atm. O_2. Cyclohexanone was the sole product detected. Reaction efficiencies based on $4e^-$/ketone.

[b] Catalytic turnovers, based on moles of oxygenated product per mole of complex added, of 1.5 at 25C and of 6.6 at 100C are observed.

Table XVI. (Continued).

	catalyst conc. (mM)	reaction efficiency ($\pm 5\%$)
b. KO$_2$(s)[c,d]		
	56	41
	28	29
	14	25
	7	15
	3.5	8

[c] Slurry of KO$_2$ in pyridine (1.545 mmol/mL) added to reaction solution at 56 mM concentration. Reaction time, 15 minutes. Solvent : Py/HOAc (6:1 by volume), 1M C$_6$H$_{12}$. Cyclohexanone was the sole product detected. Reaction efficiencies based on 4KO$_2$/ketone (Ref. 138).

[d] Use of lower concentrations of KO$_2$(s) results in lower efficiencies while use of soluble (Bu$_4$N)O$_2$ gives no observable products (Ref. 138).

dependence on catalyst concentration. Use of lower concentrations of $KO_2(s)$ (or in use of a lower concentration $KO_2(s)$/pyridine slurry) give lower efficiencies. The yield with ground $KO_2(s)$ is a slightly higher than with unground $KO_2(s)$. The opposite is true for $(Me_4N)O_2$. The completely soluble ground $(Me_4N)O_2$ gives no observable products, while the unground $(Me_4N)O_2$ (56 mM) forms a suspension and has an efficiency of 9%.

The reaction efficiencies for the "$Fe(PA)_2$" (isolated brown powder) catalyst in the conversion of cyclohexane to cyclohexanone are given in Table XVII; the optimal catalyst concentration is in the range from 1 to 3.5 mM. Catalytic turnovers (based on moles of oxygenated product per mole of iron complex added) of 2-5 are observed for concentrations of 3.75 mM or less. The reactions with $KO_2(s)$ give comparable results to the electrochemical experiments, but with lower efficiencies. The yields with "$Fe(PA)_2$" are higher than with $(Py)_4FeCl_2$.

Table XVIII summarizes the results for the ketonization of cyclohexane with 3.5 mM "$Fe(PA)_2$" (brown powder) catalyst in various solvents. The optimal solvent is a Py/HOAc mixture with a mole ratio of 2:1. The electrochemical system is insensitive to water content, but the yields for the $KO_2(s)$ system are substantially decreased by the presence of water. In the MeCN and Py/H_2O solvents, the catalyst precipitates as a rust-red solid. In pure pyridine a precipitate is not observed, but the solution becomes red. With Py/HOAc mole ratios below 2:1, the reaction efficiencies are greatly reduced.

Table XVII. Reaction Efficiencies for the Iron-Catalyzed Conversion of Cyclohexane to Cyclohexanone by Electrochemically Reduced Dioxygen in Pyridine/HOAc.[a]

catalyst conc. (mM)	reaction efficiency (±5%)
30 (suspension)	52
15	76
7.5	77
3.8[c]	80
2.5	83
1.9	79
0.9	86
0.5	40
0	0

a. $(O_2 + 2e^-)$[b]

[a] "Fe(PA)$_2$" (isolated brown powder) used as the catalyst.

[b] Controlled-potential electrolysis (-0.6 V vs. SCE) performed with glassy-carbon plate working electrodes to 25C. Solvent composition: Py/HOAc/H$_2$O (10:1:1 by volume), 1 M C$_6$H$_{12}$, 0.1 M tetraethyl-ammonium perchlorate, 1 atm. O$_2$. Cyclohexanone was the sole product detected. Reaction efficiencies based on 4e$^-$/ketone.

[c] Catalytic turnovers, based on moles of oxygenated product per mole of complex added, are observed at concentrations of 3.8 mM or less.

Table XVII. (Continued).

	catalyst conc. (mM)	reaction efficiency (±5%)
b. $KO_2(s)$[d]		
	56	46
	3.5	43

[d] Slurry of KO_2 in pyridine (1.633 mmol/mL) added to reaction solution at 56 mM concentration. Reaction time, 15 minutes. Solvent : Py/HOAc (6:1 by volume), 1M C_6H_{12}. Cyclohexanone was the sole product detected. Reaction efficiencies based on $4KO_2$/ketone (Ref. 138).

Table XVIII. Reaction Efficiencies for the Iron-Catalyzed Conversion of Cyclohexane to Cyclohexanone by Electrochemically Reduced Dioxygen in Various Solvents.[a,b]

solvent composition (mole ratio)	reaction efficiency ($\pm 5\%$)
MeCN	0 (rust-colored precip.)
Pyridine	0
Py/H$_2$O (2:1)	0 (rust-colored precip.)
Py/0.1 M HClO$_4$[c]	79
Py/HOAc (10:1)	59
Py/HOAc/H$_2$O (7:1:3)	80
Py/HOAc (5:1)	100
Py/HOAc (2:1)	100
Py/HOAc (1:1)	<10

[a] 3.5 mM "Fe(PA)$_2$" (isolated brown powder) as catalyst. Controlled-potential electrolysis (-0.6 V vs. SCE) performed with glassy-carbon plate working electrodes to 25C. Solvents contained 1 M C$_6$H$_{12}$, 0.1 M tetraethylammonium perchlorate, 1 atm. O$_2$. Cyclohexanone was the sole product detected. Reaction efficiencies based on 4e$^-$/ketone.

[b] For 56 mM KO$_2$(s) (1.633 mmol/mL slurry in pyridine) and 56 mM (Py)$_4$FeCl$_2$ the optimal Py/HOAc solvent mole ratio is between 4.3:1 (highest selectivity, 99% C$_6$H$_{10}$(O)) and 1.8:1 (highest efficiency, 76% C$_6$H$_{10}$(O), 24% C$_6$H$_{11}$OH). The presence of water greatly reduces the efficiencies (Ref. 138).

[c] From 1M HClO$_4$ in MeCN.

Product Analysis and Optimization for Reaction with Hydrogen Peroxide

The reaction efficiencies for the metal-catalyzed conversion of cyclohexane to cyclohexanone by hydrogen peroxide are shown in Table XIX for several metal complexes. Cyclohexanone and cyclohexanol are the only products observed. Bipyridines and pyridine-hydrocarbon coupled products are not detected. Maximum efficiencies are obtained for a solvent composition of 2Py/HOAc (mole ratio). Product selectivity is unchanged with 3.3 mM "Fe(PA)$_2$" catalyst for Py/HOAc ratios from 5:1 to 2:1. Identical results are obtained with anhydrous HOOH in MeCN (94%, 1.6 M) or with the direct use of undiluted 50% HOOH (17.3 M). Addition of hydrogen peroxide caused the gold, orange, or red solutions in 2Py/HOAc to decolorize, then gradually return to a bronze or olive color. In pure pyridine products are not detected with [Fe(MeCN)$_4$](ClO$_4$)$_2$, (Py)$_4$FeCl$_2$, or "Fe(PA)$_2$" as catalysts, but the bronze color is quite pronounced. Use of acetonitrile as the solvent reduces the reaction efficiency and eliminates selectivity.

The highest reaction efficiences are obtained with "Fe(PA)$_2$" (isolated brown powder) as the catalyst. Substantial yields also are obtained with Fe(8Q)$_3$ (as a suspension). The manganese complexes are not soluble, but Mn(PA)$_3$·2H$_2$O dissolves to give a pale green solution upon addition of hydrogen peroxide. The "Fe(PA)$_2$" compound forms a suspension in MeCN. The efficiency of the "Fe(PA)$_2$"-catalyzed reaction is sensitive to water content, particularly at low catalyst concentrations.

The various metal catalysts have been evaluated with reaction times of 8 hours. For lower catalyst concentrations longer reaction times

Table XIX. Reaction Efficiencies for the Metal-Catalyzed Conversion of Cyclohexane to Cyclohexanone and Cyclohexanol by Hydrogen Peroxide in 2Py/HOAc.[a]

catalyst (3.3 mM)	reaction efficiency (±5%)	catalytic turnovers	products (±5%)	
			$C_6H_{10}(O)$	$C_6H_{11}OH$
a. No metal	0	—	—	—
b. Iron catalysts				
[Fe(MeCN)$_4$](ClO$_4$)$_2$	<2	—	100	0
FeCl$_3$	9	1	100	0
(Py)$_4$FeCl$_2$	16	3	69	31
"Fe(PA)$_2$"[b]	72	11	93	7
"Fe(PA)$_2$" (56 mM HOOH)	72	6	94	6
"Fe(PA)$_2$" (56 mM HOOH, 101 mM H$_2$O)[c]	58	5	94	6
0.9 mM "Fe(PA)$_2$" (56 mM HOOH)[c,d]	71	23	94	6
0.9 mM "Fe(PA)$_2$" (56 mM HOOH, 101 mM H$_2$O)[c,d]	17	5	94	6
"Fe(PA)$_2$" in Py	0	—	—	—
(Py)$_4$FeCl$_2$ in Py	0	—	—	—
[Fe(MeCN)$_4$](ClO$_4$)$_2$ in MeCN	0	—	—	—
"Fe(PA)$_2$" in MeCN	9	2	42	58

Table XIX. (Continued).

catalyst (3.3 mM)	reaction efficiency (±5%)	catalytic turnovers	products (± 5%)	
			C$_6$H$_{10}$(O)	C$_6$H$_{11}$OH
b. (cont'd)				
Fe(8Q)$_3$	47	7	90	10
Fe(acac)$_3$	<2	—	—	—
Fe(acac)$_2$	<4	1	50	50
(Py)$_4$Fe(OAc)$_2$	<2	—	—	—
Fe(ClO$_4$)$_3$	0	—	—	—
c. Other metals				
Zn(PA)$_2$·2H$_2$O	<2	—	100	0
Co(PA)$_2$	<4	—	100	0
Mn(PA)$_3$·H$_2$O	<4	—	100	0
Mn(PA)$_2$·2H$_2$O	<4	—	100	0

[a] 3.3 mM catalyst, 96 mM HOOH (94%, 1.6 M in MeCN), 1 M C$_6$H$_{12}$ in 2Pyridine/HOAc (mole ratio). Reaction time and temperature, 8 hours at 22 ± 2 °C. Cyclohexanone and cyclohexanol were the only products detected. Reaction efficiency based on 2 HOOH/ketone, HOOH/alcohol. Catalytic turnovers based on moles of substrate oxygenated per mole of metal complex added.

[b] "Fe(PA)$_2$", isolated brown powder.

[c] Ref. 138.

[d] Reaction time, 15 hours.

(15 hours) are necessary. Figure 9 provides a time profile of the products from the "Fe(PA)$_2$" catalyzed reaction of cyclohexane with hydrogen peroxide. Cyclohexanone is generated steadily at about 1 turnover every 13 minutes. The production of cyclohexanone is complete in about 2 1/4 hours. In contrast, over 90% of the cyclohexanol is generated within 30 minutes, with a total quantity equivalent to 0.75 turnover. The reactions with KO$_2$(s) in the previous section are much more rapid, and are complete within 15 minutes.

The reaction efficiencies for the conversion of cyclohexane to cyclohexanone by iron-activated hydrogen peroxide are summarized in Table XX for a variety of iron picolinate and iron dipicolinate species. The isolated powder "Fe(PA)$_2$" gives a slightly higher yield than when the complex generated in situ, and a substantially higher yield in the case of "Fe(DPA)". The addition of 0.5 equivalent of HOOH to Fe(DPA) (either the isolated complex or generated in situ), prior to addition of substrate and 100 mM HOOH, also increases the reaction efficiency. The "Fe(PA)$_2$" catalyst in a pyridine/picolinic acid (5:1 mole ratio) solvent has an efficiency of 21% and selectivity of 85% C$_6$H$_{10}$(O), 15% C$_6$H$_{11}$OH; the (Py)$_4$Fe(OAc)$_2$ catalyst has an efficiency of 28% and selectivity of 90% C$_6$H$_{10}$(O), 10% C$_6$H$_{11}$OH in the same solvent.

The products and reaction efficiencies for the "Fe(PA)$_2$" catalyzed oxygenation of several substrates by hydrogen peroxide are shown in Table XXI. Hydrocarbons are transformed to ketones via the oxygenation of a methylenic carbon. Acetylenes (e.g., PhC≡CPh) and arylolefins (e.g., cis-PhCH=CHPh) are dioxygenated to α-dicarbonyls and aldehydes,
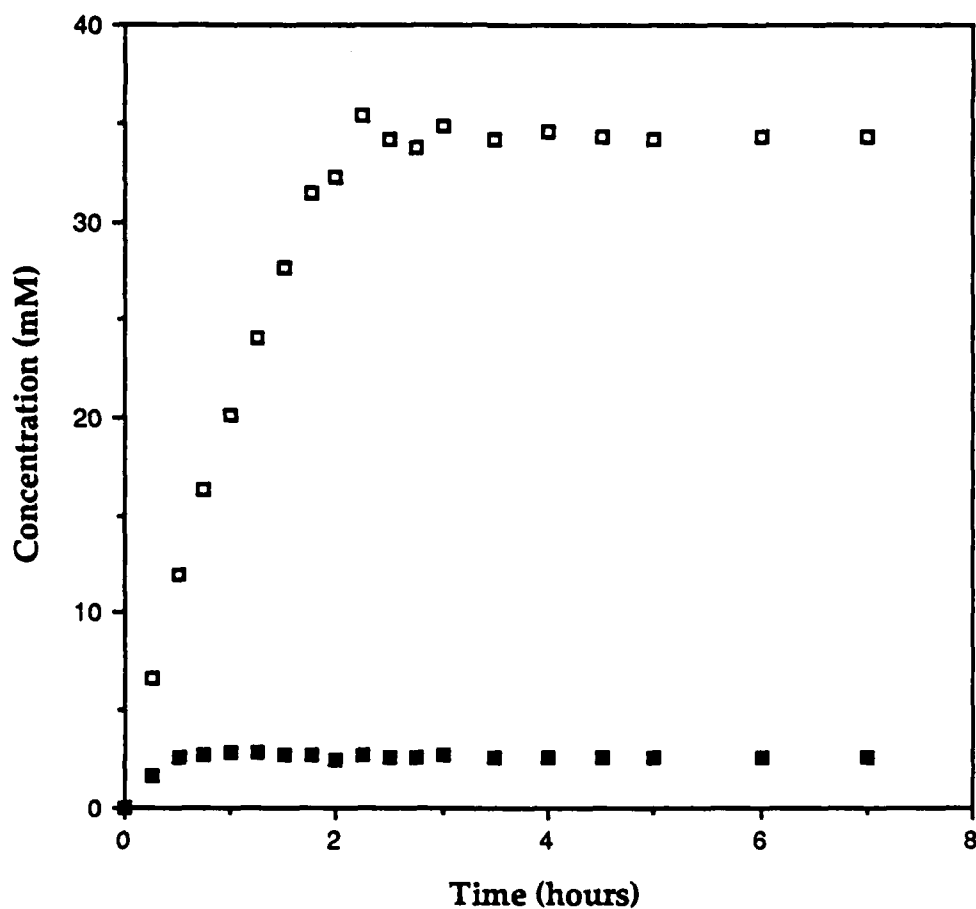
Figure 9. Time profile of products from the "Fe(PA)$_2$" catalyzed reaction of cyclohexane with hydrogen peroxide. ($\square$) Cyclohexanone, ($\blacksquare$) Cyclohexanol. Conditions: 3.3 mM "Fe(PA)$_2$" (isolated brown powder), 100 mM HOOH (82%, 3.6 M), 1 M C$_6$H$_{12}$ in 2Py/HOAc. Reaction efficiency at 2 1/4 hours, 73%.

Table XX. Reaction Efficiencies for the Iron Picolinate and Iron

Dipicolinate Catalyzed Conversion of Cyclohexane to Cyclohexanone and

Cyclohexanol by Hydrogen Peroxide in 2Py/HOAc.[a]

catalyst (3.3 mM)	reaction efficiency ($\pm$5%)	catalytic turnovers	products ($\pm$ 5%) $C_6H_{10}(O)$	$C_6H_{11}OH$
a. Iron picolinate				
"Fe(PA)$_2$"[b]	72	11	93	7
Fe^{2+} + 1PA$^-$ [c]	65	10	93	7
2PA$^-$	63	9	90	10
3PA$^-$	68	10	88	12
Fe^{3+} + 1PA$^-$ [c]	65	10	93	7
2PA$^-$	63	9	90	10
3PA$^-$	68	10	88	12
"(PA)$_2$FeOFe(PA)$_2$"[d]	62	9	91	9
Fe^{2+} + 2PA$^-$ + HOOH[c]	72	11	93	7

[a] 3.5 mM catalyst, 100 mM HOOH (94%, 1.6 M in MeCN), 1 M C_6H_{12} in 2Pyridine/HOAc (mole ratio). Reaction time and temperature, 4 hours at 22 $\pm$ 2 °C. Cyclohexanone and cyclohexanol were the only products detected. Reaction efficiency based on 2 HOOH/ketone, HOOH/alcohol. Catalytic turnovers based on moles of substrate oxygenated per mole of iron complex added.

[b] "Fe(PA)$_2$", isolated brown powder.

[c] Fe^{2+} introduced to solution as [Fe(MeCN)$_4$](ClO$_4$)$_2$; Fe^{3+} as Fe(ClO$_4$)$_3$; PA$^-$ as (Me$_4$N)PA; and DPA^{2-} as (Me$_4$N)$_2$DPA.

[d] "(PA)$_2$FeOFe(PA)$_2$", isolated pale green powder.

Table XX. (Continued).

catalyst (3.3 mM)	reaction efficiency ($\pm 5\%$)	catalytic turnovers	products ($\pm 5\%$)	
			$C_6H_{10}(O)$	$C_6H_{11}OH$
b. Iron dipicolinate				
"Fe(DPA)"[e,f]	73	12	97	3
Fe^{2+} + DPA[c]	33	5	87	13
(after 8 hours)	38	6	92	8
"Fe(DPA)" + 1/2HOOH[e,f]	76	13	97	3
Fe^{2+} + DPA + 1/2HOOH[c]	41	6	89	11
(after 8 hours)	48	7	92	8

[e] "Fe(DPA)", isolated brown powder.
[f] Ref. 138.

Table XXI. Products and Reaction Efficiencies for the Iron-Catalyzed

Ketonization of Methylenic Carbon and the Dioxygenation of Acetylenes

and Arylolefins by Hydrogen Peroxide in 2Py/HOAc.[a]

substrate (1 M)	reaction efficiency (±5%)	catalytic turnovers	products (± 5%)
cyclohexane	72	6	cyclohexanone (97%) cyclohexanol (3%)
n-hexane[b]	52	4	3-hexanone (53%) 2-hexanone (46%) 1-hexanol (<2%)
$PhCH_2CH_3$	51	5	$PhC(O)CH_3$ (>96%)
$PhCH_2Ph$ (0.6 M)[b]	35	3	$PhC(O)Ph$ (>96%)
2-methyl-butane[b]	32	3	3-methyl-2-butanone (95%) 2-methyl-1-butanol (<5%)
adamantane (0.1 M)[b]	–	–	2-adamantanone (43%) 1-adamantanol (29%) two others (28%)
cyclohexanol	25	4	cyclohexanone (>95%)
cyclohexanone	0	–	
cyclohexene[b]	59	5	2-cyclohexene-1-one (>95%)

[a] 3.5 mM "Fe(PA)₂" (isolated brown powder) catalyst, 56 mM HOOH
(50% in H_2O, 17.3 M)), 1 M substrate in 2Pyridine/HOAc (mole ratio).
Reaction time and temperature, 4 hours at 22 ± 2 °C. Reaction efficiency
based on 2 HOOH/ketone, HOOH/alcohol. Catalytic turnovers based on
moles of substrate oxygenated per mole of iron complex added.

Table XXI. (Continued).

substrate (1 M)	reaction efficiency (±5%)	catalytic turnovers	products (± 5%)
PhC≡CPh (0.6 M)[b,c]	40	3	PhC(O)C(O)Ph (>97%)
c-PhCH=CHPh[b,d]	36	4	PhCH(O) (75%) PhHC—CHPh (25%)
t-PhCH=CHMe[b]	48	4	PhCH(O) (63%) PhHC—CHMe (16%) two others (21%)
1,3-cyclohexadiene[b]	33	5	benzene (>95%)
1,4-cyclohexadiene[b]	26	4	phenol (>95%)

[b] Ref. 138.

[c] With m-ClPhC(O)OOH and t-BuOOH (in place of HOOH) the conversion efficiencies were 10% and 0%, respectively.

[d] With m-ClPhC(O)OOH and t-BuOOH the conversion efficiencies were 11% and 95%, respectively, to give PhCH(O)/epoxide ratios of 1:1.2 and 1:16.

respectively. Cyclohexanone is unreactive, while cyclohexanol has limited reactivity relative to cyclohexane.

In the Py/HOAc solvent system a binuclear iron-μ-dioxygen complex, $[(Ph_3PO)_4FeOOFe(OPPh_3)_4](ClO_4)_4$,[139] reacts with excess cyclohexane to give cyclohexanone exclusively (56 mM iron complex, 1 M C_6H_{12}, 15 min. reaction time, 3% efficiency); and with excess $PhC\equiv CPh$ to give $PhC(O)C(O)Ph$ exclusively (56 mM iron complex, 0.6 M $PhC\equiv CPh$, 15 min. reaction time, 3% efficiency). In MeCN, neither substrate reacts with the iron complex; however, the addition of sufficient acid (3.7 M $HClO_4$) causes $PhC\equiv CPh$ to be transformed almost completely within 10 minutes to yield 78% $PhC(O)C(O)Ph$ and 14% $PhC(O)OH$.[138]

Electrochemistry and Spectroscopy

Figure 10 illustrates the cyclic voltammograms for dioxygen and hydrogen peroxide in pyridine and in pyridine/acetic acid solvents. In pyridine dioxygen exhibits a reversible one-electron couple at -0.89 V vs. SCE, while in Py/HOAc an irreversible two-electron reduction is observed ($E_{p,c}$, -1.00 V vs. SCE for an O_2-saturated (1 atm.) solution). After reduction a reverse scan yields a new oxidation peak ($E_{p,a}$, +1.25 V). The oxidation of hydrogen peroxide in 2Py/HOAc occurs at +1.25 V vs. SCE. Following the oxidation of HOOH, a reverse scan yields a reduction peak ($E_{p,c}$, -0.70 V), which increases in peak height with the addition of dioxygen.

The cyclic voltammogram of $(Py)_4FeCl_2$ in pyridine (Figure 11) exhibits an irreversible oxidation ($E_{p,a}$, -0.09 V). In the presence of dioxygen the reversible couple for dioxygen is observed as well as a

Figure 10. Cyclic voltammograms: (a) O_2, saturated solution in Py;

(b) O_2, saturated solution in Py/HOAc (4.3:1 mole ratio); (c) O_2, in

2Py/HOAc (mole ratio); (d) 7 mM HOOH in 2Py/HOAc (mole ratio)

(0.1 M tetraethylammonium perchlorate). Conditions: scan rate, 0.1 V s^{-1};

ambient temperature; glassy-carbon working electrode (0.09 cm^2); saturated

calomel electrode (SCE) vs. NHE, +0.242 V.

(a) O₂ in Py

(b) O₂ in Py/HOAc

100µA

E,V vs. SCE

E,V vs. SCE

(c) O₂ in 2Py/HOAc

50µA

(d) 7mM HOOH in 2Py/HOAc

E,V vs SCE

Figure 11. Cyclic voltammograms: (a) 3.5 mM $(Py)_4FeCl_2$ in Py;
(b) a + O_2; (c) 3.5 mM $(Py)_4FeCl_2$ in Py/HOAc (4.3:1 mole ratio); (d) c + O_2
(0.1 M tetraethylammonium perchlorate). Conditions: scan rate, 0.1 V s^{-1};
ambient temperature; glassy-carbon working electrode (0.09 cm^2); saturated
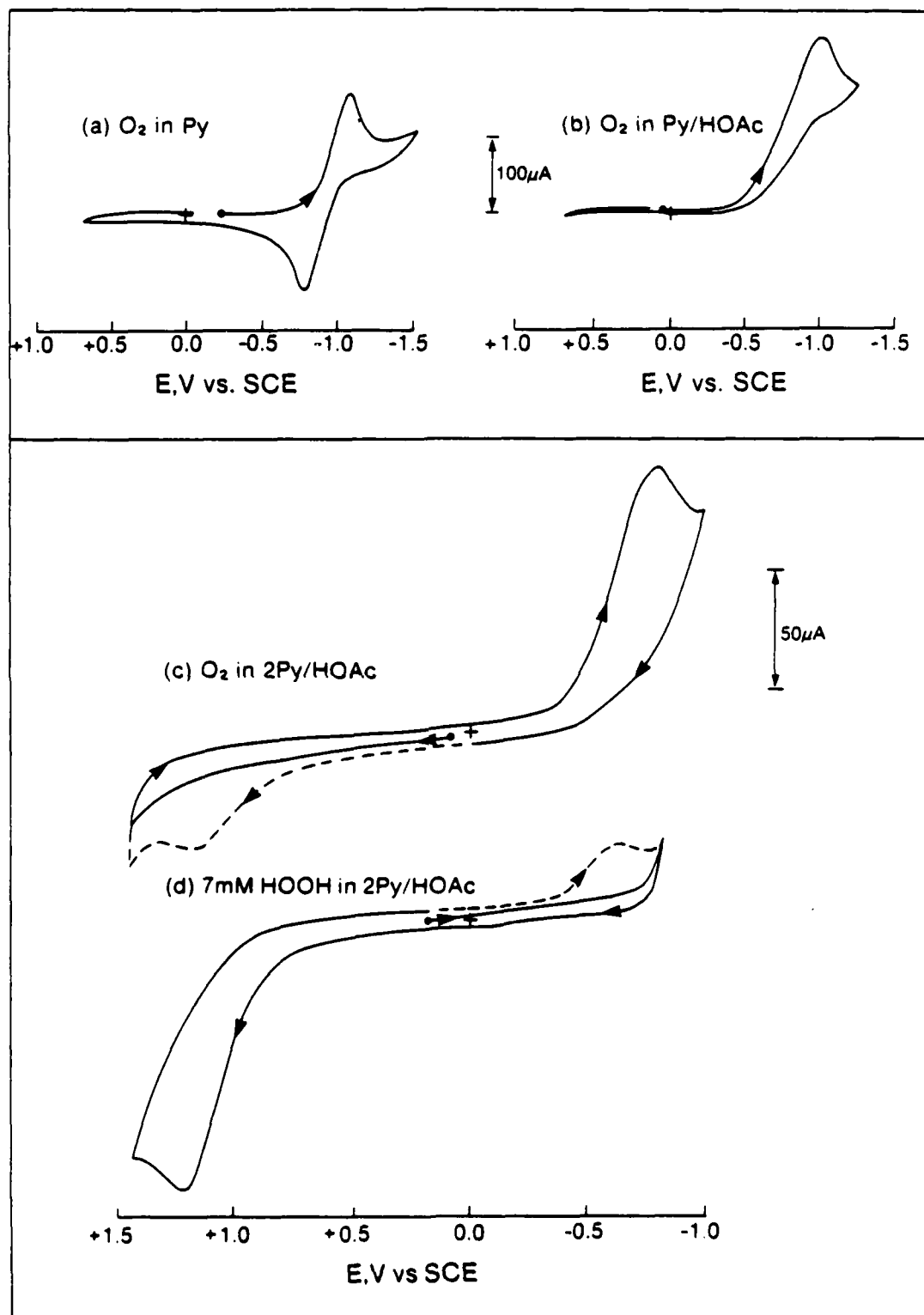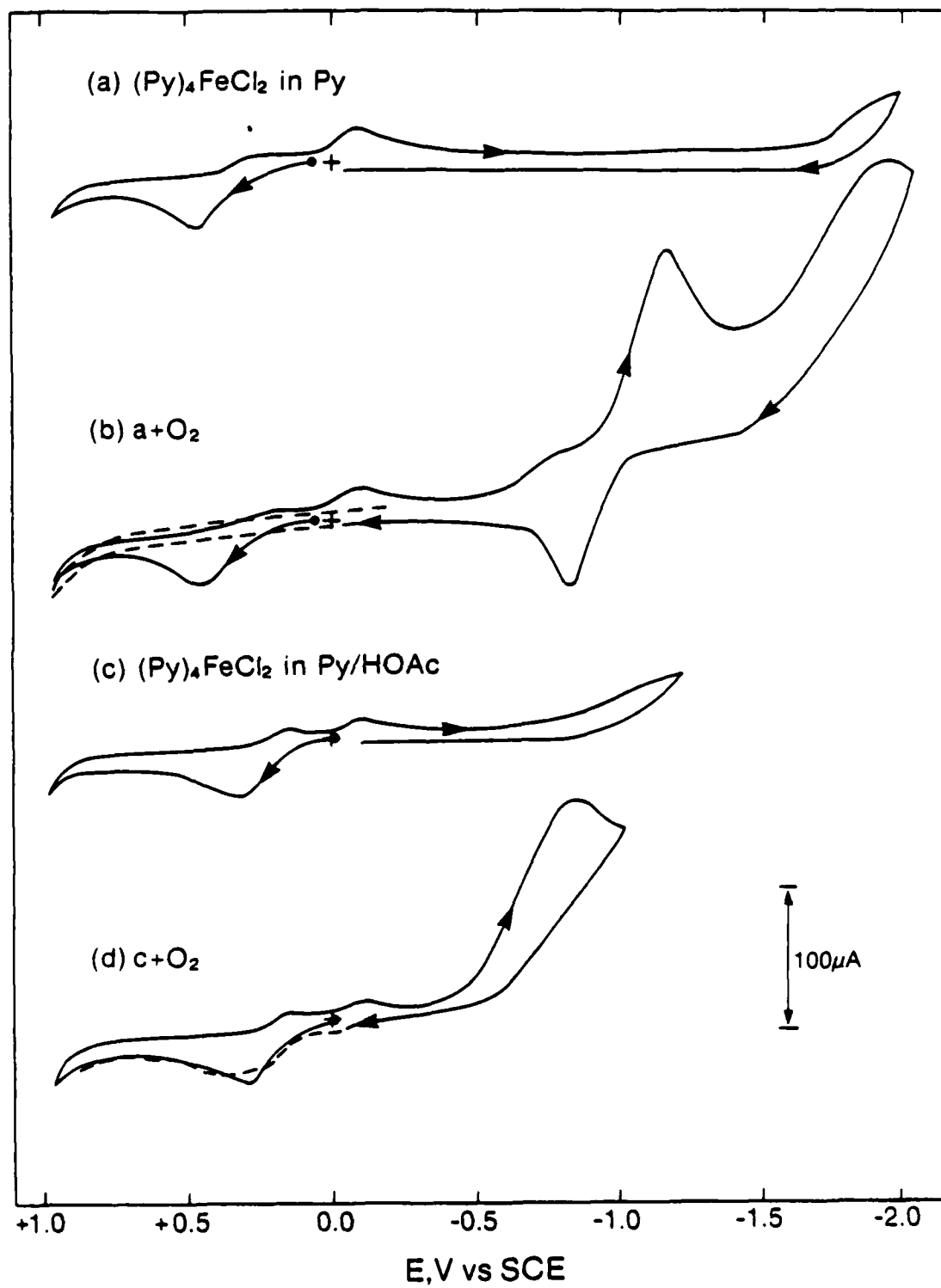calomel electrode (SCE) vs. NHE, +0.242 V.

(a) (Py)$_4$FeCl$_2$ in Py

(b) a+O$_2$

(c) (Py)$_4$FeCl$_2$ in Py/HOAc

(d) c+O$_2$

100μA

E,V vs SCE

pre-peak at -0.77 V. No electrochemical features are seen for the iron complex with an initial negative scan. An initial positive scan with subsequent reversal reveals that the electrochemistry of the iron complex is unchanged prior to the reduction of dioxygen. Bubbling argon through the solution first removes the reversible oxygen couple and then the pre-peak. Further removal of dioxygen leads to the reappearance of the oxidation peak for $(Py)_4FeCl_2$. In Py/HOAc (4.3:1 mole ratio) the oxidation of $(Py)_4FeCl_2$ is shifted ($E_{p,a}$, +0.33 V vs. SCE). The reduction peak at -0.09 V remains, but is somewhat diminished in peak height. Both features become quasi-reversible with $E_{p,c}$, +0.19 V and $E_{p,a}$, -0.01 V, respectively. With dioxygen present an irreversible two-electron reduction peak occurs at -0.85 V, and the oxidation peak of the iron complex is slightly broadened, and appears to be a combinatin of two oxidation features. Partial removal of dioxygen by bubbling argon through the solution results in the shift of the irreversible reduction peak to -0.75 V and the return of the oxidation peak to its original shape.

The electrochemical behavior of $FeCl_3$ is similar to that of $(Py)_4FeCl_2$ with respect to the presence of dioxygen. In pyridine, the cyclic voltammogram of $FeCl_3$ has a semi-reversible couple at +0.30 V vs. SCE and a reduction peak at -0.10 V, which indicates the presence of two species. In the presence of dioxygen, a pre-peak (-0.85 V) to the reversible couple of dioxygen is present and no oxidation peak is observed for $FeCl_3$. In Py/HOAc (4.3:1 mole ratio) the reduction peak at -0.10 V becomes a fully reversible couple ($E_{1/2}$, -0.05 V), and the semi-reversible couple shifts to

-0.26 V and is reduced in peak height. In the presence of dioxygen an irreversible reduction occurs at -0.75 V. The reversible couple at -0.05 is unchanged, but the oxidation peak of the other couple is substantially enhanced.

The electrochemistry of "Fe(PA)$_2$" (isolated brown powder) in 2Py/HOAc is shown in Figure 12. In addition to the reversible couple at +0.18 V vs. SCE, which also is observed for Fe(PA)$_2$ that is generated in situ, a small reduction peak is seen at -0.08 V and a second small reduction peak at -0.65 V. Addition of dioxygen to the solution does not cause any change in the redox features of the complex. The oxidation peak (previously observed to be coupled to the irreversible reduction of dioxygen) is not seen. With the addition of hydrogen peroxide (from 1/4 to 2 equivalents), the reduction peak at -0.08 V is enhanced and broadened. No reduction peak for dioxygen is observed after the oxidation of HOOH. In 2Py/HOAc, the addition of 2 HOOH to "Fe(PA)$_2$" results in the gradual growth of an oxidation peak at +1.00 V. The initial oxidation for the iron complex with a positive scan is lost, but gradually returns. The reaction is complete after 15 minutes and no further changes are observed in the electrochemistry, even after 72 hours (Figure 12).

This behavior contrasts with that for iron picolinate and iron dipicolinate complexes in DMF.[140] The stoichiometric addition of HOOH to a solution of Fe(PA)$_2$ in DMF causes the appearance of two reduction peaks at -0.53 V and -0.92 V, and of an oxidation peak at +0.95 V vs. SCE. The reduction peak for the Fe(PA)$_2$ complex is suppressed and the oxidation peak is decreased to one-half of its original height. The

Figure 12. Cyclic voltammograms: (a) 3.5 mM "Fe(PA)$_2$" (isolated brown powder); (b) a plus 2 equivalents of HOOH; (c) b, after 24 hours in 2Py/HOAc (mole ratio) (0.1 M tetraethylammonium perchlorate). Conditions: scan rate, 0.1 V s^{-1}; ambient temperature; glassy-carbon working electrode (0.09 cm^2); saturated calomel electrode (SCE) vs. NHE, +0.242 V.

(a) "Fe(PA)₂" in Py/HOAc

50μA

10μA

(a)

(b) a + 2 HOOH

(b)

(c) b, after 24 hours

(c)

+1.5   +1.0   +0.5   0.0   -0.5   -1.0

+0.5   0.0   -0.5

E,V vs SCE

E,V vs SCE
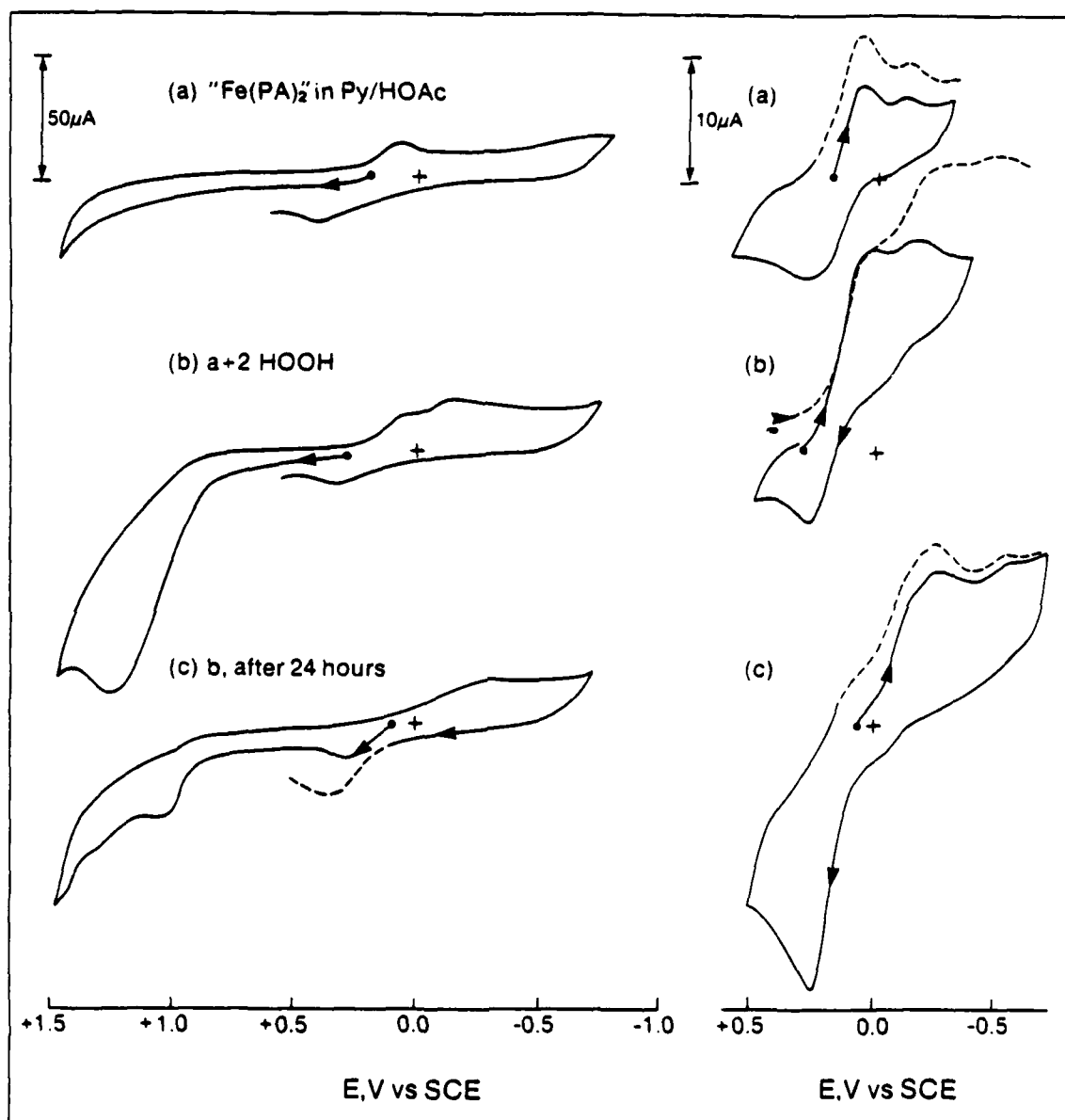
electrochemistry of the isolated pale green powder "$(PA)_2FeOFe(PA)_2$" has the same features. With Fe(DPA) the addition of HOOH suppresses the original redox features of the complex and generates a redox couple at -0.30 V that has a peak height equivalent to one-half the total height of the original peaks. Identical electrochemistry is observed after the reaction of Fe(DPA) and O_2 at a 4:1 stoichiometry, although a new reduction peak is observed at -0.22 V in the presence of dioxygen. The reaction of $Fe(PA)_2$ with dioxygen results in similar electrochemical behavior as that observed for the addition of 1 HOOH but with a much larger reduction peak at -0.92 V. The addition of excess HOOH to the $Fe(PA)_2$ or Fe(DPA) solutions causes the appearance of an oxidation peak at +0.95 V, and the rapid and complete decomposition of HOOH to molecular oxygen within 30 minutes. At the end of this time, the electrochemistry for the stoichiometric addition of HOOH is observed.

The UV/visible spectrum of $Fe(PA)_2$ in 2Py/HOAc is shown in Figure 13. The 2Py/HOAc (mole ratio) solvent absorbs below 340 nm. Iron(II) (as $[Fe(MeCN)_4](ClO_4)_2$) has an absorption maximum at 380 nm in this solvent. Addition of PA^- (as $(Me_4N)PA$) causes the maximum to shift to longer wavelengths until at two equivalents $[Fe(PA)_2]$ the maximum is at 402 nm. Addition of 1/2 equivalent of hydrogen peroxide decolorizes the golden solution to give an absorption below 350 nm and a shoulder at 400 nm. Further addition of HOOH removes the shoulder at 400 nm.

Figure 13. UV/visible spectra: (a) 0.75 mM Fe(PA)$_2$ [Fe(MeCN)$_4$(ClO$_4$)

plus 2 (Me$_4$N)PA]; (b) a plus HOOH in 2Py/HOAc (mole ratio), 1 M C$_6$H$_{12}$.

(a) Fe(PA)$_2$ in Py/HOAc

(b) a + HOOH
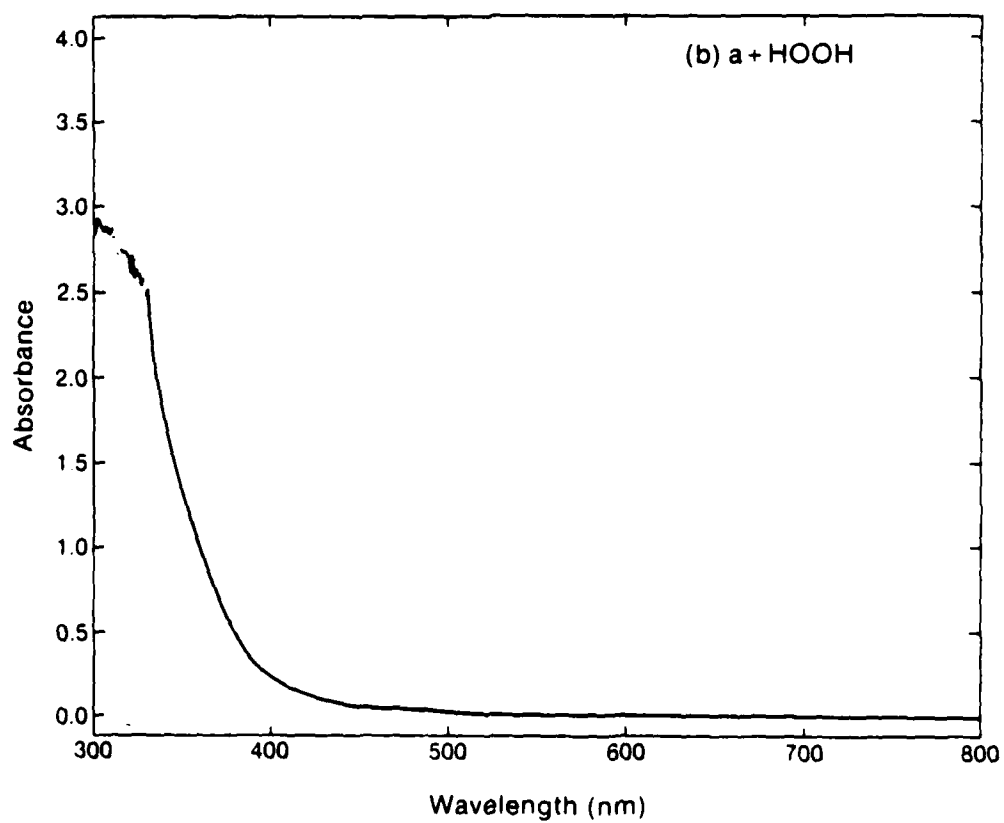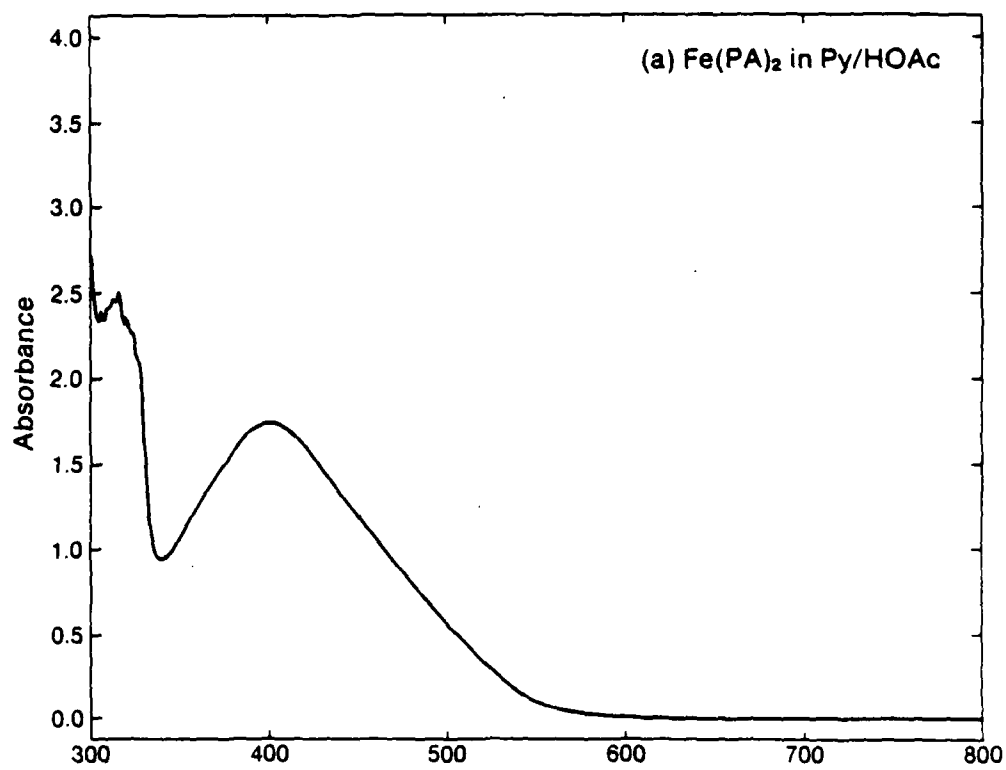
Discussion

The results for the optimization of the transformation of cyclohexane to cyclohexanone via superoxide ion chemistry (Tables XVI, XVII, and XVIII) are similar to those for heterogeneous iron-dioxygen systems in pyridine/acetic acid solvents.[63-68] The optimal efficiencies obtained for the O_2^- systems when the iron catalyst and superoxide source are in suspension, and the lack of reactivity when all species are fully soluble, are consistent with heterogeneous processes.

The irreversible two-electron reduction of dioxygen in 2Py/HOAc and the subsequent detection of the oxidation peak for hydrogen peroxide at +1.25 V vs. SCE (Figure 10) clearly indicate that dioxygen is reduced to hydrogen peroxide in this solvent, and that free superoxide ion is not present. Free superoxide ion is incompatible with a protic solvent matrix (the proton-induced disproportionation of superoxide ion to hydrogen peroxide and dioxygen is essentially a diffusion-controlled process[141]). The difference in product distribution for electrochemically reduced oxygen (to HOOH) and for hydrogen peroxide with the $(Py)_4FeCl_2$ catalyst, and the much higher efficiency for the electrochemical process indicate that the electrochemical process may also involve a surface reaction (in this case, the electrode surface). The results with the $Fe(PA)_2$ catalyst (Tables XVII, XVIII, XIX, and XX) are more ambiguous. While the electrochemical process may involve a surface reaction, a reaction pathway that involves electrochemically produced hydrogen peroxide (or intermediates) is equally probable.

The far greater reactivity of iron catalysts in the hydrogen peroxide system as compared to manganese or cobalt is apparent from the data in Table XIX. The ligand and solvent dependencies also are apparent (Tables XVIII, XIX, and XX). The iron picolinate and iron dipicolinate systems, which contain pyridyl-nitrogen and carboxylate donors analogous to the pyridine and acetic acid of the solvent, are the most effective catalysts. The highest selectivities are achieved with metal-ligand stoichiometries that give coordinately unsaturated complexes. The $Fe(8Q)_3$ complex which contains pyridyl-nitrogen and phenoxide donors is the only other catalyst to give comparable yields and selectivity.

The conversion efficiencies and products for various organic substrates in the reaction with iron-activated hydrogen peroxide (Table XXI) indicate that hydrocarbon substrates are transformed to ketones via the direct oxygenation of a methylenic carbon. Alcohols are detected as minor products. The relative reaction efficiencies for cyclohexane, cyclohexene, n-hexane, and 2-methyl-butane are roughly proportional to the number of $\left(>CH_2 \right)$ groups per molecule (6, 4, 4, and 1), which indicates that the HOOH system is selectively reactive with methylenic carbon. The absence of any reaction for cyclohexanone is surprising, as is the limited reactivity of cyclohexanol relative to cyclohexane (~1/3). Acetylenes and arylolefins are dioxygenated to α-dicarbonyls and aldehydes, respectively, with epoxides detected as minor products from the reactions with arylolefins. These product distributions indicate that the reaction mechanism must include pathways for both dioxygenation and monooxygenation.

The failure to detect bipyridines or pyridine-hydrocarbon coupled products does not exclude the formation of hydroxyl radicals by a process similar to Fenton chemistry. Fully 30% of the hydrogen peroxide is unaccounted for in the iron picolinate catalyzed system. Pyridine is an excellent trap for hydroxyl radical,

$$\cdot OH + Py \rightarrow (1/n)(Py \cdot OH)_n \qquad k, 3 \times 10^9 \, M^{-1}s^{-1} \qquad (9)$$
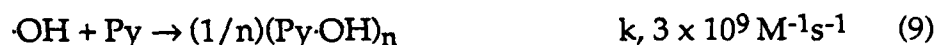
via formation of a pyridine-hydroxyl radical adduct.[142,143] This species is a brown-bronze diamagnetic polymer that is inert and does not have a significant UV/visible spectrum. The formation of this polymer in these catalytic systems is reasonable given (a) the tendency for radical chemistry in iron-hydrogen peroxide systems, (b) the observation of a bronze colored product in these reaction solutions, and (c) the failure to detect this product by gas chromatography-mass spectrometry or UV/visible spectroscopy.

The cyclic voltammogram for $(Py)_4FeCl_2$ and O_2 in pyridine (Figure 11) contains the reversible couple for O_2/O_2^- and a pre-peak indicative of a Lewis acid-base interaction to form the metal-superoxide adduct.[144] In the Py/HOAc solvent the only indication of an interaction between the metal complex and the reduced dioxygen is a slight broadening of the oxidation peak for the iron complex. The similar cyclic voltammograms for $(Py)_4FeCl_2$ and $FeCl_3$ in both Py and Py/HOAc solvents are consistent with EC processes in which hydrolysis plays a dominant role (Scheme VII) (the similar electrochemistry expected for $-Cl$,
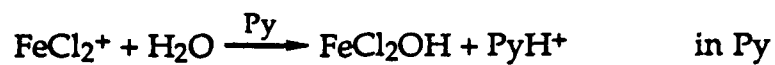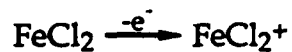
–OH, and –OAc ligands prevents conclusive assignments of the redox active species).

The cyclic voltammograms of "Fe(PA)$_2$" (isolated brown powder) (Figure 12) indicate that the complex is partially oxidized and that more than one stable species is present (reduction at -0.08 V). The oxidation of hydrogen peroxide in the presence of Fe(PA)$_2$ does not produce a reduction peak for dioxygen, but enhances and broadens the peak at -0.08 V. Iron complexes are known to have a tendency to form µ-oxo dimers.[61,145-147] The [Fe(2-Me-8Q)$_2$]$_2$O dimer is stable in neutral and basic DMSO solutions and has a redox couple at -0.78 V vs. SCE.[61] Peroxo-bridged iron dimers also are known.[139,148] The electrochemistry of the [(Ph$_3$PO)$_4$FeOOFe(OPPh$_3$)$_4$](ClO$_4$)$_4$ species in MeCN is dominated by an irreversible oxidation peak at +1.8 V vs. SCE, which is similar to that for free HOOH (+2.1 V) in that solvent.[139] The reduction of "Fe(PA)$_2$" at -0.65 V may be attributed to a µ-oxo dimer and the oxidation peak at +1.00 V, which appears upon addition of excess hydrogen peroxide, may indicate the formation of a µ-peroxo species. These assignments are supported by the electrochemical behavior of iron picolinate and iron dipicolinate complexes in DMF.[140] Stoichiometric addition of HOOH to a solution of Fe(PA)$_2$ in DMF causes the appearance of two reduction peaks that are attributable to the µ-oxo and µ-peroxo dimers, and an oxidation peak at +0.95 V that is characteristic of a peroxy group. With Fe(DPA) only the µ-oxo species appears to form on the basis of the electrochemical measurements. Hence, the µ-peroxo dimer probably collapses to the µ-oxo dimer. The reaction of Fe(DPA) with molecular oxygen also forms

Scheme VII.

Redox behavior of $(Py)_4FeCl_2$ and $FeCl_3$ in Py and Py/HOAc

    Couple at ~ +0.3 V

      Oxidation

$$FeCl_2 \xrightarrow{-e^-} FeCl_2^+$$

$$FeCl_2^+ + H_2O \xrightarrow{Py} FeCl_2OH + PyH^+ \qquad \text{in Py}$$

$$\text{or } FeCl_2^+ + HOAc \xrightarrow{Py} FeCl_2OAc + PyH^+ \quad \text{in Py/HOAc}$$

      Reduction

$$FeCl_2^+ \xrightarrow{+e^-} FeCl_2$$
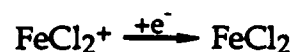
    Couple at ~ -0.05 V

      Reduction

$$FeCl_3 \xrightarrow{+e^-} FeCl_3^- \longrightarrow FeCl_2 + Cl^-$$

$$\text{or } FeCl_2OH \xrightarrow{+e^-} FeCl_2OH^- \longrightarrow FeCl_2 + {}^-OH$$

$$FeCl_2OH^- + HOAc \longrightarrow FeCl_2OAc^- + H_2O$$

$$\text{or } FeCl_2OAc \xrightarrow{+e^-} FeCl_2OAc^-$$

      Oxidation

$$FeCl_3^- \xrightarrow{-e^-} FeCl_3$$

$$\text{or } FeCl_2OAc^- \xrightarrow{-e^-} FeCl_2OAc$$
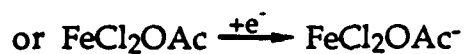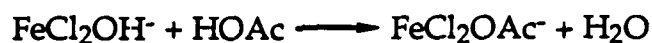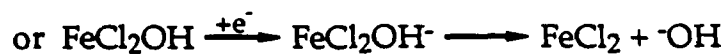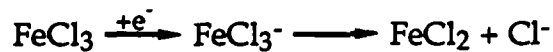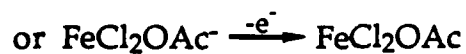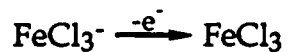
the μ-oxo dimer. The existence of a (DPA)Fe(OO)· intermediate with a reduction at -0.22 V has been confirmed by a rotated ring-disk experiment.[140] In 2Py/HOAc the oxidation peak for the μ-peroxo species is observed for both Fe(PA)$_2$ and Fe(DPA), and the rapid catalytic decomposition of HOOH does not occur, both observations indicate the presence of a stable μ-peroxo species.

Reaction pathways consistent with these observations are presented in Scheme VIII. A parallel scheme applies to the Fe(DPA) system. The stabilities of the μ-oxo and μ-peroxo species depend on the ligand and the solvent. The electrochemical results indicate that the μ-peroxo species is less stable in the Fe(DPA) system, which is consistent with the faster decomposition of HOOH by this complex and its greater reaction efficiency with substrates. The absence of rapid catalytic decomposition of HOOH by these iron complexes in 2Py/HOAc is consistent with the stability of the μ-peroxo species in this solvent. Thus, in the absence of substrate the μ-peroxo species does not quickly decompose to the μ-oxo dimer and dioxygen, which would interrupt the catalytic cycle. This also rationalizes the catalytic efficiency of these iron complexes for the oxygenation of substrates in 2Py/HOAc. Almost no substrate oxygenation occurs in DMF or DMSO because HOOH decomposition is the dominant pathway.

The reaction scheme for μ-oxo dimer formation, the reactivity of Fe(2-Me-8Q)$_2$ (which is known to form a μ-oxo dimer) with O$_2$, O$_2$·, and HOOH,[61] the dioxygenations of substrates by the Fe(PA)$_2$/HOOH system, and the parallel dioxygenations by the μ-peroxo species [(Ph$_3$PO)$_4$FeOOFe(OPPh$_3$)$_4$](ClO$_4$)$_4$[139,140] prompt the proposal that

Scheme VIII.

$$2(PA)_2Fe + HOOH \longrightarrow (PA)_2FeOFe(PA)_2 + H_2O$$

$$(PA)_2FeOFe(PA)_2 + HOOH \longrightarrow [(PA)_2FeOOFe(PA)_2] + H_2O$$

$$[(PA)_2FeOOFe(PA)_2] \longrightarrow 2(PA)_2Fe + {}^1O_2$$
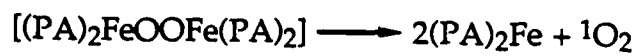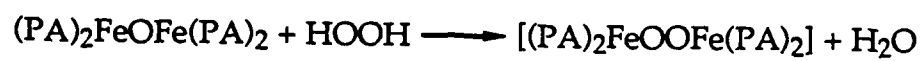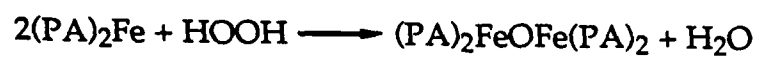
$[(PA)_2FeOOFe(PA)_2]$ is the active form of the catalyst. A dimeric catalyst requires that the catalytic turnovers in the tables be doubled. Reaction pathways for substrate transformations by this catalyst are presented in Scheme IX. On the basis of the higher reaction efficiencies achieved with the partially oxidized, isolated powders that contain the μ-oxo dimer, or with the pre-addition of 1/2 equivalent of HOOH to the reaction mixture, the initial step in the catalytic reaction cycle appears to be the activation of $Fe(PA)_2$ to $(PA)_2FeOFe(PA)_2$. The latter reacts with HOOH to give $[(PA)_2FeOOFe(PA)_2]$. This species transforms methylenic carbons to ketones and dioxygenates acetylenes and arylolefins. A small fraction of the $Fe(PA)_2$ pre-catalyst apparently forms a one-to-one adduct with HOOH to give a species, $[(PA)_2Fe(HOOH)]$, that is an effective monooxygenase. The $Fe(PA)_2/KO_2(s)/(2Py/HOAc)$ and $Fe(PA)_2/(O_2 + 2e^-)/(2Py/HOAc)$ systems probably form the same reactive intermediates as the $Fe(PA)_2/HOOH/(2Py/HOAc)$ system; and the other heterogeneous iron-dioxygen systems[63-68] probably form similar reactive intermediates with chemistry that parallels that in Scheme IX.

Scheme IX.

Dioxygenation of substrate

$2(PA)_2Fe + HOOH \longrightarrow (PA)_2FeOFe(PA)_2 + H_2O$

$(PA)_2FeOFe(PA)_2 + HOOH \longrightarrow [(PA)_2FeOOFe(PA)_2] + H_2O$

$[(PA)_2FeOOFe(PA)_2] \longrightarrow$

- $\xrightarrow{C_6H_{12}} C_6H_{10}(O) + H_2O + 2(PA)_2Fe$
- $\xrightarrow{PhC \equiv CPh} PhC(O)C(O)Ph + 2(PA)_2Fe$
- $\xrightarrow{c\text{-}PhCH=CHPh} 2PhCH(O) + 2(PA)_2Fe$

Monooxygenation of substrate

$(PA)_2Fe + HOOH \longrightarrow [(PA)_2Fe(HOOH) \longleftrightarrow (PA)_2Fe=O(H_2O)]$

$[(PA)_2Fe=O(H_2O)] \longrightarrow$

- $\xrightarrow{C_6H_{12}} C_6H_{11}OH + H_2O + Fe(PA)_2$
- $\xrightarrow{C_6H_{11}OH} C_6H_{10}(O) + H_2O + Fe(PA)_2$
- $\xrightarrow{c\text{-}PhCH=CHPh} c\text{-}PhHC\overset{O}{-}CHPh + H_2O + Fe(PA)_2$
- $\xrightarrow{1,3\text{-}CHD} PhH + 2H_2O + Fe(PA)_2$
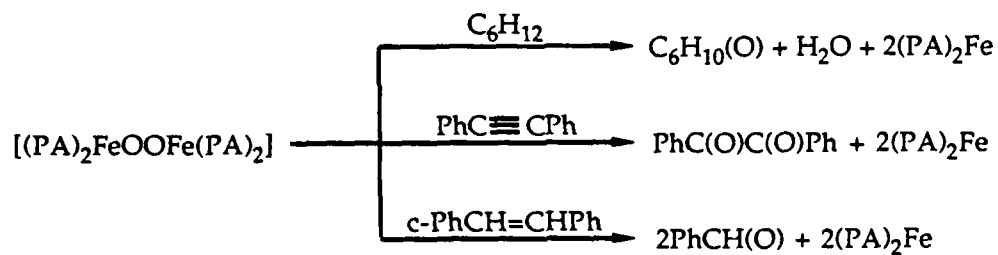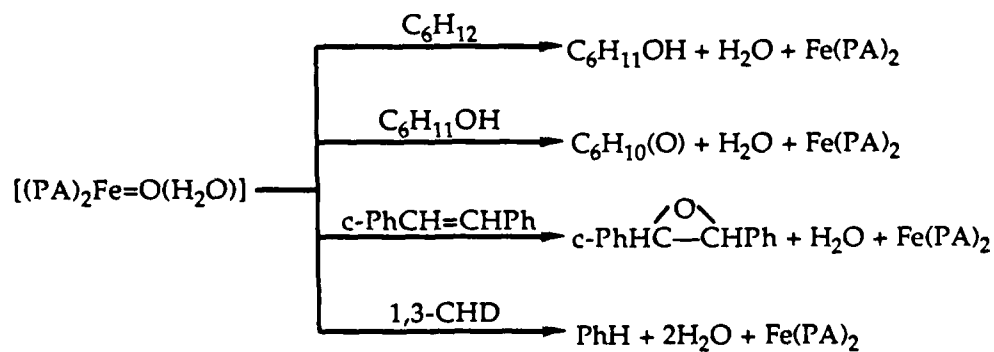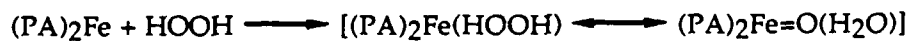
CHAPTER V

CONCLUSIONS

The oxidation potentials for a series of ML_3 complexes [M = Mn, Fe, Co, and Zn; L = acetylacetonate, 8-quinolinolate, picolinate, 2,2'-bipyridine, and 1,10-phenathroline] have been determined by cyclic voltammetry in aprotic solvents. With the exceptions of solvent and H_2O ligands, the oxidations of the manganese, iron, and cobalt complexes occur at substantially less positive potentials than those for (a) their zinc analogues, (b) the free ligand anions, and (c) the solvated M(II) ions, and are clearly ligand-centered. The removal of an electron from the valence shell of the ligand is easier than removal from the metal center and the ligand radical product is stabilized by the formation of a metal (d-electron)–ligand (p-electron) covalent bond. The negative shift in potential for these ligand oxidations is proportional to their metal-ligand covalent bond energies. Apparent metal-ligand covalent bond energies range from 6 kcal/mole for $Mn(8Q)_3$ to 35 kcal/mole for $Co(PA)_3$. The reductions for the bipyridine and phenanthroline complexes of these transition metals also are ligand-centered with bond energies ranging from greater than 23 kcal/mole for the manganese complexes to greater than 45 kcal/mole for the cobalt complexes.

The X-ray absorption edge energies for a series of oxidized and reduced manganese complexes have been determined and correlated with the electrochemical results. The edge energy for manganese (d^5sp) is 6546.0 ± 0.3 eV, for manganese (d^4sp^2), 6550.0 ± 0.5 eV, and for manganese

(d^5sp) covalently bonded to an oxidized ligand, 6548.3 ± 0.5 eV. A sp

manganese covalency change ($d^5sp \rightarrow d^4sp^2$) causes a shift in edge energy

of 4.3 eV, and the formation of a d-p covalent bond [MnL_2 ($d^5sp + 2 \cdot L$) $\rightarrow$

$Mn(\cdot L)(L^-)_2$ ($d^5sp + 2 \cdot L, + \cdot L$)] from a ligand-centered oxidation corresponds

to an average shift in edge energy of 2.3 eV per bond formed. Formulation

of MnO_4^- as [$Mn(\cdot O \cdot)_3(\cdot O^-)$]$^-$ with seven Mn-O covalent bonds leads to a

predicted edge energy of 6557.5 eV, which is identical to that observed.

The optimization of the selective ketonization of cyclohexane to

cyclohexanone by an iron/reduced oxygen catalyst system in a mixed

pyridine/acetic acid solvent has been investigated. The addition of

hydrogen peroxide to a solution that contains bis(picolinato)iron(II) and

cyclohexane in a pyridine/acetic acid solvent system (2:1 mole ratio)

results in the direct transformation of cyclohexane to cyclohexanone with

an efficiency of 72% (based on 2 HOOH/ketone). Similar results are

obtained for systems that utilize superoxide ion or electrochemically

reduced dioxygen in place of hydrogen peroxide. Other hydrocarbon

substrates are transformed to ketones via the direct oxygenation of a

methylenic carbon with reaction efficiencies roughly proportional to the

number of $\left(\overset{\displaystyle \diagdown}{\diagup} CH_2 \right)$ groups per molecule. Acetylenes (e.g., $PhC \equiv CPh$) and

arylolefins (e.g., *cis*-$PhCH=CHPh$) are dioxygenated to α-dicarbonyls and

aldehydes, respectively. Monooxygenation of substrates to minor products

appears to require a [$(PA)_2Fe(HOOH)$] catalyst. An iron picolinate μ-peroxo

bridged dimer, [$(PA)_2FeOOFe(PA)_2$], is proposed as the active form of the

catalyst responsible for dioxygenation.

REFERENCES AND NOTES

1. Jørgensen, C. K. *Oxidation Numbers and Oxidation States*; Springer: New York, 1969.

2. Sawyer, D. T. *Comments Inorg. Chem.* **1987**, *6(2)*, 103.

3. Sanderson, R. T. *Polar Covalence*; Academic Press: New York, 1983.

4. For a brief summary containing pertinent references see Huheey, J. E. *Inorganic Chemistry*, 2nd Ed.; Harper & Row, Publishers: New York, 1978, pp. 159-173.

5. Pauling, L. *J. Am. Chem. Soc.* **1932**, *54*, 3570.

6. Pauling, L. *The Nature of the Chemical Bond*, 2nd Ed.; Cornell University Press: Ithaca, New York, 1940, p. 58.

7. Mulliken, R. S. *J. Chem. Phys.* **1934**, *2*, 782; **1935**, *3*, 573.

8. Allred, A. L.; Rochow, E. G. *J. Inorg. Nucl. Chem.* **1958**, *5*, 264.

9. *CRC Handbook of Chemistry and Physics*, 68th Ed.; Chemical Rubber Company: Cleveland, Ohio, 1987, E62-63, E76-77.

10. Nelson, D. D., Jr.; Fraser, G. T.; Klemperer, W. *Science* **1987**, *238*, 1670.

11. Hinze, J.; Jaffé, H. H. *J. Am. Chem. Soc.* **1962**, *84*, 540.

12. Hinze, J.; Jaffé, H. H. *J. Phys. Chem.* **1963**, *67*, 1501.

13. Hinze, J.; Whitehead, M. A.; Jaffé, H. H. *J. Am. Chem. Soc.* **1963**, *85*, 148.

14. Huheey, J. E. *J. Phys. Chem.* **1965**, *69*, 3284.

15. Iczkowski, R. P.; Margrave, J .L. *J. Am. Chem. Soc.* **1961**, *83*, 3547.

16. Sanderson, R. T. *Inorg. Chem.* **1986**, *25*, 3518.

17. Sanderson, R. T. *Science* **1957**, *114*, 670.

18. Parr, R. G.; Donnelly, R. A.; Levy, M.; Palke, W. E. *J. Chem. Phys.* **1978,** *68,* 3801.

19. Politzer, P.; Weinstein, H. *J. Chem. Phys.* **1979,** *71,* 4218.

20. Schilling, J. B.; Goddard, W. A. III; Beauchamp, J. L. *J. Am. Chem. Soc.* **1987,** *109,* 5573.

21. Di Bella, S.; Fragalà, I.; Granozzi, G. *Inorg. Chem.* **1986,** *25,* 3997.

22. Low, J. J.; Goddard, W. A. III. *J. Am. Chem. Soc.* **1986,** *108,* 6115.

23. Harrison, J. F. *J. Phys. Chem.* **1986,** *90,* 3313.

24. Christe, K. O. *Inorg. Chem.* **1986,** *25,* 3721.

25. Sugimoto, H.; Tung, H.-C.; Sawyer, D. T. *J. Am. Chem. Soc.* **1988,** *110,* 2465.

26. Jørgensen, C. K. *Inorg. Chem.* **1969,** *3,* 1201.

27. Sawyer, D. T. *Comments Inorg. Chem.* **1984,** *3,* 133.

28. Cass, M. E.; Gordon, N. R.; Pierpont, C. G. *Inorg. Chem.* **1986,** *25,* 3962.

29. Buchanan, R. M.; Wilson-Blumenberg, C.; Trapp, C.; Larsen, S. K.; Greene, D. L.; Pierpont, C. G. *Inorg. Chem.* **1986,** *25,* 3070.

30. Lynch, M. W.; Hendrickson, D. N.; Fitzgerald, B. J.; Pierpont, C. G. *J. Am. Chem. Soc.* **1984,** *106,* 2041.

31. Buchanan, R. M.; Pierpont, C. G. *J. Am. Chem. Soc.* **1980,** *102,* 4951.

32. Haga, M.-A.; Dodsworth, E. S.; Lever, A. B. P.; Boone, S. R.; Pierpont, C. G. *J. Am. Chem. Soc.* **1986,** *108,* 7413.

33. Haga, M.-A.; Dodsworth, E. S.; Lever, A. B. P. *Inorg. Chem.* **1986,** *25,* 447.

34. Bradbury, J. R.; Schultz, F. A. *Inorg. Chem.* **1986,** *25,* 4416.

35. Jones, S. E.; Leon, L. E.; Sawyer, D. T. *Inorg. Chem.* **1982,** *21,* 3692.

36. Bodini, M. E.; Copia, G.; Robinson, R.; Sawyer, D. T. *Inorg. Chem.* **1983**, *22*, 126.

37. Geiger, D. K.; Ferraudi, G.; Madden, K.; Granifo, J.; Rillema, D. P. *J. Phys. Chem.* **1985**, *89*, 3890.

38. Sawyer, D. T.; Srivatsa, G. S.; Bodini, M. E.; Schaefer, W. P.; Wing, R. M. *J. Am. Chem. Soc.* **1986**, *108*, 936.

39. Tsang, P. K. S.; Cofré, P.; Sawyer, D. T. *Inorg. Chem.* **1987**, *26*, 3604.

40. Hay, R. W. *Bio-inorganic Chemistry*; John Wiley and Sons, Inc.: New York, 1984.

41. Sawyer, D. T. *Chemtech* **1988**, *18*, 369.

42. Barinskii, R. L. *Zh. Strukt. Khim.* **1960**, *1*, 200.

43. Srivastava, U. C.; Nigam, H. L. *Coord. Chem. Rev.* **1972**, *9*, 275.

44. Nigam, A. K.; Guptas, M. K. *J. Phys. F: Metal Phys.* **1974**, *4*, 1084.

45. Ghatikar, M. N.; Padalia, B. D. *J. Phys. C: Solid State Phys.* **1978**, *11*, 1941.

46. Murugesan, T.; Sarode, P. R.; Gopalakrishnan, J.; Rao, C. N. R. *J. Chem. Soc., Dalton Trans.* **1980**, 837.

47. Fenton, H. J. H. *J. Chem. Soc.* **1894**, *65*, 899; **1896**, *69*, 546.

48. Haber, F.; Weiss, J. *Proc. Roy. Soc. (London)* **1934**, *A147*, 332.

49. Walling, C. *Acc. Chem. Res.* **1975**, *8*, 125.

50. Sheldon, R. A.; Kochi, J. K. *Metal-Catalyzed Oxidations of Organic Compounds*; Academic Press, Inc.: New York, 1981.

51. Groves, J. T. In *Metal Ion Activation of Dioxygen*; Spiro, T. G., Ed.; Wiley-Interscience: New York, 1980, pp. 125-162.

52. Bray, W. C.; Gorin, M. H. *J. Am. Chem. Soc.* **1932**, *54*, 2124.

53. Sugimoto, H.; Sawyer, D. T. *J. Am. Chem. Soc.* **1984**, *106*, 4283.

54. Sugimoto, H.; Sawyer, D. T. *J. Am. Chem. Soc.* **1985**, *107*, 5712.

55. Sawyer, D. T.; Sugimoto, H. In *Frontiers in Bioinorganic Chemistry;* Xavier, A. V., Ed.; VCH Publishers: Deerfield Beach, FL, 1986, pp.236-245.

56. Sugimoto, H.; Sawyer, D. T. *J. Org. Chem.* **1985**, *50*, 1784.

57. Sugimoto, H.; Spencer, L.; Sawyer, D. T. *Proc. Natl. Acad. Sci. USA* **1987**, *84*, 1731.

58. Yamaguchi, K.; Sawyer, D. T. *Inorg. Chem.* **1985**, *24*, 971.

59. Yamaguchi, K. S.; Spencer, L.; Sawyer, D. T. *FEBS* **1986**, *197*, 249.

60. Howie, J. K.; Sawyer, D. T. *J. Am. Chem. Soc.* **1976**, *98*, 6698.

61. Seo, E. T.; Riechel, T. L.; Sawyer, D. T. *Inorg. Chem.* **1977**, *16*, 734.

62. Bannister, W. H.; Bannister, J. V.; Searle, A. J. F.; Thornalley, P. J. *Inorg. Chim. Acta.* **1983**, *78*, 139.

63. Barton, D. H. R.; Gastiger, M. J.; Motherwell, W. B. *J. Chem. Soc., Chem. Commun.* **1983**, 41.

64. Barton, D. H. R.; Boivin, J.; Motherwell, W. B.; Ozbalik, N.; Schwartzentruber, K. M.; Jankowski, K. *Nouv. J. Chim.* **1986**, *10*, 387.

65. Balavoine, G.; Barton, D. H. R.; Boivin, J.; Gref, A.; Ozbalik, N.; Rivière, H. *Tetrahedron Letts.* **1986**, *27*, 2849.

66. Balavoine, G.; Barton, D. H. R.; Boivin, J.; Gref, A.; Ozbalik, N.; Rivière, H. *J. Chem. Soc., Chem. Commun.* **1986**, 1727.

67. Balavoine, G.; Barton, D. H. R.; Boivin, J.; Gref, A.; Le Coupanec, P.; Ozbalik, N.; Pestana, A.; Rivière, H. *Tetrahedron* **1988**, *44*, 1091.

68. Barton, D. H. R.; Boivin, J.; Ozbalik, N.; Schwartzentruber, K. M.; Jankowski, K. *Tetrahedron Letts.* **1985**, *26*, 447.

69. Sawyer, D. T.; Roberts, J. L., Jr. *Experimental Electrochemistry for Chemists*; Wiley: New York, 1974; pp. 44-46, 144-145, 336-339.

70. Belli, M.; Scafati, A.; Biaconi, A.; Mobilio, S.; Palladino, L.; Reale, A.; Burattini, E. *Solid State Commun.* **1980**, *35*, 335.

71. Apte, M. Y.; Mande, C. *J. Phys. Chem. Solids* **1980**, *41*, 307.

72. Bortolini, O.; Ricci, M.; Meunier, B. *Nouv. J. Chim.* **1986**, *10*, 39.

73. Evans, D. F. *J. Chem. Soc.* **1959**, 2003.

74. Carlin, R. L. *Magnetochemistry*; Springer-Verlag: New York, 1986.

75. Selwood, P. W. *Magnetochemistry*, 2nd Ed.; Interscience: New York, 1956.

76. Brevard, C.; Granger, P. *Handbook of High Resolution Multinuclear NMR*; Wiley-Interscience: New York, 1981.

77. Larsson, R.; Eskilsson, O. *Acta. Chem. Scand.* **1969**, *23*, 1765.

78. Nakamoto, K.; McCarthy, R. J.; Ruby, A.; Martell, A. E. *J. Am. Chem. Soc.* **1961**, *83*, 1066.

79. Basu, S.; Chatterji, Z. *Physik. Chem.* **1958**, *209*, 361.

80. Barnum, D. W. *J. Inorg. Nucl. Chem.* **1961**, *21*, 221.

81. Summers, J. Ph.D. Dissertation, University of Michigan, 1968; available from University Microfilms International, Ann Arbor, MI.

82. Ray, M. M.; Adhya, J. N.; Biswas, D.; Poddar, S. N. *Aust. J. Chem.* **1966**, *19*, 1737.

83. Morrison, M. M.; Sawyer, D. T. *Inorg. Chem.* **1978**, *17*, 333.

84. Schilt, A. A.; Taylor, R. C. *J. Inorg. Nucl. Chem.* **1959**, *9*, 211.

85. Chiswell, B.; O'Reilly, E. J. *Inorg. Chim. Acta.* **1973**, *7*, 707.

86. Bannister, E.; Cotton, F. A. *J. Chem. Soc.* **1960**, 1878.

87. Aghabozorg, H.; Palenik, G. J.; Stoufer, R. C.; Summers, J. *Inorg. Chem.* **1982**, *21*, 3903.

88. Williams, D. E. *J. Inorg Nucl. Chem.* **1966**, *28*, 1895.

89. Prabhakaran, C. P.; Patel, C. C. *J. Inorg. Nucl. Chem.* **1968**, *30*, 867.

90. Kleinstein, A.; Webb, G. A. *J. Inorg. Nucl. Chem.* **1971**, *33*, 405.

91. Reiff, W. M.; Baker, W. A. *Inorg. Chem.* **1970**, *9*, 570.

92. Nyholm, R. S.; Turco, A. *J. Chem. Soc.* **1962**, 1121.

93. Nyholm, R. S.; Turco, A. *Chem. Ind. (London)* **1960**, 74.

94. Plaksin, P. M.; Stoufer, R. C.; Mathew, M.; Palenik, G. J. *J. Am. Chem. Soc.* **1972**, *94*, 2121.

95. Goodwin, H. A.; Sylva, R. N. *Aust. J. Chem.* **1967**, *20*, 629.

96. Matsushita, T.; Spencer, L.; Sawyer, D. T. *Inorg. Chem.* **1988**, *27*, 1167.

97. Furman, N. H. *Standard Methods of Chemical Analysis*, 6th Ed., Vol. I; D. Van Nostrand, Inc.: Princeton, NJ, 1962; pp. 537-538.

98. Karayannis, N. M.; Mikulski, C. M.; Strocko, M. J.; Pytlewski, L. L.; Labes, M. M. *J. Inorg. Nucl. Chem.* **1970**, *32*, 2629.

99. Baudisch, O.; Hartung, W. H. In *Inorganic Synthesis*, Vol. I; Booth, H. S., Ed.; McGraw-Hill Book Company, Inc.: New York, 1939, p. 184.

100. Charles, R. G.; Freiser, H.; Friedal, R.; Hilliard, L. E.; Johnston, W. D. *Spectrochimica Acta.* **1956**, *8*, 1.

101. Ohkaku, N.; Nakamoto, K. *Inorg. Chem.* **1971**, *10*, 798.

102. Tackett, J. E.; Sawyer, D. T. *Inorg. Chem.* **1969**, *3*, 692.

103. Rane, A. V.; Ravi, U. V. *Spectrochimica Acta.* **1982,** *38A(8),* 937.

104. Wheeler, S. H.; Zingheim, S. C.; Nathan, L. C. *J. Inorg. Nucl. Chem.* **1978,** *40,* 779.

105. Bryant, B. E.; Fernelius, W. C. In *Inorganic Synthesis V;* Moeller, T., Ed.; McGraw-Hill: New York, 1957; pp. 188-189.

106. Bauer, H. F.; Drinkard, W. C. *J. Am. Chem. Soc.* **1960,** *82,* 5031.

107. Kolthoff, I. M.; Sandell, F. B. *Textbook of Quantitative Inorganic Analysis,* 3rd Ed.; The MacMillan Company: New York, 1956, p. 600.

108. Sawyer, D. T.; Calderwood, T. S.; Yamaguchi, K.; Angelis, C. T. *Inorg. Chem.* **1982,** *22,* 2577.

109. Yamaguchi, K.; Calderwood, T. S.; Sawyer, D. T. *Inorg. Chem.* **1986,** *25,* 1289.

110. Cofré, P.; Sawyer, D. T. *Inorg. Chem.* **1986,** *25,* 2084.

111. Baker, B. C.; Sawyer, D. T. *Anal. Chem.* **1968,** *40,* 1945.

112. Lannon, M.; Lappin, A. G.; Segal, M. G. *J. Chem. Soc., Dalton Trans.* **1986,** 619.

113. Charles, R. G. *J. Phys. Chem.* **1957,** *61,* 1640.

114. The dominant form of isolated manganic triacetate is $[Mn_3O(OAc)_6](OAc)(HOAc)$ with a tridentate oxo-ion bridging the three Mn ions. Hessel, L. W.; Romers, C. *Rev. Trav. Chim.* **1969,** *88,* 645.

115. Bard, A. J.; Parsons, R.; Jordan, V., Eds. *Standard Potentials in Aqueous Solution;* Marcel Dekker, Inc.: New York, 1985.

116. Yamaguchi, K. S.; Sawyer, D. T. *Isr. J. Chem.* **1985,** *25,* 164.

117. Sock, O.; Lemoine, P.; Gross, M. *Spectrochimica Acta.* **1981,** *26,* 99.

118. Gritzner, G.; Murauer, H.; Gutmann, V. *J. Electroanal. Chem.* **1979**, *101*, 177.

119. Ferric acetate exists as $[Fe_3(OAc)_6](OAc)_3$, $[Fe_3(OAc)_6(OH)](OAc)_2$, or $[Fe_3(OAc)_6(OH)_2](OAc)$. Sidgwick, N. W. *The Chemical Elements and Their Compounds*, Vol. II; Clarendon Press: Oxford, 1950, p. 1363.

120. Ferric acetate also may form oxo-bridged trinuclear species analogous to manganic triacetate (Ref. 114). Cotton, F. A.; Wilkinson, G. *Advanced Inorganic Chemistry*, 3rd Ed.; Interscience Publishers: New York, 1972, p. 866.

121. Cobaltic triacetate, $[(OAc)_2Co(\mu\text{-}OH)_2Co(OAc)_2](HOAc)$, exists as a binuclear compound containing bidentate acetates and μ-hydroxo bridges. Koubek, E.; Edwards, J. O. *J. Inorg. Nucl. Chem.* **1963**, *25*, 1401; Lande, S. S.; Falk, C. D.; Kochi, J. K. *J. Inorg. Nucl. Chem.* **1971**, *33*, 4101.

122. Cobaltic triacetate also may form a trinuclear oxo-bridged species analogous to manganic triacetate (Ref. 114). Ziolkowski, J. J.; Pruchnik, F.; Szymanska-Buzar, T. *Inorg. Chim. Acta.* **1973**, *7*, 473.

123. Cotton, F. A.; Holm, R. H. *J. Am. Chem. Soc.* **1960**, *82*, 2979.

124. Bhathager, S. S.; Khanna, M. L.; Nergi, M. B. *Phil. Mag.* **1938**, *25*, 234.

125. Jannakoudakis, A. D.; Tsiamis, C.; Jannakoudakis, P. D.; Theodoridu, E. *J. Electroanal. Chem.* **1985**, *184*, 123.

126. Cotton, F. A.; Soderberg, R. H. *Inorg. Chem.* **1964**, *3*, 1.

127. Cotton, F. A.; Elder, R. C. *Inorg. Chem.* **1965**, *4*, 1145.

128. Barrette, W. C.; Johnson, H. W., Jr.; Sawyer, D. T. *Anal. Chem.* **1984**, *56*, 1890.

129. Barnum, D. W. *J. Inorg. Nucl. Chem.* **1961,** 22, 183.

130. Brown, N. M. D.; McMonagle, J. B.; Greaves, G. N. *J. Chem. Soc., Faraday Trans. I* **1984,** 80, 589.

131. Apte, M. Y.; Mande C. *J. Phys. C: Solid State Phys.* **1982,** 15, 607.

132. Chin, D.-H.; Sawyer, D. T.; Schaefer, W. P.; Simmons, C. J. *Inorg. Chem.* **1983,** 22, 7527.

133. Cotton, F. A.; Wilkinson, G. *Advanced Inorganic Chemistry,* 4th Ed.; John Wiley & Sons, Inc.: New York, 1980, pp. 766-783.

134. Basolo, F.; Pearson, R. G. *Mechanisms of Inorganic Reactions,* 2nd Ed.; John Wiley & Sons, Inc.: New York, 1967.

135. Dessy, R. E.; Stary, F. E.; King, R. B.; Waldrop, M. *J. Am. Chem. Soc.* **1966,** 88, 471.

136. Mazur, S.; Ohkubo, K. *J. Am. Chem. Soc.* **1975,** 97, 2911.

137. Soar, J.; Smith, D. E.; Cais, M. *J. Am. Chem. Soc.* **1985,** 107, 6807.

138. Data supplied by Ceshing Sheu of this laboratory.

139. Sawyer, D. T.; McDowell, M. S.; Spencer, L.; Tsang, P. K. S. *Inorg. Chem.* **1989,** in press.

140. Data supplied by Dr. Pablo Cofré of the Universidad Catòlica de Chile.

141. Chin, D.-H.; Chiericato, G., Jr.; Nanni, E. J., Jr.; Sawyer, D. T. *J. Am. Chem. Soc.* **1982,** 104, 1296.

142. Dorfman, L. F.; Adams, G. E. *Natl. Stand. Ref. Data Ser. (U. S. Natl. Bur. Stand.)* **1973,** *NSRDS-NBS* 46, 20 (SD catalog No. C13.48:46).

143. Roberts, J. L., Jr.; Morrison, M. M.; Sawyer, D. T. *J. Am. Chem. Soc.* **1978,** 100, 329.

144. Sawyer, D. T.; Chiericato, G., Jr.; Angelis, C. T.; Nanni, E. J., Jr.; Tsuchiya, T. *Anal. Chem.* **1982,** *54,* 1720.

145. Ehman, D. L.; Sawyer, D. T. *Inorg. Chem.* **1969,** *8,* 900.

146. Wilkins, R. G.; Yelin, R. E. *Inorg. Chem.* **1969,** *8,* 1470.

147. Schugar, H. J.; Hubbard, A. T.; Anson, F. C.; Gray, H. B. *J. Am. Chem. Soc.* **1969,** *41,* 71.

148. Hester, R. E.; Nour, E. M. *J. Raman Spectrosc.* **1981,** *11,* 35.

VITA

Silvia Ann Richert (née Beatty) ████████████████████
████████████████████████████ in 1979 and earned a B.S. in
Chemistry, Mathematics, and Humanities from the United States Air
Force Academy in 1983. After being commissioned as a second lieutenant
in the U.S. Air Force, she attended Harvard University on a National
Science Foundation Graduate Fellowship and completed an A.M. in
Chemistry in 1984. She then was stationed at the Air Force Weapons
Laboratory at Kirtland AFB, New Mexico as a Laser Research Chemist
from 1984 to 1986. In 1986 she was selected for a Ph.D. educational
assignment and began attending Texas A&M University. ████████████
████████████████████